

Politecnico di Torino

Politecnico di Torino

Master's Degree in

Energy and Nuclear Engineering

Renewable Energy Systems

Academic Year 2025/2026

Graduation Session: September 2026

Hydrogen Integration in a Grid-Connected Microgrid for the Glass Industry: PEM Electrolyzer Modelling considering Degradation under Different Energy Management Frameworks

Supervisors:

Marta Gandiglio

Eduardo Prieto-Araujo

Lorenzo Bruno

Esteban Daniel Gonzalez Iakl

Paolo Marocco

Candidate:

Chiara Barettini

UPC

CITCEA UPC

Abstract

The decarbonization of energy-intensive industrial processes represents a major challenge in the transition towards low-carbon energy systems. In this context, hydrogen offers a potential option for reducing fossil-fuel consumption in high-temperature applications where complete electrification may be difficult to achieve. This thesis investigates the integration of photovoltaic generation, PEM electrolyzer, and compressed hydrogen storage in a grid-connected microgrid for the partial substitution of natural gas in a continuous glass-melting furnace.

A numerical model of the integrated energy system is developed using plant-specific energy-demand and photovoltaic-generation data provided by a company in the glass manufacturing sector.

Particular attention is devoted to the PEM electrolyzer, whose performance is described through a detailed electrochemical model that determines cell voltage, hydrogen production, and conversion efficiency as a function of the operating point. A literature-based degradation model is additionally implemented to represent the evolution of electrolyzer performance as a function of operating time and load conditions.

The analysis is developed in two stages. First, a deterministic rule-based strategy is implemented to manage photovoltaic and grid electricity, hydrogen production, storage, and furnace supply according to a predefined operating hierarchy. Different hydrogen-substitution levels are investigated to assess the behaviour and technical limitations of the integrated system.

In the second stage, the developed PEM electrochemical and degradation models are integrated into an existing optimization-based Energy Management System formulated for the same industrial application but including additional system-level energy flows and operating constraints. The EMS uses a rolling-horizon formulation to coordinate the system energy flows by minimizing energy and carbon-emission-related costs while satisfying the relevant component and energy-balance constraints. The original constant-efficiency representation of the electrolyzer is replaced through an iterative coupling procedure, allowing the operating point and degradation-dependent PEM performance to influence the optimized system dispatch.

Finally, the two energy-management strategies are analyzed through technical, energy, economic, and environmental indicators to assess their implications for hydrogen integration in the considered industrial application.

Contents

Abstract 2

1 Introduction **10**

1.1 Role of Hydrogen in Decarbonization 10

1.2 Hydrogen Properties 12

1.3 Hydrogen Production Pathways 14

1.3.1 Green Hydrogen 14

1.3.2 Yellow Hydrogen 15

1.3.3 Other Hydrogen Production Pathways 15

1.4 Power-to-X 16

1.4.1 Power-to-Hydrogen 17

1.4.2 Hydrogen-Derived Power-to-X Pathways 17

1.4.3 Role of Power-to-X in Integrated Energy Systems 18

1.4.4 Power-to-Hydrogen in Industrial Microgrids 18

1.5 Hydrogen in High-Temperature Industries 19

1.5.1 Hydrogen Application in the Glass Industry 19

1.6 The H2GLASS Project 20

1.7 Thesis Objectives 21

2 Theoretical Background **23**

2.1 Water Electrolysis Technologies 23

2.1.1 Electrolyzer Categories 23

2.1.2 Comparison of Electrolyzer Technologies 27

2.2 PEM Electrolyzer Degradation 27

2.2.1 Main Degradation Mechanisms 28

2.2.2 Influence of Operating Conditions 28

2.2.3 Effect of Degradation on Electrolyzer Performance 29

2.3 Hydrogen Storage 30

2.3.1 Hydrogen Storage Technologies 30

2.4 Hydrogen Compression 32

2.5 Fundamentals of Optimization and Energy Management Systems 33

2.5.1 Mathematical Optimization 33

2.5.2 Main Classes of Optimization Problems 34

2.5.3 Energy Management Systems 34

3 Methodology **36**

3.1 System Description 36

3.2 Input Data and Main Assumptions . . . 38
3.2.1 Input Data and Pre-processing . . . 38
3.2.2 Main Modelling Assumptions . . . 39
3.3 System Component Models . . . 40
3.3.1 Glass Furnace Energy Demand . . . 40
3.3.2 PEM Electrolyzer Model . . . 41
3.3.3 Hydrogen Compression Model . . . 48
3.3.4 Hydrogen Storage Model . . . 49
3.4 PEM Electrolyzer Degradation Model . . . 50
3.5 Rule-Based Energy Management . . . 54
3.6 Optimization-Based Energy Management . . . 57
3.7 Performance Assessment Methodology . . . 65

4 Case Study and Results **69**
4.1 Simulation Setup . . . 69
4.1.1 Simulation Parameters . . . 69
4.1.2 Investigated Scenarios . . . 71
4.2 Rule-Based Energy Management Results . . . 72
4.2.1 Scenario-Specific Operating Behaviour . . . 72
4.2.2 Comparative Assessment of the Rule-Based Scenarios . . . 84
4.3 Optimization-Based Energy Management System . . . 94
4.3.1 Optimization-Specific Simulation Parameters . . . 94
4.3.2 Selected-Day Operating Behaviour . . . 95
4.3.3 Annual Technical and Energy Performance . . . 98
4.3.4 Effect of the Detailed PEM Representation and Degradation . . . 100
4.3.5 Economic and Environmental Performance . . . 103
4.4 Cross-Framework Discussion . . . 106
4.4.1 Interpretation of the Two Analyses . . . 106
4.4.2 PEM Operation and Degradation . . . 106
4.4.3 System-Level Implications . . . 107

5 Conclusion **109**
5.1 Limitations and Future Developments . . . 110

List of Figures

1.1 H2GLASS project 21

2.1 Schematic representation of an alkaline electrolyzer. 24
2.2 Schematic representation of a PEM electrolyzer. 25
2.3 Schematic representation of a solide oxide electrolyzer. 26
2.4 Schematic representation of an AEM electrolyzer. 27

3.1 Schematic representation of the grid-connected industrial microgrid considered in this work. 37

4.1 Hydrogen demand and hydrogen supplied to the furnace for the 5% hydrogen-share scenario. 72
4.2 Electrical power balance during the selected operating period for the 5% hydrogen-share scenario. 73
4.3 Level of Hydrogen in the storage unit for the 5% hydrogen-share scenario. 73
4.4 Fresh and degradation-adjusted PEM LHV efficiencies for the 5% hydrogen-share scenario. 74
4.5 Hydrogen demand and hydrogen supplied to the furnace for the 10% hydrogen-share scenario. 76
4.6 Level of Hydrogen in the storage unit for the 10% hydrogen-share scenario. 76
4.7 Hydrogen demand, supplied hydrogen, and residual deficit for the 15% hydrogen-share scenario. 78
4.8 Level of Hydrogen in the storage unit for the 15% hydrogen-share scenario. 79
4.9 Hydrogen demand, supplied hydrogen, and residual deficit for the 20% hydrogen-share scenario. 80
4.10 Level of Hydrogen in the storage unit for the 20% hydrogen-share scenario. 81
4.11 Fresh and degradation-adjusted PEM LHV efficiencies for the 20% hydrogen-share scenario. 81
4.12 Hydrogen demand, supplied hydrogen, and residual deficit for the 25% hydrogen-share scenario. 83
4.13 Comparison between the target hydrogen share and the effective annual hydrogen contribution achieved for the investigated rule-based scenarios. 85
4.14 Annual hydrogen production obtained with the fresh and degradation-adjusted PEM models for the investigated rule-based scenarios. 86

4.15 Degradation-related hydrogen-production loss and hydrogen-target coverage for the investigated rule-based scenarios. 87
4.16 Specific electrical energy consumption obtained with the fresh and degradation-adjusted PEM models for the investigated rule-based scenarios. 88
4.17 Annual PEM electricity supply from photovoltaic generation and from the electrical grid for the investigated rule-based scenarios. 89
4.18 Annual operational emissions for the 100% natural-gas baseline and the investigated rule-based hydrogen-share scenarios, including direct natural-gas and indirect grid-electricity contributions. 90
4.19 Annual energy and carbon-related operating costs for the 100% natural-gas baseline and the investigated rule-based hydrogen-share scenarios. 91
4.20 Net incremental energy and carbon-related operating cost per unit of hydrogen effectively supplied to the furnace for the investigated rule-based scenarios. 92
4.21 PEM electrical input power and electricity-price profile during selected day 180. . . 95
4.22 Hydrogen charging and discharging power and tank state of charge during selected day 180. 96
4.23 Composition of the useful energy supplied to the furnace during selected day 180. . 97
4.24 Daily hydrogen production and average hydrogen-tank state of charge over the annual simulation. 99
4.25 Annual electrical-energy supply and demand of the optimization-based system. . . 100
4.26 Daily average relative difference between the fresh electrochemical PEM efficiency and the constant 65% efficiency assumption at the operating points associated with the final degradation-aware EMS dispatch. 101
4.27 Daily fresh and degradation-adjusted PEM efficiency over the annual simulation. . . 102
4.28 Annual energy and carbon-related operating costs for the reconstructed 100% natural-gas baseline and the optimization-based configuration. 104
4.29 Annual operational emissions for the reconstructed 100% natural-gas baseline and the optimization-based configuration, including direct natural-gas and indirect grid-electricity contributions. 105

List of Tables

1.1 Comparison of selected physical, energetic, and combustion properties of hydrogen and methane. 12

2.1 Comparison of the main water electrolysis technologies. 27

4.1 General plant and simulation parameters adopted in the rule-based implementation. 69
4.2 Main parameters adopted in the PEM electrochemical model. 70
4.3 Main parameters adopted in the hydrogen compression model. 71
4.4 Main parameters adopted in the hydrogen storage model. 71
4.5 PEM operating range obtained in the 5% hydrogen-share scenario. 74
4.6 PEM operating range obtained in the 10% hydrogen-share scenario. 77
4.7 PEM operating range obtained in the 15% hydrogen-share scenario. 79
4.8 Main indicators of the investigated rule-based scenarios. 84
4.9 Main simulation parameters specific to the optimization-based EMS. 94
4.10 Main annual technical performance indicators of the optimization-based EMS. . . . 98
4.11 Annual economic and environmental performance of the reconstructed 100% natural-gas baseline and the optimization-based configuration. 103

1. Introduction

The transition toward a climate-neutral energy system represents one of the major technological and societal challenges of the twenty-first century. Decarbonizing energy-intensive industries is particularly difficult because of their high energy consumption, continued reliance on fossil fuels, and demand for high-temperature heat [1, 2, 3].
Among the different solutions being investigated, hydrogen has emerged as a promising energy carrier for reducing fossil fuel consumption in industrial applications where direct electrification remains difficult. When produced using low-carbon electricity, hydrogen can significantly reduce greenhouse gas emissions and support the transition toward more sustainable industrial energy systems [3, 1].
The glass industry represents a particularly relevant application due to the high energy demand of continuously operated melting furnaces and their dependence on fossil fuels, primarily natural gas. The partial substitution of natural gas with hydrogen therefore represents a potential pathway for reducing the carbon footprint of glass manufacturing [4].
This thesis focuses on the integration of hydrogen into a grid-connected industrial microgrid for glass production. The system under investigation includes photovoltaic generation, a PEM electrolyzer, hydrogen compression and storage systems, and a hybrid natural gas-hydrogen combustion system for high-temperature heat generation.
The work is closely connected to the European H2GLASS project and aims to assess the technical, energetic, economic, and environmental implications of hydrogen integration in a grid-connected industrial energy system for glass manufacturing[5].

1.1 Role of Hydrogen in Decarbonization

The growing penetration of renewable energy sources is reshaping modern energy systems, but electricity alone cannot address all decarbonization needs. Several applications require alternative solutions capable of delivering energy in forms that can be stored, transported, and used where direct electrification is not technically or economically suitable. Hydrogen can help address this challenge by providing a way to use renewable energy in a variety of applications that are difficult to electrify directly. Its ability to connect different energy sectors and provide low-carbon alternatives to fossil fuels has therefore made it an increasingly important component of long-term decarbonization strategies.
Unlike primary energy sources, hydrogen is an energy carrier that is not naturally available in significant quantities in its molecular form and must therefore be produced from compounds that contain hydrogen. Its strategic relevance therefore lies in its ability to store, transport, and deliver energy, enabling low-carbon energy to be transferred across different sectors and applications [3, 1].
One of the most important features of hydrogen is its potential to facilitate sector coupling. Elec-

tricity generated from renewable sources can be converted into hydrogen through water electrolysis and subsequently stored for later use. This conversion creates a link between the power sector and energy-consuming sectors where direct use of electricity is not always possible. It also provides an additional option for managing the variability of renewable generation. In this way, hydrogen can contribute both to the decarbonization of end-use sectors and to greater flexibility of energy systems characterized by increasing shares of variable renewable sources.

Hydrogen can be used in several ways depending on the application. It can be used as an energy carrier for applications requiring high-grade thermal energy, as a chemical feedstock in industrial processes, and as a medium for long-duration energy storage. Hydrogen is already extensively used in sectors such as ammonia production, petroleum refining, and methanol synthesis, where replacing conventionally produced hydrogen with low-emission alternatives can reduce greenhouse gas emissions. At the same time, new applications are being investigated in sectors where conventional decarbonization options remain limited, including energy-intensive industries and selected transport applications [3].

The potential contribution of hydrogen to decarbonization, however, depends fundamentally on how it is produced. Current global hydrogen production remains predominantly based on fossil fuels. According to the International Energy Agency, global hydrogen demand reached approximately 97 Mt in 2023, while low-emission hydrogen accounted for less than 1% of total production. In the same year, hydrogen production was also responsible for approximately 920 Mt of CO_2 emissions, highlighting the substantial environmental impact of conventional production pathways [3].

These data underline an essential distinction between the use of hydrogen and its actual contribution to climate mitigation. Although hydrogen does not generate direct CO_2 emissions when used as a fuel, its overall environmental performance depends on the energy sources and technologies employed for its production. Hydrogen can therefore contribute effectively to decarbonization only when its production is associated with sufficiently low lifecycle greenhouse gas emissions.

Despite its potential, hydrogen should not be regarded as a universal substitute for conventional energy carriers. Its production involves energy conversion losses, while compression, storage, transportation, and final utilization introduce additional technical and economic challenges. Large-scale deployment also requires dedicated infrastructure, appropriate safety measures, and substantial investment throughout the hydrogen value chain. For applications that can be efficiently electrified directly, the direct use of electricity may therefore represent a more energy-efficient solution. Hydrogen is instead particularly relevant where direct electrification is technically challenging or where a molecular energy carrier is specifically required [1, 2, 3]. This is particularly relevant for energy-intensive industries that require a continuous supply of high-temperature heat. In these applications, replacing conventional fossil fuels is difficult, making hydrogen a possible alternative for reducing their dependence on fossil fuels.

1.2 Hydrogen Properties

Hydrogen has distinctive physical, energetic, and combustion properties that differ significantly from conventional hydrocarbon fuels. These characteristics strongly influence the technologies required for its storage, transportation, and utilization and are therefore fundamental for understanding both the opportunities and the technical challenges associated with its integration into energy and industrial systems.

Under ambient conditions, molecular hydrogen (H_2) is a colorless, odorless, and non-toxic diatomic gas with a molar mass of approximately 2.016 g/mol. Being the lightest molecule, hydrogen has a very low gaseous density, approximately 0.09 kg/m^3 under normal conditions. This characteristic has important practical consequences, particularly for storage and transportation, since a relatively large volume is needed to contain a given mass of hydrogen [6].

From an energetic perspective, hydrogen is characterized by a particularly high energy content per unit of mass. Its lower heating value (LHV) is approximately 120 MJ/kg, while its higher heating value (HHV) is approximately 142 MJ/kg [6]. The difference between these two values depends on whether the latent heat associated with the condensation of the water produced during utilization is recovered.

A comparison between the main physical, energetic, and combustion properties of hydrogen and methane is provided in Table 1.1. The comparison highlights the distinctive characteristics of hydrogen, particularly its high gravimetric energy content, low gaseous density, wide flammability range, and high reactivity compared with methane.

Table 1.1: Comparison of selected physical, energetic, and combustion properties of hydrogen and methane.

Property	**Hydrogen**	**Methane**
Molecular mass [g/mol]	2.016	16.04
Lower heating value [MJ/kg]	~120	~50
Gas density [kg/m^3]	~0.09	~0.66–0.72
Flammability range in air [vol.%]	4.1–74	5.3–15
Minimum ignition energy [mJ]	~0.02	~0.28
Maximum laminar burning velocity [m/s]	~2.91	~0.37

Source: adapted from [7, 8].

On a mass basis, hydrogen therefore contains considerably more energy than conventional hydrocarbon fuels. The situation is substantially different when energy content is considered on a volumetric basis. Because of its very low density under ambient conditions, gaseous hydrogen has a low volumetric energy density compared with conventional fuels. Consequently, practical storage generally requires increasing its density through physical or chemical methods. The most common physical options include compression at high pressure and liquefaction at cryogenic temperatures, while alternative approaches involve solid-state storage or conversion into hydrogen carriers. Compressed gaseous hydrogen systems can operate at several pressure levels depending on the application, with pressures up to several hundred bar used when high storage density is required. These storage re-

quirements introduce additional energy consumption, infrastructure needs, and technical complexity into the hydrogen value chain.

Hydrogen also exhibits combustion characteristics that differ considerably from those of conventional hydrocarbon fuels such as natural gas. Hydrogen-air mixtures are flammable over a wide range of concentrations, approximately 4.1-74 vol.% under ambient conditions, and hydrogen requires a very low minimum ignition energy. Moreover, its high laminar burning velocity and rapid chemical kinetics result in faster flame propagation compared with methane [6]. These properties allow hydrogen combustion over a broad range of mixture compositions, but they also increase the risk of phenomena such as flashback, particularly in premixed combustion systems.

The high reactivity of hydrogen has important implications for the design and operation of combustion equipment. Burner geometries and control strategies originally developed for natural gas may require modifications as the hydrogen fraction in the fuel increases. Changes in flame speed, flame structure, heat transfer, and combustion stability must therefore be considered when introducing hydrogen either through mixing with natural gas or by complete fuel substitution [4].

An additional aspect concerns pollutant formation. Hydrogen contains no carbon and therefore its combustion does not directly produce CO_2, carbon monoxide, or carbonaceous particulate matter originating from the fuel. However, combustion with air can still generate nitrogen oxides (NO_x). Their formation depends strongly on local flame temperature, oxygen concentration, residence time, and combustion conditions. For this reason, appropriate burner design and combustion strategies are required to control NO_x emissions in hydrogen-fired systems. [4].

Hydrogen also presents specific characteristics relevant to safety and infrastructure design. Its small molecular size and high diffusivity increase its tendency to leak through small openings and permeate certain materials. At the same time, its low density promotes rapid upward dispersion when released in open or well-ventilated environments. The combination of a wide flammability range and low ignition energy nevertheless requires careful leak detection, ventilation, ignition-source control, and appropriate system design. Hydrogen flames can also be difficult to detect visually under certain conditions, introducing additional requirements for flame detection and safety systems [6, 8].

Material compatibility represents another important consideration. Exposure to hydrogen can negatively affect the mechanical properties of some metallic materials through phenomena generally referred to as hydrogen embrittlement. The susceptibility to these phenomena depends on several factors, including material composition and microstructure, hydrogen pressure, temperature, stress state, and operating conditions. Pipelines, storage vessels, valves, seals, and other components intended for hydrogen service must thus be designed using suitable materials and engineering standards [9].

Overall, hydrogen combines a high gravimetric energy content with low volumetric energy density, high diffusivity, and distinctive combustion characteristics. These properties affect the production, compression, storage, transportation, and use of hydrogen and must be considered when integrating hydrogen into industrial energy systems.

1.3 Hydrogen Production Pathways

Although hydrogen is always the same chemical species, the environmental impact associated with its production can vary significantly depending on the feedstock, conversion technology, and energy source employed. Hydrogen can be produced through several pathways, ranging from conventional fossil-based processes to water electrolysis powered by low-carbon electricity. For this reason, a color-based nomenclature has become widely used to distinguish different production routes and provide an intuitive indication of their associated environmental characteristics [10, 11].
The color classification, however, is not formally standardized, and definitions may vary across the scientific literature and industrial applications. More importantly, a color label alone does not provide a complete assessment of the environmental performance of hydrogen. The actual greenhouse gas emissions associated with each pathway depend on several factors, including the carbon intensity of the energy supply, upstream emissions, methane leakage, conversion efficiency, carbon capture rates, and the system boundaries considered in lifecycle assessments. Quantitative indicators, generally expressed in $kgCO_2$-eq per kg_{H_2}, provide a more rigorous basis for comparing alternative hydrogen production pathways [10].
Despite these limitations, the color-based nomenclature remains useful for distinguishing the main hydrogen production routes and their potential environmental impacts.

1.3.1 Green Hydrogen

Green hydrogen generally refers to hydrogen produced through water electrolysis using electricity generated from renewable energy sources, such as solar photovoltaic, wind, or hydropower [10, 11]. During electrolysis, electrical energy is used to split water into hydrogen and oxygen, thus converting renewable electricity into a chemical energy carrier that can subsequently be stored, transported, or used in different end-use applications.
The main environmental advantage of this pathway derives from the absence of direct fossil fuel consumption during hydrogen production and from the low carbon intensity that can be achieved when the electrolyzer is supplied with renewable electricity. Nevertheless, green hydrogen should not automatically be considered completely emission-free on a lifecycle basis. There may still be emissions due to manufacturing, construction, and operation of renewable generation assets, electrolyzers, storage systems, and associated infrastructure. The actual environmental impact therefore depends on the entire supply chain [10].
Water electrolysis can be performed using different technologies, including alkaline water electrolysis, proton exchange membrane (PEM) electrolysis, anion exchange membrane (AEM) electrolysis, and solid oxide electrolysis [12]. Their operating principles, characteristics, advantages, and limitations are discussed in detail in the following sections. Among these technologies, PEM electrolysis was selected for the system investigated in this thesis because of its suitability for dynamic operation in combination with variable renewable electricity generation.
Despite its potential for low-emission hydrogen production, renewable electrolysis still faces impor-

tant economic and technical challenges. Electricity consumption represents a major contribution to hydrogen production costs, while electrolyzer investment costs, infrastructure requirements, and the availability of sufficiently low-cost renewable electricity strongly influence its economic competitiveness. Nevertheless, renewable hydrogen remains an important option for reducing emissions and supporting the decarbonization of applications where direct electrification is difficult [3, 1].

1.3.2 Yellow Hydrogen

Yellow hydrogen is similarly produced through water electrolysis, but using electricity from the electrical grid rather than exclusively from renewable sources. In this pathway, the electrolysis process itself does not generate direct CO_2 emissions; however, the overall environmental impact of hydrogen production depends strongly on the origin and carbon intensity of the electricity used to supply the electrolyzer.

Since grid electricity may originate from a combination of renewable, nuclear, and fossil-based generation, the carbon footprint associated with hydrogen production can vary significantly depending on the electricity mix. Furthermore, as the generation mix changes over time, the carbon intensity of grid-based hydrogen production may also vary according to the period during which the electrolyzer operates. For this reasons, hydrogen produced through grid-powered electrolysis cannot automatically be considered renewable or low-emission solely because electrolysis is used as the production technology [10].

It should be noted that the term *yellow hydrogen* is not defined consistently throughout the literature. While it is used in some classifications to identify hydrogen produced through electrolysis using grid electricity, other classifications associate yellow hydrogen specifically with solar-powered electrolysis. This difference shows that hydrogen color terminology is not fully standardized. The production pathway should be clearly defined when using these labels [10, 11].

In the system investigated in this thesis, hydrogen can be produced using either on-site photovoltaic electricity or electricity imported from the external grid. Depending on the electricity source, these production pathways can be associated with green and yellow hydrogen, respectively.

1.3.3 Other Hydrogen Production Pathways

In addition to green and yellow hydrogen, several other color labels are commonly used to identify hydrogen according to its production pathway [10, 11]:

- **Grey hydrogen** is generally produced from fossil fuels, most commonly natural gas through steam methane reforming (SMR), without carbon capture. In this process, methane reacts with steam to produce hydrogen, while the carbon contained in the feedstock is ultimately released as CO_2, resulting in significant greenhouse gas emissions.
- **Blue hydrogen** is also produced from fossil fuels, typically natural gas through processes such as steam methane reforming, but incorporates carbon capture and storage (CCS) to reduce

the amount of CO_2 released into the atmosphere. Its effective carbon intensity depends strongly on the carbon capture rate, upstream methane emissions, and the additional energy requirements associated with the capture and storage processes.

- **Turquoise hydrogen** is produced through methane pyrolysis, in which methane is thermally decomposed into hydrogen and solid carbon rather than CO_2. Depending on the energy source used to provide the required process heat and on the management and long-term fate of the solid carbon produced, environmental performance may vary.
- **Pink hydrogen** generally refers to hydrogen produced through water electrolysis using electricity generated from nuclear energy. Since color terminology is not standardized, the terms *red* or *purple hydrogen* may also appear in the literature in association with nuclear-based hydrogen production pathways.
- **Brown or black hydrogen** is hydrogen produced through coal gasification, with the specific terminology depending on the type of coal used. In the absence of carbon capture and storage, these production pathways are characterized by high greenhouse gas emissions.

1.4 Power-to-X

The growing use of renewable energy sources is changing the operation of modern energy systems. Electricity generation from solar photovoltaic and wind technologies is inherently dependent on weather conditions and may therefore not always coincide with the temporal profile of energy demand. As renewable penetration increases, greater flexibility is required to integrate variable electricity generation efficiently and to extend the use of low-carbon energy beyond applications that can be directly electrified.

Within this context, the term *Power-to-X* (PtX) refers to a broad family of technologies and conversion pathways in which electrical energy is transformed into another energy carrier, fuel, chemical product, or useful form of energy. The "X" represents the final product or energy vector obtained from electricity and may include hydrogen, synthetic gases, liquid fuels, chemicals, or heat. When supplied by renewable or other low-carbon electricity, PtX technologies can contribute to transferring low-carbon energy from the power sector to applications in industry, transport, heating, and the chemical sector [13].

A central concept associated with Power-to-X is *sector coupling*, namely the integration of the electricity sector with other energy-consuming sectors through energy conversion and storage technologies. Rather than considering electricity, gas, heat, transport, and industrial systems as independent infrastructures, sector coupling enables energy to be exchanged and converted among them. In this way, PtX technologies can act as an interface between renewable electricity generation and applications that require fuels, chemical feedstocks, or high-temperature thermal energy [13].

1.4.1 Power-to-Hydrogen

Power-to-Hydrogen (PtH_2) is a particularly relevant PtX pathway because hydrogen can be used directly as an energy carrier or as an intermediate for the production of other fuels and chemicals. In a Power-to-Hydrogen system, electrical energy is supplied to an electrolyzer to split water into hydrogen and oxygen according to the overall reaction [12]:

$$2H_2O \rightarrow 2H_2 + O_2 \tag{1.1}$$

The resulting hydrogen stores part of the electrical energy supplied to the electrolysis process in chemical form. Its environmental performance depends primarily on the origin of the electricity used for electrolysis and on the emissions associated with the overall production chain. When electrolysis is supplied by renewable or other sufficiently low-carbon electricity, hydrogen can provide a pathway for transferring low-carbon energy to applications where the direct use of electricity may be technically difficult or unsuitable [10, 3].
Once produced, hydrogen can be used as an industrial feedstock or fuel, stored for later utilization, or further converted into other energy carriers and chemical products.

1.4.2 Hydrogen-Derived Power-to-X Pathways

Hydrogen produced through electrolysis can be further combined with other compounds to synthesize fuels and chemicals with characteristics suited to different applications [13].
In *Power-to-Methane* pathways, electrolytic hydrogen is combined with carbon dioxide through methanation to produce synthetic methane. The resulting gas can potentially benefit from existing natural-gas infrastructure, although its overall environmental performance depends strongly on the origin of the electricity and CO_2 used in the process.
Hydrogen and captured CO_2 can also be used to produce methanol and other synthetic hydrocarbons. These pathways are generally included within broader *Power-to-Liquid* or *e-fuel* concepts and are of particular interest for applications where high-energy-density liquid fuels remain difficult to replace through direct electrification.
Another important pathway is the production of ammonia from hydrogen and nitrogen. In this case, electrolytic hydrogen can be combined with nitrogen obtained from air and subsequently converted into ammonia, which is already extensively used as an industrial feedstock and is also being investigated as an energy carrier and fuel. The use of low-emission hydrogen can contribute to reducing emissions associated with conventional ammonia production.
Beyond hydrogen-derived pathways, electricity can also be converted directly into useful thermal energy through technologies such as heat pumps, electric boilers, and other electric heating systems. These applications are commonly described as *Power-to-Heat*. Unlike hydrogen-based pathways, they do not require the intermediate production of a chemical energy carrier and can provide a highly efficient option where direct electrification of heat demand is technically feasible.

1.4.3 Role of Power-to-X in Integrated Energy Systems

From an energy-system perspective, Power-to-X technologies can provide several complementary functions. Their contribution depends on the specific technology, system configuration, operating strategy, and timescale considered [13].

First, flexible PtX units can increase the utilization of renewable electricity by adjusting their operation according to electricity availability. During periods of high renewable generation, electricity can be converted into hydrogen or other products rather than being curtailed, provided that sufficient conversion and storage capacity is available.

Second, the conversion of electricity into storable energy carriers can provide temporal flexibility between energy production and final consumption. Hydrogen and hydrogen-derived fuels can be stored and subsequently used when required, allowing them to provide longer-duration energy storage than technologies mainly designed for short-term electrical balancing.

Third, PtX facilitates sector coupling by connecting the electricity sector with industrial, transport, and chemical applications through the production of hydrogen and other electricity-derived energy carriers.

These benefits must nevertheless be considered together with the energy losses introduced by successive conversion steps. Each transformation from electricity to hydrogen and, where applicable, from hydrogen to synthetic fuels or other products reduces the overall energy efficiency of the pathway. For this reason, direct electrification is generally preferable from an energy-efficiency perspective whenever it is technically and economically feasible, whereas PtX becomes particularly valuable where electricity must be stored over longer periods or converted into a molecular energy carrier for specific end uses [13].

1.4.4 Power-to-Hydrogen in Industrial Microgrids

Power-to-Hydrogen can play a particularly relevant role in industrial microgrids combining renewable generation, flexible electricity consumption, hydrogen storage, and industrial demand. In these systems, the electrolyzer represents a controllable electrical load whose operating profile can be coordinated with renewable electricity availability, electricity prices, hydrogen demand, and storage conditions [14, 15].

For example, hydrogen production can be increased during periods of high photovoltaic generation, allowing a larger fraction of locally generated renewable electricity to be utilized. When grid connection is available, electrolyzer operation may also be coordinated with electricity market conditions.

The hydrogen produced can subsequently be compressed and stored, decoupling the timing of hydrogen production from its final consumption. This flexibility is particularly valuable for industrial processes characterized by continuous or relatively inflexible energy demand, since variable renewable electricity can be converted into a storable fuel and supplied to the process according to its operational requirements.

The effective integration of these components requires coordinated energy management. Decisions concerning electrolyzer operation, renewable electricity utilization, grid imports, hydrogen storage charging and discharging, and final hydrogen consumption are strongly interconnected. Optimization-based energy management systems can be employed to determine economically efficient operating strategies while satisfying technical and operational constraints [14, 15].
The Power-to-Hydrogen configuration described above is directly connected to the system investigated in this thesis, where photovoltaic generation is integrated with a PEM electrolyzer, hydrogen compression and storage, grid electricity, and hydrogen consumption in a glass manufacturing process. The resulting system can therefore be interpreted as a Power-to-Hydrogen application within an industrial microgrid, in which an energy management system coordinates the interaction between electricity generation, hydrogen production and storage, and industrial energy demand.

1.5 Hydrogen in High-Temperature Industries

Hydrogen is considered a potential option for decarbonizing several energy-intensive industries requiring high-temperature process heat, including iron and steel, glass, cement, and ceramics. Its potential role, however, differs according to the characteristics of the industrial process and to whether hydrogen is required as a fuel, a chemical reactant, or both [16].
In iron and steel production, hydrogen can perform both an energetic and a chemical function. In addition to its potential use as a fuel for high-temperature heat generation, hydrogen can act as a reducing agent in direct reduced iron processes, replacing carbon-based reductants. In industries such as glass and ceramics, by contrast, hydrogen is primarily considered as a potential substitute for fossil fuels used to provide process heat. Depending on the existing equipment and process requirements, it may be introduced by partially blending it with natural gas or through more extensive fuel substitution[16, 4].
As discussed previously, the substitution of natural gas with hydrogen is not a direct one-to-one fuel replacement because of the different physical and combustion properties of the two fuels. In industrial furnaces, these differences can affect burner operation, flame characteristics, heat-transfer mechanisms, and temperature distribution, potentially requiring adaptations to fuel-supply systems, burners, control strategies, and safety measures [16, 17]. These aspects are particularly important in continuous production processes, where stable thermal conditions and reliable fuel supply are essential to maintain productivity and product quality.
Among these applications, glass manufacturing represents a particularly relevant case because of its high process temperatures, continuous furnace operation, dependence on fossil fuels, and stringent product-quality requirements.

1.5.1 Hydrogen Application in the Glass Industry

Glass manufacturing is an energy-intensive industrial process in which the melting stage represents the dominant thermal-energy requirement. Raw materials are heated in melting furnaces to

temperatures commonly reaching approximately 1400–1600 °C, depending on the type of glass and production process. Industrial furnaces generally operate continuously for extended periods, making process stability, fuel availability, and operational reliability essential requirements [4].
Several decarbonization options have been proposed for the glass sector, including improvements in energy efficiency, increased use of recycled glass or cullet, electric and hybrid melting, alternative low-carbon fuels, and carbon capture technologies. Among these options, hydrogen can partially or completely replace natural gas as a furnace fuel. Partial hydrogen–natural gas substitution is particularly relevant for existing facilities, as it may allow a progressive reduction in fossil-fuel consumption while retaining part of the existing furnace infrastructure [4, 17].
Hydrogen substitution can affect furnace operation because changes in flame characteristics and combustion-gas composition may influence temperature distribution, heat transfer to the glass melt, and NO_x formation [4, 17]. These aspects may require adaptations to burner design and combustion-control strategies. However, such furnace-level phenomena fall outside the scope of the present work, which focuses on the energy-system integration of hydrogen and the associated energy management strategies.
Beyond the furnace itself, the continuous nature of glass production requires a reliable hydrogen supply capable of meeting the process energy demand without compromising operational continuity. This represents an important challenge for the integration of renewable hydrogen in the glass industry and is among the aspects investigated within the European H2GLASS project, introduced in the following section.

1.6 The H2GLASS Project

H2GLASS is a European research and innovation project aimed at supporting the decarbonization of energy-intensive industries through the development and demonstration of hydrogen-based technologies. Funded under the Horizon Europe programme, the project investigates the integration of hydrogen into industrial glass production and the development of technologies supporting its implementation [5, 18].
The main objective of H2GLASS is to develop and validate the technological solutions required to enable the progressive replacement of fossil fuels with hydrogen in high-temperature industrial processes. Particular attention is devoted to the possibility of achieving high hydrogen shares, up to full hydrogen combustion, while maintaining the product quality, process efficiency, operational reliability, and safety requirements characteristic of industrial glass production.
Achieving this transition requires addressing several interconnected technological challenges. The project therefore investigates hydrogen combustion and hydrogen-ready burner technologies, the management of flame characteristics and pollutant emissions, the supply of hydrogen for industrial applications, and the integration of advanced monitoring and control systems. Digital technologies, including digital twins, are also considered to support process optimization, combustion control, predictive maintenance, and risk management [5].



Figure 1.1: H2GLASS project

Launched in 2023 and coordinated by SINTEF Energy Research, H2GLASS brings together partners from across Europe and combines research activities with industrial-scale demonstration [18]. The multidisciplinary consortium includes industrial companies, research institutions, universities, technology providers, and engineering organizations, combining expertise in glass manufacturing, hydrogen technologies, combustion systems, industrial engineering, energy systems, digitalization, and safety [5, 18].

A central characteristic of the project is its strong focus on industrial demonstration. The technologies and solutions developed within H2GLASS are intended to be validated under representative industrial operating conditions through several large-scale demonstrators. These activities primarily address the glass sector, while also considering the transferability of the developed hydrogen-based solutions to other energy-intensive industries characterized by high-temperature process requirements [5, 18].

The present thesis is closely connected to activities carried out within H2GLASS project. The case study builds on an industrial system configuration related to that investigated within H2GLASS, with part of the input data provided by an industrial partner participating in the project. Furthermore, the optimization-based energy management framework considered in this work originates from activities developed within H2GLASS.

1.7 Thesis Objectives

The work presented in this thesis was carried out at the Centre for Technological Innovation in Static Converters and Drives (CITCEA-UPC), Universitat Politècnica de Catalunya (UPC), within the context of the H2GLASS project.

The main objective of this thesis is to investigate the integration of hydrogen into the energy supply

of a continuous glass-melting furnace, with particular attention to the role and performance of the PEM electrolyzer within the overall industrial energy system. The study aims to assess the technical, energetic, economic, and environmental implications of partially replacing natural gas with hydrogen produced on site through water electrolysis, using photovoltaic generation and grid electricity together with hydrogen compression and storage.

A central objective is to represent PEM electrolyzer performance beyond a constant-efficiency approximation. A detailed electrochemical model is therefore adopted to account for the dependence of hydrogen production and conversion efficiency on the electrolyzer operating conditions. Particular attention is also given to PEM degradation, with the aim of quantifying its effect on hydrogen-production capability and electrical energy requirements over the considered operating period.

At system level, the thesis investigates how different hydrogen-substitution targets affect the operation and limitations of the integrated system, considering PEM utilization, hydrogen storage, electricity supply, and natural-gas fallback. The analysis also examines how the detailed electrochemical and degradation-dependent PEM representation can be integrated into an optimization-based Energy Management System (EMS), allowing electrolyzer performance to interact with system-level dispatch and with the coordinated use of the available energy resources.

Overall, the work aims to identify the main factors governing the feasibility and performance of hydrogen integration in the considered glass-industry application, including hydrogen-substitution level, electrolyzer capacity and operating conditions, PEM degradation, hydrogen-storage flexibility, energy-management decisions, and electricity-supply conditions.

2. Theoretical Background

This chapter provides the theoretical background required to describe the main technologies and concepts considered in the energy system investigated in this thesis. The principal water electrolysis technologies are introduced and compared, with particular attention to proton exchange membrane water electrolysis and the degradation phenomena affecting PEM electrolyzer performance. The chapter then presents the main principles and technologies associated with hydrogen storage and compression, together with the role of the glass furnace as the final industrial energy demand. Finally, the fundamental concepts of mathematical optimization and energy management systems are introduced, providing the theoretical basis for the rule-based and optimization-based energy management approaches considered in the following chapters.

2.1 Water Electrolysis Technologies

Water electrolyzers are electrochemical devices that convert electrical energy into chemical energy by splitting water into hydrogen and oxygen. When powered by renewable electricity, such as photovoltaic or wind energy, they enable the production of green hydrogen, which is considered a key energy carrier for the decarbonization of hard-to-abate sectors.
The overall electrochemical reaction is:

$$H_2O \rightarrow H_2 + \frac{1}{2}O_2 \tag{2.1}$$

Electrolyzers play a strategic role in integrated energy systems because they allow excess renewable electricity to be stored in the form of hydrogen, which can later be used as a fuel, chemical feedstock, or energy storage medium. This capability is particularly important in industrial applications characterized by continuous energy demand and variable renewable generation[19, 12].

2.1.1 Electrolyzer Categories

The four main water electrolysis technologies currently under development and commercialization are:

- Alkaline Electrolyzers (AE),
- Proton Exchange Membrane Electrolyzers (PEMEC),
- Solid Oxide Electrolysis Cells (SOEC),
- Anion Exchange Membrane Electrolyzers (AEM).

These technologies differ in terms of electrolyte type, operating temperature, current density, efficiency, dynamic response, and technological maturity [12, 19].

AE

Alkaline electrolyzers are the most mature and commercially established technology. They use a concentrated aqueous solution of potassium hydroxide (KOH) or sodium hydroxide (NaOH) as electrolyte, while hydroxide ions (OH^-) are the charge carriers.
The half-cell reactions are:

$$\text{Cathode:} \quad 2H_2O + 2e^- \rightarrow H_2 + 2OH^- \tag{2.2}$$

$$\text{Anode:} \quad 2OH^- \rightarrow \frac{1}{2}O_2 + H_2O + 2e^- \tag{2.3}$$

Alkaline systems are characterized by relatively low capital cost and long lifetime, but they exhibit lower current densities and slower dynamic response compared to PEM systems.

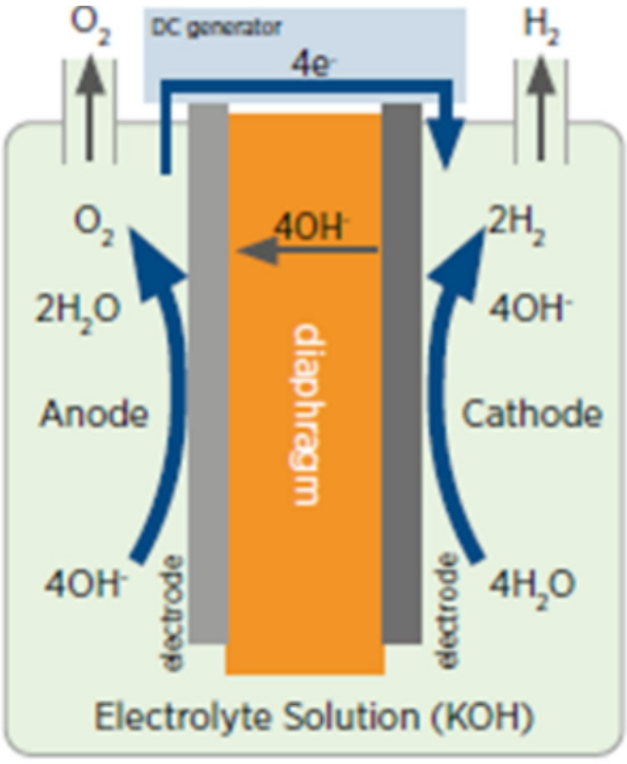


Figure 2.1: Schematic representation of an alkaline electrolyzer. Reproduced from [12].

PEMEC

Proton Exchange Membrane Electrolyzers use a solid polymer electrolyte membrane, typically based on perfluorosulfonic acid (PFSA), such as Nafion, which conducts protons (H^+) from the anode to the cathode.
The electrochemical reactions are:

$$\text{Anode:} \quad H_2O \rightarrow 2H^+ + \frac{1}{2}O_2 + 2e^- \tag{2.4}$$

$$\text{Cathode:} \quad 2H^+ + 2e^- \rightarrow H_2 \tag{2.5}$$

PEM electrolyzers typically operate at temperatures between 50 and 80 °C and can produce high-purity hydrogen at elevated pressure. Their main advantages are:

- high current density;
- compact design;
- rapid start-up and shut-down;
- excellent dynamic response;
- high hydrogen purity.

The main disadvantages are the higher capital cost and the use of noble metal catalysts, such as iridium and platinum.

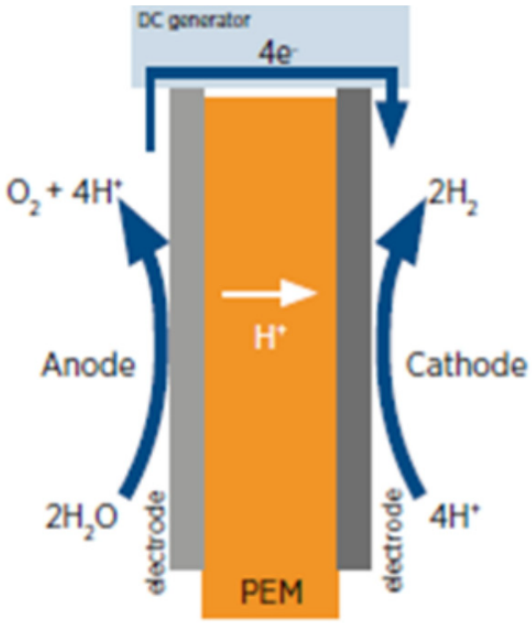


Figure 2.2: Schematic representation of a PEM electrolyzer. Reproduced from [12].

SOEC

Solid Oxide Electrolysis Cells operate at high temperatures, typically between 700 and 1000 °C, using a ceramic electrolyte that conducts oxygen ions (O^{2-}).
The half-cell reactions are:

$$\text{Cathode:} \quad H_2O + 2e^- \rightarrow H_2 + O^{2-} \tag{2.6}$$

$$\text{Anode:} \quad O^{2-} \rightarrow \frac{1}{2}O_2 + 2e^- \tag{2.7}$$

The high operating temperature reduces the electrical energy required for water splitting and allows very high efficiencies, especially when waste heat is available. However, thermal stresses and material degradation remain major challenges.

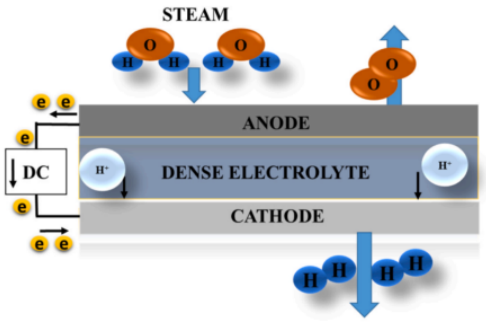


Figure 2.3: Schematic representation of a solid oxide electrolyzer. Reproduced from [20].

AEM

Among emerging technologies, Anion Exchange Membrane (AEM) electrolyzers are attracting increasing interest. These systems combine some advantages of alkaline and PEM technologies by using a polymer membrane that transports hydroxide ions.
The half-cell reactions are:

$$\text{Cathode:} \quad 2H_2O + 2e^- \rightarrow H_2 + 2OH^- \tag{2.8}$$

$$\text{Anode:} \quad 2OH^- \rightarrow H_2O + \frac{1}{2}O_2 + 2e^- \tag{2.9}$$

AEM electrolyzers can potentially use non-precious catalysts and dilute alkaline solutions, but their durability and membrane stability still require significant improvement.

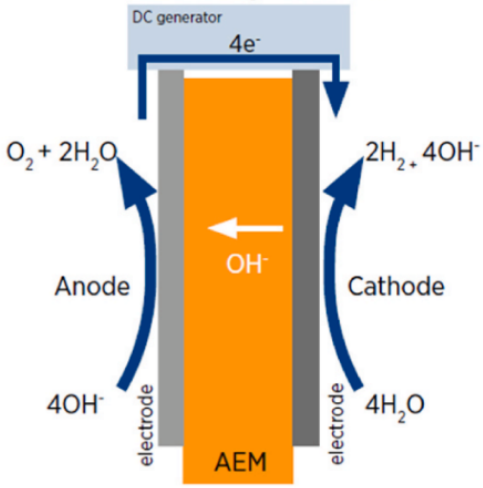


Figure 2.4: Schematic representation of an AEM electrolyzer. Reproduced from [12].

2.1.2 Comparison of Electrolyzer Technologies

The main characteristics of the considered electrolyzer technologies are compared in Table 2.1 [12, 21].

Table 2.1: Comparison of the main water electrolysis technologies.

Parameter	AE	PEMEC	SOEC	AEM
Electrolyte	KOH/NaOH	Polymer membrane	Solid oxide	KOH/NaOH
Operating temperature [°C]	70–90	50–80	700–850	40–60
Nominal current density [A/cm^2]	0.2–0.8	1–2	0.3–1	0.2–2
Cell pressure [bar]	< 30	< 70	< 10	< 35
Hydrogen purity [%]	99.5–99.9998	99.9–99.9999	99.9	99.9–99.9999
Development status	Mature	Commercialized	R&D	R&D

Among these technologies, PEMEC is particularly suitable for renewable-powered industrial microgrids because of its fast response, compact design, and ability to operate efficiently under highly variable electrical input. For these reasons, PEM water electrolysis is selected as the reference hydrogen production technology for the energy system investigated in this thesis.

2.2 PEM Electrolyzer Degradation

Despite the favorable characteristics of proton exchange membrane water electrolysis, long-term durability remains one of the main challenges associated with this technology. During operation, the different components of a PEM electrolyzer are exposed to demanding electrochemical, thermal, and mechanical conditions that progressively affect their properties and performance. These degradation phenomena can lead to an increase in cell voltage for a given current density, a reduction in efficiency, and ultimately a decrease in the useful lifetime of the electrolyzer [22].

The analysis of degradation is particularly relevant when PEM electrolyzers are coupled with variable renewable energy sources, as variations in operating power, start-up and shut-down events, and partial-load operation may influence the ageing behaviour of the system[22].

2.2.1 Main Degradation Mechanisms

Degradation in PEM water electrolyzers does not result from a single phenomenon but from the combined ageing of several components of the electrochemical cell. The main mechanisms involve the electrocatalysts, the proton exchange membrane, the porous transport layers, and other structural and interfacial components of the cell [22].

One of the most critical regions is the anode, where the oxygen evolution reaction takes place under highly oxidative and acidic conditions. These severe operating conditions require highly stable electrocatalytic materials, with iridium-based catalysts being widely used because of their activity and corrosion resistance. Nevertheless, catalyst degradation may occur through mechanisms such as dissolution, particle growth, agglomeration, and changes in catalyst morphology. These processes can progressively reduce the electrochemically active surface area and increase the activation losses associated with the oxygen evolution reaction [22].

The proton exchange membrane is another component directly affected by ageing. Its function is to conduct protons between the electrodes while maintaining electrical insulation and limiting the mixing of hydrogen and oxygen. During long-term operation, the membrane may undergo chemical and mechanical degradation. Chemical degradation can alter the polymer structure and reduce membrane integrity, while repeated hydration and dehydration cycles can generate mechanical stresses, dimensional changes, and eventually the formation of defects. Membrane thinning or damage may increase gas crossover between the anode and cathode compartments, with negative consequences for efficiency, performance, and operational safety [22, 23].

Degradation can also affect the porous transport layers and other electrically conductive components of the cell. Surface oxidation, corrosion, changes in porosity, and increasing interfacial contact resistance may progressively deteriorate electrical and mass transport within the electrolyzer. These phenomena can increase ohmic losses and may negatively affect water distribution and gas removal from the electrode regions[22].

The different degradation mechanisms are strongly interconnected. Changes occurring in one component may alter the operating conditions of adjacent components and accelerate additional ageing processes. Consequently, the overall degradation of a PEM electrolyzer should be regarded as the result of multiple interacting electrochemical, chemical, thermal, and mechanical phenomena rather than as the deterioration of a single component.

2.2.2 Influence of Operating Conditions

The degradation rate of a PEM electrolyzer depends strongly on its operating conditions. Current density, temperature, pressure, water quality, operating profile, and the frequency of transient events can all influence the ageing behaviour of the system [22].

Operation at high current density increases hydrogen production but also exposes the cell components to more demanding electrochemical conditions. Higher current densities can increase overpotentials, heat generation, and local stresses within the membrane-electrode assembly, potentially accelerating some degradation mechanisms.

Temperature also plays an important role. Increasing operating temperature generally improves reaction kinetics and can reduce certain electrochemical losses. However, excessively high temperatures or repeated thermal cycling may accelerate material degradation and impose additional mechanical stresses on cell components. A compromise is therefore required between improved electrochemical performance and long-term durability.

Dynamic operation represents an additional consideration when PEM electrolyzers are integrated with variable renewable generation. Rapid variations in electrical input, repeated start-up and shut-down events, and changes in operating conditions may introduce transient electrochemical and mechanical stresses. Their influence on degradation depends on the specific operating profile and system design, making durability an important consideration in the operation of renewable-powered PEM electrolyzers.

Water quality is also essential for maintaining long-term performance. Impurities entering the electrolyzer may contaminate the membrane or catalyst layers and negatively affect electrochemical activity and ionic conductivity. PEM electrolyzers therefore generally require high-purity water and appropriate water treatment systems [22].

2.2.3 Effect of Degradation on Electrolyzer Performance

From a system-level perspective, one of the most relevant consequences of degradation is the progressive deterioration of the relationship between electrical input and hydrogen production. As the electrochemical components age, additional voltage may be required to maintain the same operating current.

The cell voltage can generally be expressed as the sum of the reversible thermodynamic voltage and the different irreversible voltage losses[23]:

$$V_{\text{cell}} = E_{\text{rev}} + \eta_{\text{act}} + \eta_{\text{ohm}} + \eta_{\text{conc}}, \tag{2.10}$$

where E_{rev} is the reversible cell voltage, while η_{act}, η_{ohm}, and η_{conc} represent activation, ohmic, and concentration overvoltages, respectively.

As discussed above, degradation can affect one or more of these contributions. Catalyst ageing can increase activation losses, membrane deterioration and increasing contact resistance can contribute to higher ohmic losses, while changes in porous structures and mass-transport characteristics may influence concentration-related losses. As a result, the polarization characteristics of the electrolyzer progressively change during its operating lifetime[22].

For a given current density, an increase in cell voltage corresponds to a higher electrical power requirement. Since hydrogen production is primarily related to the electrical current through Faraday's law, more electrical energy may be required to produce the same amount of hydrogen as

degradation progresses. As a result, the electrical efficiency of the electrolyzer tends to decrease over its operating lifetime[23, 22].
Over the lifetime of an electrolyzer, performance degradation can generally be discussed in terms of Beginning-of-Life (BOL) and End-of-Life (EOL) conditions, representing the initial and final stages of component performance, respectively. The progressive deterioration between these conditions is particularly relevant at system level, since a larger electrical energy input may be required to produce a given amount of hydrogen as degradation progresses. The degradation model adopted in this thesis does not aim to reproduce the complete evolution from BOL to EOL; instead, it represents the performance evolution over the investigated operating period using degradation-dependent efficiency data, as described in Chapter 3.4.

2.3 Hydrogen Storage

Hydrogen storage is a fundamental component of integrated hydrogen energy systems, as it allows hydrogen production to be temporally decoupled from its final utilization. This function is particularly important when hydrogen is produced through water electrolysis powered by variable renewable energy sources. In such systems, electricity availability may not coincide with the hydrogen demand profile, especially when the final user is an industrial process characterized by continuous or relatively inflexible operation.
Storage therefore provides an important source of operational flexibility. Hydrogen produced during periods of high renewable electricity availability can be accumulated and subsequently used when renewable generation is insufficient or when hydrogen demand exceeds instantaneous production. In this way, hydrogen storage acts as a buffer between the electricity and hydrogen subsystems and facilitates the integration of variable renewable generation with continuous industrial energy demand.
The selection of an appropriate storage technology depends on several factors, including the amount of hydrogen to be stored, storage duration, required charging and discharging rates, operating conditions, available space, safety requirements, and economic considerations. Different storage technologies may therefore be suitable depending on the scale and characteristics of the application [24, 25].

2.3.1 Hydrogen Storage Technologies

Hydrogen storage technologies can generally be distinguished according to the physical or chemical form in which hydrogen is stored. The main alternatives include compressed gaseous hydrogen, liquid hydrogen, and material-based storage systems. Additional options, including underground geological storage and hydrogen carriers, may become particularly relevant for large-scale or long-duration applications [24, 25].

Compressed Gaseous Hydrogen

Compressed gaseous hydrogen is one of the most established and commercially available hydrogen storage technologies. In this approach, gaseous hydrogen is compressed and stored in pressure vessels specifically designed for hydrogen service.

Depending on the application, storage pressures can range from relatively low pressures to several hundred bar, with pressures of 350 and 700 bar commonly adopted in high-pressure hydrogen storage applications. Increasing the storage pressure increases hydrogen density and therefore reduces the volume required to store a given mass. However, higher pressures also increase compression energy requirements and impose more demanding requirements on pressure vessels and auxiliary components [25].

Pressure vessels used for compressed hydrogen storage can be manufactured using different materials and structural configurations. Conventional metallic vessels provide high mechanical strength but are generally relatively heavy, while composite vessels can reduce vessel weight but typically involve greater manufacturing complexity and cost.

Compressed gaseous storage is particularly attractive for stationary applications in which technological maturity, operational flexibility, and relatively simple system integration are important. Its suitability however depends strongly on the required storage capacity and duration, and alternative technologies may become more appropriate as the scale of hydrogen storage increases [24].

Liquid Hydrogen

Hydrogen can also be stored in liquid form by cooling it below its boiling temperature, approximately $-253\,^{\circ}\mathrm{C}$ at atmospheric pressure. Liquefaction substantially increases hydrogen density compared with storage as a gas under ambient conditions, making liquid hydrogen attractive when high volumetric storage density is required [24, 25].

However, cryogenic storage introduces significant technical and energetic challenges. Hydrogen liquefaction requires considerable energy, while storage vessels require advanced thermal insulation to minimize heat transfer from the surroundings. Despite insulation, heat ingress can cause gradual evaporation of the stored hydrogen, resulting in *boil-off* and requiring appropriate pressure-management strategies.

For these reasons, liquid hydrogen storage is particularly relevant when high volumetric density is a priority, including some large-scale storage and transportation applications. For stationary buffering applications where storage density is less critical, compressed gaseous storage may provide a technically simpler solution.

Material-Based and Chemical Storage

An alternative approach consists of storing hydrogen through physical or chemical interactions with other materials. These technologies include metal hydrides, adsorption-based systems, chemical hydrides, and hydrogen carriers.

Metal hydrides store hydrogen through reversible interactions between hydrogen and metallic materials or alloys. These systems can achieve high volumetric hydrogen densities and may operate at lower pressures than conventional high-pressure compressed storage. Yet, their practical performance depends strongly on the properties of the storage material, including gravimetric capacity, thermodynamics, reaction kinetics, thermal-management requirements, durability, and cost [26].
Adsorption-based systems use porous materials with high specific surface areas to physically adsorb hydrogen. Their storage performance depends strongly on material characteristics as well as operating pressure and temperature, and many advanced materials remain under research and development.
Hydrogen can also be stored indirectly using chemical carriers. Examples include ammonia and liquid organic hydrogen carriers (LOHCs), in which hydrogen is chemically incorporated into another compound and subsequently recovered when required. Such approaches may offer advantages for large-scale storage or transportation but require additional conversion processes and infrastructure, introducing further energy losses and system complexity [24].
Another important solution for very large quantities of hydrogen is underground geological storage, particularly in salt caverns. This approach can provide very large storage capacities and is particularly relevant for long-duration or seasonal storage. Its applicability is closely related to the availability of suitable geological formations and differs substantially from above-ground pressurized storage systems used for smaller stationary applications [24].
Among the available storage technologies, compressed gaseous hydrogen storage is adopted in the system investigated in this thesis due to its technological maturity, operational flexibility, and suitability for stationary applications. The specific storage configuration and its mathematical representation are presented in Chapter 3.

2.4 Hydrogen Compression

Hydrogen compression represents an important auxiliary process in hydrogen production and storage systems. Hydrogen produced by an electrolyzer may need to be compressed to a higher pressure before being introduced into a pressurized storage system. The compression process requires additional electrical energy and therefore contributes to the overall energy consumption and efficiency of the hydrogen production chain [27].
The energy required for compression depends primarily on the hydrogen mass flow rate, inlet and outlet pressures, gas temperature, compressor configuration, and compression efficiency. When large pressure ratios are required, compression can be divided into multiple stages. Intermediate cooling between successive compression stages reduces the gas temperature and can decrease the overall compression work compared with an equivalent single-stage compression process [27, 28].
From an energy-system perspective, the compressor therefore represents an auxiliary electrical load and must be considered when evaluating the net electrical energy required to produce and store a given amount of hydrogen.
In the system investigated in this thesis, hydrogen produced by the PEM electrolyzer is compressed

before entering the pressurized storage system. The methodology adopted for modelling hydrogen compression, including the compressor configuration, operating pressures, efficiency assumptions, and calculation of compression power is described in Chapter 3.

2.5 Fundamentals of Optimization and Energy Management Systems

The increasing integration of renewable energy sources, energy conversion technologies, storage systems, and industrial loads has made the operation of modern energy systems increasingly complex. Different components must interact while satisfying energy balances, technical limitations, and operational requirements under conditions that may vary over time.
Energy management provides a framework for coordinating the operation of the different components of an integrated energy system, while mathematical optimization offers systematic methods for determining operating decisions according to predefined objectives and constraints. These concepts are particularly relevant in systems characterized by multiple interconnected energy flows and storage technologies, where decisions concerning one component may directly influence the operation of the others [29, 30].

2.5.1 Mathematical Optimization

Optimization is the mathematical process of identifying the best solution among a set of feasible alternatives according to a specified objective. In engineering applications, it provides a systematic framework for determining operating or design decisions while accounting for the physical, technical, and operational constraints of the system [29].
A generic constrained optimization problem can be expressed as:

$$\min_{\mathbf{x}} \; f(\mathbf{x}) \tag{2.11}$$

subject to:

$$g_i(\mathbf{x}) \leq 0, \qquad i = 1, \ldots, m, \tag{2.12}$$

$$h_j(\mathbf{x}) = 0, \qquad j = 1, \ldots, p, \tag{2.13}$$

where $\mathbf{x}$ represents the vector of *decision variables*, $f(\mathbf{x})$ is the *objective function*, while $g_i(\mathbf{x})$ and $h_j(\mathbf{x})$ represent inequality and equality constraints, respectively [31, 32].
The decision variables represent the quantities whose values can be determined by the optimization algorithm. In energy-system applications, they may include power flows, equipment operating points, storage charging and discharging rates, energy imports or exports, and other controllable quantities.

The objective function defines the mathematical criterion according to which alternative feasible solutions are evaluated. Depending on the purpose of the analysis, optimization may be used to minimize quantities such as operating costs, energy consumption, fuel consumption, or environmental impact, or to maximize efficiency, renewable energy utilization, or other performance indicators.
Constraints define the feasible operating region of the problem. Equality constraints are commonly used to represent physical relationships such as energy and mass balances, whereas inequality constraints can describe equipment capacities, operating limits, storage boundaries, minimum requirements, and other technical or operational restrictions.
The solution of an optimization problem thus identifies the values of the decision variables that provide the best value of the objective function while simultaneously satisfying all imposed constraints.

2.5.2 Main Classes of Optimization Problems

Optimization problems can be classified according to the mathematical characteristics of their objective function, constraints, and decision variables. In Linear Programming (LP), the objective function and constraints are linear and the decision variables are continuous. When integer or binary variables are introduced while preserving linear relationships, the formulation becomes a Mixed-Integer Linear Programming (MILP) problem. Nonlinear relationships lead instead to Nonlinear Programming (NLP), or Mixed-Integer Nonlinear Programming (MINLP) when both continuous and integer variables are present [33, 32].
The mathematical formulation involves a compromise between modelling detail and computational complexity. Detailed component models may contain nonlinear relationships that cannot always be incorporated directly into an optimization framework without increasing computational requirements. Simplified representations, approximations, or iterative procedures can therefore be adopted to preserve relevant physical behaviour while maintaining computational tractability [31].

2.5.3 Energy Management Systems

An Energy Management System (EMS) coordinates the operation of the different components of an energy system according to technical and operational requirements. Its decisions may account for factors such as energy generation and demand, storage conditions, equipment operating limits, and energy prices [30].
Different approaches can be adopted to implement an EMS. Rule-based strategies determine system operation according to predefined rules and priorities. Their behaviour is then directly determined by the operating logic established in advance. Optimization-based strategies, instead, determine the operating decisions by solving a mathematical optimization problem defined through decision variables, an objective function, and a set of constraints.
For systems whose operation is interconnected over time, optimization can be performed over a sequence of future time intervals rather than independently at each instant. This is particularly relevant in the presence of storage, since decisions taken at one time influence the energy available

in subsequent periods. In a rolling- or receding-horizon approach, the optimization problem is repeatedly solved over a moving time horizon as system operation progresses [34].
In this thesis, both rule-based and optimization-based energy-management approaches are considered. Their specific implementation and mathematical formulation are presented in Chapter 3.

3. Methodology

This chapter presents the methodological framework adopted to investigate the integration of hydrogen production and utilization within a grid-connected industrial energy system for glass manufacturing. The analysis combines component-level modelling with energy-management strategies to evaluate the operation of the overall system under time-varying operating conditions.
The overall system configuration and the interactions among its main components are first introduced, together with the input data and main modelling assumptions. The component models are then presented according to the implementation adopted in the first, rule-based stage of the analysis, which provides the detailed physical formulation of the main system components.
Particular attention is devoted to the Proton Exchange Membrane (PEM) electrolyzer, which represents the hydrogen production unit of the system. A detailed electrochemical model is employed to determine its operating behaviour, hydrogen production, and conversion efficiency as a function of the operating conditions. A degradation model is additionally introduced to account for the progressive evolution of electrolyzer performance during operation.
The analysis is subsequently developed in two stages. In the first stage, a rule-based energy-management strategy is used to investigate the operation of the considered system configuration under progressively increasing hydrogen-substitution levels. The operation of the different components is coordinated according to predefined control rules, allowing the technical response and limitations of the integrated system to be assessed as the hydrogen contribution is increased.
In the second stage, the detailed PEM electrochemical and degradation models developed in this work are integrated into an existing optimization-based Energy Management System (EMS). The optimization framework is formulated for the same industrial application, while including additional system-level energy flows, operating constraints, and degrees of freedom. The original constant-efficiency representation of the PEM electrolyzer is replaced through an iterative coupling procedure, allowing its operating-point- and degradation-dependent performance to influence the optimized system operation.
Where possible, the main physical parameters are maintained consistently between the two frameworks, while differences in modelling formulation are retained according to the specific objectives of each analysis. Both are performed over an annual simulation horizon in order to capture seasonal variations in energy demand, photovoltaic generation, hydrogen production and storage, and grid electricity use.

3.1 System Description

The system investigated in this work consists of a grid-connected industrial microgrid in which on-site hydrogen production and renewable electricity are integrated to investigate the partial decarbonization of a continuous glass melting furnace. The proposed configuration combines photo-

voltaic electricity generation, a PEM electrolyzer, hydrogen compression and storage, the existing natural-gas supply, and the external electrical grid.
A schematic representation of the proposed system is shown in Figure 3.1.

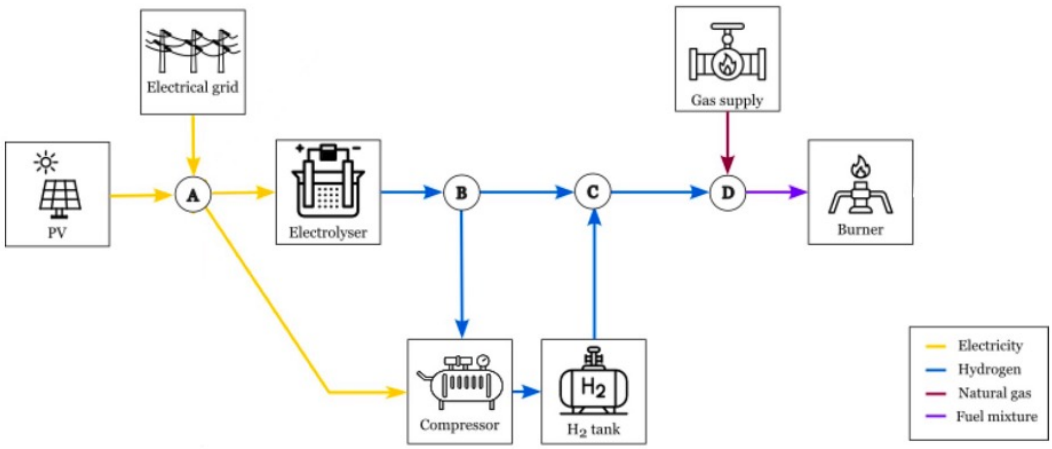


Figure 3.1: Schematic representation of the grid-connected industrial microgrid considered in this work.

The photovoltaic (PV) system provides renewable electricity for hydrogen production. The generated electricity is supplied to the Proton Exchange Membrane (PEM) electrolyzer, where electrical energy is converted into chemical energy in the form of hydrogen through water electrolysis. Since photovoltaic generation is variable over time and the installed PV capacity is fixed according to the existing industrial-site configuration, the available renewable generation may not always be sufficient to meet the electrical demand of the hydrogen production system. The system is therefore also connected to the public electrical grid, which provides an additional source of electricity when required.
The hydrogen produced by the PEM electrolyzer can be supplied directly to the glass furnace or directed towards the storage system. Before entering the pressurized storage tank, hydrogen is compressed by a multi-stage compressor to the required storage pressure. The storage system introduces temporal flexibility by decoupling hydrogen production from hydrogen consumption: hydrogen can be accumulated when production exceeds immediate requirements and subsequently withdrawn when needed.
The glass furnace represents the final energy consumer considered in the system and is characterized by a continuous thermal demand. Natural gas represents the conventional furnace fuel, while hydrogen produced on site is introduced as an alternative energy carrier to reduce natural-gas consumption.

3.2 Input Data and Main Assumptions

3.2.1 Input Data and Pre-processing

The simulation framework is driven by time-dependent input data describing the operation of the industrial energy system over the considered simulation period. All original input time series are provided with a temporal resolution of 15 minutes. The temporal treatment of these data depends on the adopted simulation framework and is specified in the corresponding sections.
The input dataset includes:

- the thermal load profile of the glass furnace;
- the photovoltaic (PV) energy production profile;
- the electricity price profile;
- the natural gas price profile.

These input profiles are used as the common basis for the two energy-management frameworks considered in this work. In addition, the optimization-based EMS includes an industrial electrical load and an additional furnace load used in the definition of the total furnace energy demand. Within this formulation, part of the furnace demand can also be supplied through direct electric heating. These features are not included in the rule-based formulation.
The furnace thermal load is provided in per-unit form and converted into thermal energy using a reference energy value according to

$$E_{\mathrm{th},k} = PU_k E_{\mathrm{base}}, \tag{3.1}$$

where PU_k is the normalized furnace load at timestep k and E_{base} is the reference thermal energy associated with one 15-minute interval, defined as

$$E_{\mathrm{base}} = 1000\ \mathrm{kWh}. \tag{3.2}$$

The resulting quantity therefore represents the thermal energy required by the furnace during each simulation interval.
Since the simulation frameworks operate on power quantities, the energy values provided in the original input dataset are converted into average power values over the corresponding time interval. For the original 15-minute temporal resolution, the timestep is defined as

$$\Delta t = 900\ \mathrm{s} = 0.25\ \mathrm{h}. \tag{3.3}$$

The average power associated with the energy quantity E_k over timestep k is therefore calculated as

$$P_k = \frac{E_k}{\Delta t} \tag{3.4}$$

where Δt is expressed in hours when E_k is given in kWh and P_k in kW. For $\Delta t = 0.25$ h, this relation becomes

$$P_k = 4E_k. \tag{3.5}$$

Similarly, electricity and natural-gas prices, originally provided in EUR/MWh, are converted into EUR/kWh for use in the economic calculations.

3.2.2 Main Modelling Assumptions

The integrated energy system is represented through a set of modelling assumptions introduced to define the system boundaries and maintain an appropriate balance between physical detail and computational complexity. The main assumptions adopted throughout the simulation framework are summarized below.

- Each simulation interval is treated as a quasi-steady operating condition. Time-dependent input variables and calculated power flows are represented by their average values over the corresponding timestep.
- The glass furnace is treated as a continuous thermal load whose demand is imposed externally through the input profile. Its internal processes of thermo-fluid-dynamic, combustion, and heat-transfer are not explicitly modeled. Instead, the furnace is represented through its energy demand, which is satisfied by the energy carriers considered in each system configuration.
- Photovoltaic generation is treated as an externally imposed time-dependent input. The physical behaviour of the PV system, including solar irradiance conversion, module temperature effects, inverter operation, and electrical conversion losses, is not explicitly modelled.
- The electrical grid is assumed to be available as an external source of electricity whenever additional electrical energy is required by the system. The detailed physical behaviour and capacity constraints of the external electrical network are outside the system boundaries.
- Hydrogen storage is represented through an energy-based lumped model. The stored hydrogen content is tracked through its equivalent LHV energy content rather than through a detailed thermodynamic description of pressure, temperature, and real-gas behaviour inside the vessel.
- Hydrogen leakage and storage losses are neglected. The stored hydrogen content therefore changes only as a result of charging and discharging, according to the corresponding energy balance and the imposed storage limits.

These assumptions define the common modelling framework adopted throughout the study. Component- and strategy-specific assumptions and parameters are introduced separately in the corresponding sections.

3.3 System Component Models

This section presents the mathematical models adopted to represent the main components of the integrated energy system in the rule-based implementation. The modelling approach is modular, with the glass furnace demand, PEM electrolyzer, hydrogen compression system, and hydrogen storage system represented separately and subsequently coupled within the overall simulation framework.
The PEM electrolyzer is described through a detailed electrochemical and performance model, whereas the remaining components are represented through simplified energy or thermodynamic formulations consistent with the system-level scope of the study. The same PEM electrochemical formulation is adopted in both energy-management frameworks. In addition, the main physical parameters of the system components are aligned, where possible, to maintain consistency in the physical representation of the industrial system. Nevertheless, some components and operating constraints are represented differently due to the specific structure and requirements of each energy-management framework. These differences are described in the corresponding sections.
The mathematical formulation of each system component is presented in this chapter, whereas the specific numerical parameters adopted for the case study are reported in Chapter 4, *Case Study and Results*.

3.3.1 Glass Furnace Energy Demand

The glass furnace represents the final industrial energy consumer considered in the system. According to the assumptions introduced in the previous section, it is represented through an externally imposed thermal energy demand that must be continuously satisfied.
Following the input pre-processing procedure described in the previous section, the corresponding average thermal power demand at timestep k is denoted by $P_{\mathrm{th},k}$.
In the rule-based implementation, the total furnace thermal demand is divided into two target contributions: one associated with hydrogen and the other with natural gas. A prescribed hydrogen energy share, denoted by $x_{\mathrm{H_2}}$, defines the fraction of the total thermal demand that has to be supplied by hydrogen.
The target hydrogen contribution is therefore calculated as

$$P_{\mathrm{H_2,target},k} = x_{\mathrm{H_2}} P_{\mathrm{th},k}, \tag{3.6}$$

while the complementary natural gas contribution is

$$P_{\mathrm{NG,target},k} = \left(1 - x_{\mathrm{H_2}}\right) P_{\mathrm{th},k}. \tag{3.7}$$

The hydrogen share $x_{\mathrm{H_2}}$ is defined on an energy basis and therefore represents the fraction of the total furnace energy demand assigned to hydrogen, rather than a mass- or volume-based fuel blending ratio. This share can be varied between simulation scenarios to investigate different levels of natural gas substitution. The imposed furnace load profile therefore remains unchanged, while the target

contributions assigned to hydrogen and natural gas vary according to the selected scenario.
Once the target hydrogen thermal contribution has been determined, the corresponding hydrogen mass flow rate required by the furnace is calculated from the lower heating value of hydrogen:

$$\dot{m}_{\mathrm{H_2,target},k} = \frac{P_{\mathrm{H_2,target},k}}{\eta_{\mathrm{bur}}\, LHV_{\mathrm{H_2}}\, 3600}, \tag{3.8}$$

where $\dot{m}_{\mathrm{H_2,target},k}$ is expressed in $\mathrm{kg\,s^{-1}}$, $LHV_{\mathrm{H_2}} = 33.33\ \mathrm{kWh\,kg^{-1}}$ is the lower heating value of hydrogen, and η_{bur} represents the thermal efficiency associated with fuel utilization in the furnace burner.
For a given hydrogen mass flow rate actually supplied to the furnace, the corresponding useful thermal contribution is calculated as

$$P_{\mathrm{H_2,supplied},k} = \eta_{\mathrm{bur}}\, \dot{m}_{\mathrm{H_2,supplied},k}\, LHV_{\mathrm{H_2}} 3600. \tag{3.9}$$

The difference between the target and the actual hydrogen contribution defines the unmet hydrogen energy demand:

$$P_{\mathrm{H_2,unmet},k} = \max\left(0,\ P_{\mathrm{H_2,target},k} - P_{\mathrm{H_2,supplied},k}\right). \tag{3.10}$$

If the prescribed hydrogen contribution cannot be fully supplied, the unmet portion is compensated by additional natural gas in order to maintain the total furnace thermal demand. The resulting natural gas contribution is therefore expressed as

$$P_{\mathrm{NG,actual},k} = P_{\mathrm{NG,target},k} + P_{\mathrm{H_2,unmet},k}. \tag{3.11}$$

The corresponding natural-gas fuel input required to provide this useful thermal contribution is calculated as

$$P_{\mathrm{NG,fuel},k} = \frac{P_{\mathrm{NG,actual},k}}{\eta_{\mathrm{bur}}}, \tag{3.12}$$

where $P_{\mathrm{NG,fuel},k}$ represents the LHV-based natural-gas energy input to the burner.
Accordingly, the total thermal demand supplied to the furnace is

$$P_{\mathrm{furnace,supplied},k} = P_{\mathrm{H_2,supplied},k} + P_{\mathrm{NG,actual},k}, \tag{3.13}$$

Within the rule-based framework, the compensation of any unmet hydrogen contribution by natural gas ensures that the imposed furnace thermal demand is continuously satisfied.

3.3.2 PEM Electrolyzer Model

The Proton Exchange Membrane (PEM) electrolyzer represents the core conversion component of the hydrogen production system. Its purpose is to convert the electrical power supplied to the stack into hydrogen through water electrolysis.

A detailed electrochemical model is adopted to characterize the nonlinear relationship between current density, cell voltage, stack power, hydrogen production, and conversion efficiency. The electrolyzer is represented at both cell and stack level: the electrochemical behaviour is first evaluated for a single cell as a function of current density, while the overall stack performance is subsequently obtained from the number of cells and their active area.
The PEM electrolyzer model consists of a forward electrochemical formulation coupled with an inverse numerical procedure. The forward model evaluates, for a given current density, the corresponding cell voltage, stack power, hydrogen production rate, and conversion efficiencies.
When the electrolyzer operating point is prescribed in terms of the electrical power supplied to the stack rather than the current density, an inverse numerical procedure is employed to determine the current density corresponding to the given stack-power setpoint. Once the current density is identified, the forward electrochemical model is used to evaluate the corresponding electrochemical and performance quantities.

Electrochemical and Performance Model

The operating voltage of a PEM electrolyzer cell is determined by the reversible thermodynamic voltage and by the additional voltage losses associated with electrochemical kinetics, ohmic resistance, and mass transport. The resulting cell voltage can therefore be expressed as:

$$V_{\text{cell}} = E_{\text{rev}} + \eta_{\text{act,a}} + \eta_{\text{act,c}} + \eta_{\text{ohm}} + \eta_{\text{conc,a}} + \eta_{\text{conc,c}}, \tag{3.14}$$

where E_{rev} is the reversible cell voltage, η_{act} represents the activation overpotential, η_{ohm} the ohmic overpotential, and η_{conc} the concentration overpotential. The subscripts a and c refer respectively to the anodic and cathodic contributions.

Reversible Voltage

The reversible voltage represents the minimum theoretical electrical potential required to drive the water electrolysis reaction under reversible conditions.
The standard reversible voltage is corrected as a function of the operating temperature according to:

$$E^0(T) = 1.229 - 0.00085\,(T - 298.15)\,, \tag{3.15}$$

where T is the cell operating temperature expressed in kelvin.
The effect of the hydrogen and oxygen operating pressures is subsequently included through the Nernst equation:

$$E_{\text{rev}} = E^0(T) + \frac{RT}{2F} \ln\left[\left(\frac{p_{\text{H}_2}}{p_0}\right)\left(\frac{p_{\text{O}_2}}{p_0}\right)^{1/2}\right], \tag{3.16}$$

where R is the universal gas constant, F is Faraday's constant, p_{H_2} and p_{O_2} are the hydrogen and oxygen partial pressures, and $p_0 = 1$ bar is the reference pressure.

Activation Overpotential

Activation losses account for the additional voltage required to overcome the kinetic barriers associated with the electrochemical reactions occurring at the electrodes.

For both the anode and cathode, the activation overpotential is described through an inverse hyperbolic sine formulation derived from the Butler–Volmer relationship:

$$\eta_{\text{act}} = \frac{RT}{\alpha n F} \operatorname{asinh}\left(\frac{i}{2i_0}\right), \tag{3.17}$$

where i is the current density, i_0 is the exchange current density, α is the charge transfer coefficient, and n is the number of electrons involved in the corresponding electrode reaction.

The anodic and cathodic activation losses are evaluated separately using their respective electrochemical parameters.

Ohmic Overpotential

Ohmic losses mainly arise from proton transport through the polymer electrolyte membrane and from additional electrical contact resistances within the cell.

The proton conductivity of the Nafion membrane is modelled as:

$$\kappa = (0.005139\lambda - 0.00326) \exp\left[1268\left(\frac{1}{303} - \frac{1}{T}\right)\right], \tag{3.18}$$

where λ represents the membrane water content.

The area-specific membrane resistance is then calculated as:

$$R_{\text{mem}} = \frac{t_{\text{mem}}}{\kappa}, \tag{3.19}$$

where t_{mem} is the membrane thickness.

An additional contact resistance is included, leading to the total area-specific resistance ASR, expressed in $\Omega\,\text{cm}^2$:

$$ASR = R_{\text{mem}} + R_{\text{contact}}. \tag{3.20}$$

The resulting ohmic overpotential is therefore:

$$\eta_{\text{ohm}} = i\, ASR. \tag{3.21}$$

Concentration Overpotential

At high current densities, mass transport limitations may result in additional voltage losses as the operating current approaches the limiting current density.

These losses are represented as:

$$\eta_{\text{conc}} = -\frac{RT}{nF} \ln\left(1 - \frac{i}{i_{\text{lim}}}\right), \tag{3.22}$$

where i_{lim} is the limiting current density.

The concentration overpotentials are evaluated separately for the anodic and cathodic sides. In the numerical implementation, the current density used in this expression is constrained to remain slightly below the corresponding limiting current density, avoiding the logarithmic singularity as $i \to i_{\text{lim}}$.

Cell and Stack Electrical Quantities

Once the different voltage contributions have been evaluated, the total operating voltage of a single cell is obtained from Equation 3.14.

The electrical current flowing through one cell is related to the current density through:

$$I = iA_{\text{cell}}, \tag{3.23}$$

where A_{cell} is the electrochemically active cell area.

The total stack voltage is obtained by assuming the cells to be electrically connected in series:

$$V_{\text{stack}} = N_{\text{cells}} V_{\text{cell}}, \tag{3.24}$$

where N_{cells} is the total number of cells in the stack.

The electrical power absorbed by the stack is thus:

$$P_{\text{stack}} = V_{\text{stack}} I = N_{\text{cells}} V_{\text{cell}} i A_{\text{cell}}. \tag{3.25}$$

This relationship is nonlinear because the cell voltage itself depends on the current density through the activation, ohmic, and concentration losses.

Hydrogen Production

Hydrogen production is calculated through Faraday's law.

For a single cell, the hydrogen molar flow rate associated with the electrical current is:

$$\dot{n}_{\text{H}_2,\text{cell}} = \frac{I}{2F}. \tag{3.26}$$

A unit Faradaic efficiency is assumed, such that the entire electrical current contributes to hydrogen production according to Faraday's law.

Considering the complete stack, the total hydrogen molar production rate becomes:

$$\dot{n}_{\text{H}_2} = N_{\text{cells}} \frac{I}{2F}. \tag{3.27}$$

The corresponding hydrogen mass flow rate is obtained as:

$$\dot{m}_{\text{H}_2} = \dot{n}_{\text{H}_2} M_{\text{H}_2}, \tag{3.28}$$

where M_{H_2} is the molar mass of hydrogen.

The chemical power associated with the produced hydrogen, expressed on a lower-heating-value basis, is therefore:

$$P_{\mathrm{H_2,LHV}} = \dot{m}_{\mathrm{H_2}} LHV_{\mathrm{H_2}}. \tag{3.29}$$

When $\dot{m}_{\mathrm{H_2}}$ is expressed in kg/s and $LHV_{\mathrm{H_2}}$ in J/kg, Equation 3.29 directly provides the hydrogen power in watts.

Performance Indicators

The electrochemical model evaluates the LHV-based stack conversion efficiency as the ratio between the chemical power of the produced hydrogen and the electrical power absorbed by the stack:

$$\eta_{\mathrm{energ}} = \frac{\dot{m}_{\mathrm{H_2}} LHV_{\mathrm{H_2}}}{P_{\mathrm{stack}}}. \tag{3.30}$$

The model additionally evaluates the thermoneutral voltage ratio:

$$TN = \frac{V_{\mathrm{tn}}}{V_{\mathrm{cell}}}, \tag{3.31}$$

where the thermoneutral voltage is assumed equal to:

$$V_{\mathrm{tn}} = 1.48 \text{ V}. \tag{3.32}$$

Stack Power to Current Density Inversion

As introduced above, the system-level electrical power setpoint must be converted into the corresponding electrochemical operating point. The inverse calculation can be summarized as

$$P_{\mathrm{set}} \longrightarrow i \longrightarrow V_{\mathrm{cell}},\ I,\ P_{\mathrm{stack}},\ \dot{m}_{\mathrm{H_2}},\ \eta. \tag{3.33}$$

Since the stack power is given by

$$P_{\mathrm{stack}}(i) = N_{\mathrm{cells}} A_{\mathrm{cell}} i V_{\mathrm{cell}}(i), \tag{3.34}$$

and V_{cell} is itself a nonlinear function of current density, the inverse relationship cannot be obtained explicitly. A numerical bisection procedure is therefore employed to determine the current density corresponding to the prescribed electrical power.

Power Setpoint Limitation

Before solving the inverse problem, the requested power is checked against the admissible operating limits of the electrolyzer.

If the requested electrical power is lower than or equal to the minimum operating threshold, the electrolyzer is assumed to remain switched off. Consequently, both the operating current density and the hydrogen production rate are set equal to zero.

For power requests above the minimum operating threshold, the requested electrical power is limited to the rated stack power according to

$$P_{\text{set}} = \min\left(P_{\text{set}}, P_{\text{rated}}\right), \tag{3.35}$$

thus ensuring that the operating point always remains within the admissible operating range of the electrolyzer.
The search interval for the current density is defined as

$$i \in [0, i_{\max}]\,. \tag{3.36}$$

Bisection Algorithm
The objective of the procedure is to determine the operating current density satisfying

$$P_{\text{stack}}(i) = P_{\text{set}}. \tag{3.37}$$

The initial search interval is defined as

$$i_{\text{low}} = 0, \qquad i_{\text{high}} = i_{\max}. \tag{3.38}$$

Before starting the iterative procedure, the stack power corresponding to the maximum admissible current density is evaluated:

$$P_{\text{high}} = P_{\text{stack}}\left(i_{\text{high}}\right). \tag{3.39}$$

If

$$P_{\text{set}} \geq P_{\text{high}}, \tag{3.40}$$

the requested operating point would require a current density greater than the admissible maximum. In this case, the solution is saturated at

$$i = i_{\max}. \tag{3.41}$$

Otherwise, the current density is determined iteratively.
At each iteration, the midpoint of the current-density interval is computed as

$$i_{\text{mid}} = \frac{i_{\text{low}} + i_{\text{high}}}{2}. \tag{3.42}$$

The electrochemical model is then evaluated at i_{mid} to determine the corresponding cell voltage,

$$V_{\text{cell}}\left(i_{\text{mid}}\right), \tag{3.43}$$

and the resulting stack power,

$$P_{\text{mid}} = P_{\text{stack}}\left(i_{\text{mid}}\right). \tag{3.44}$$

The calculated stack power is compared with the prescribed power setpoint.
If

$$P_{\mathrm{mid}} < P_{\mathrm{set}}, \tag{3.45}$$

the trial current density is lower than the required solution and the lower search bound is updated according to

$$i_{\mathrm{low}} = i_{\mathrm{mid}}. \tag{3.46}$$

Conversely, if

$$P_{\mathrm{mid}} \geq P_{\mathrm{set}}, \tag{3.47}$$

the trial current density is equal to or greater than the required solution, and the upper search bound is updated according to

$$i_{\mathrm{high}} = i_{\mathrm{mid}}. \tag{3.48}$$

The interval is progressively reduced around the solution by repeating the update procedure for a fixed number of iterations, providing a sufficiently accurate approximation of the operating current density.
After the iterative procedure, the operating current density is approximated as

$$i = \frac{i_{\mathrm{low}} + i_{\mathrm{high}}}{2}. \tag{3.49}$$

Once the current density has been determined, the corresponding electrochemical operating point and performance quantities are evaluated through the forward model according to the equations presented above.

Hydrogen Demand Driven Calculation

While the power-driven formulation is used when the electrolyzer operating point is prescribed in terms of electrical power, the rule-based energy management strategy frequently determines the hydrogen production required to satisfy the furnace demand. In these situations, the operating point of the electrolyzer is obtained directly from the required hydrogen production rate.
Starting from Faraday's law, the current density required to produce a prescribed hydrogen mass flow rate is calculated as

$$i_{\mathrm{req}} = \frac{2F\dot{m}_{\mathrm{H_2,req}}}{N_{\mathrm{cells}} A_{\mathrm{cell}} M_{\mathrm{H_2}}}. \tag{3.50}$$

Once the operating current density has been determined, the corresponding cell voltage is evaluated through the electrochemical model, and the associated stack power is obtained from

$$P_{\text{stack,req}} = N_{\text{cells}} V_{\text{cell}} \left(i_{\text{req}}\right) i_{\text{req}} A_{\text{cell}}. \tag{3.51}$$

The resulting operating point is subsequently checked against the maximum admissible current density and the rated stack power. If the required current density exceeds $i_{\max}$, the operating point is limited to the maximum admissible current density and the requested hydrogen production is identified as infeasible. Similarly, if the corresponding stack power exceeds P_{rated}, the operating point is limited to the current density corresponding to the rated stack power.

3.3.3 Hydrogen Compression Model

The hydrogen compression model represents the auxiliary energy consumption associated with the pressurization of hydrogen before storage. Hydrogen produced by the PEM electrolyzer is available at the electrolyzer outlet pressure, which also represents the inlet pressure of the compression system. Since the hydrogen storage system operates at a higher pressure, the fraction of hydrogen directed to storage must be compressed before entering the tank.

The compression process is represented through a multi-stage model with intermediate cooling. The overall pressure increase is distributed equally among the compression stages by assuming the same pressure ratio for each stage. The stage pressure ratio is therefore calculated as:

$$PR_{\text{stage}} = \left(\frac{p_{\text{out}}}{p_{\text{in}}}\right)^{1/n_{\text{stages}}}, \tag{3.52}$$

where p_{in} and p_{out} are the compressor inlet and outlet pressures, respectively, and n_{stages} is the number of compression stages.

For each stage, the ideal specific work required for isentropic compression is calculated according to:

$$w_{\text{s}} = \frac{\gamma}{\gamma - 1} R_{\text{H}_2} T_{\text{in}} \left[PR_{\text{stage}}^{(\gamma-1)/\gamma} - 1\right], \tag{3.53}$$

where γ is the hydrogen specific heat ratio, R_{H_2} is the specific gas constant of hydrogen, and T_{in} is the gas temperature at the inlet of each compression stage.

The actual specific compression work is higher than the ideal isentropic value because of compressor irreversibilities. The isentropic efficiency η_{is} is therefore introduced as:

$$w_{\text{stage}} = \frac{w_{\text{s}}}{\eta_{\text{is}}}. \tag{3.54}$$

Intermediate cooling between consecutive stages is assumed, such that the same inlet temperature is considered for each compression stage. Since the same pressure ratio and inlet temperature are adopted for all stages, the total specific compression work can be expressed as

$$w_{\text{tot}} = n_{\text{stages}} w_{\text{stage}}. \tag{3.55}$$

The electrical power required by the compression system depends on the hydrogen mass flow rate directed to storage. Taking into account the motor efficiency, the compressor electrical power is calculated as:

$$P_{\text{cp}} = \frac{\dot{m}_{\text{H}_2,\text{cp}} w_{\text{tot}}}{\eta_{\text{motor}}}, \tag{3.56}$$

where $\dot{m}_{\text{H}_2,\text{cp}}$ is the hydrogen mass flow rate passing through the compressor and η_{motor} is the electric motor efficiency. When the specific work is expressed in J/kg and the hydrogen mass flow rate in kg/s, the resulting compressor power is obtained in watts.
The compressor is also subject to a rated electrical power limit. As a result, the maximum hydrogen mass flow rate that can be compressed is obtained by rearranging Equation 3.56:

$$\dot{m}_{\text{H}_2,\text{cp,max}} = \frac{P_{\text{cp,rated}} \eta_{\text{motor}}}{w_{\text{tot}}}. \tag{3.57}$$

The resulting compressor capacity therefore represents an operational constraint on the hydrogen flow that can be directed to the pressurized storage system. Hydrogen supplied directly from the electrolyzer to the furnace does not undergo the storage compression process considered here, whereas hydrogen directed to the storage tank introduces an additional electrical consumption that must be accounted for by the energy-management strategy.

3.3.4 Hydrogen Storage Model

The hydrogen storage system is represented through a simplified energy-based lumped model. Rather than explicitly describing the thermodynamic evolution of hydrogen pressure, temperature, and density inside the vessel, the amount of stored hydrogen is expressed through its equivalent chemical energy content based on the lower heating value of hydrogen.
The main state variable of the storage model is therefore the tank energy, denoted by

$$E_{\text{tank},k}, \tag{3.58}$$

where $E_{\text{tank},k}$ represents the equivalent chemical energy content of the stored hydrogen at timestep k.
The storage level is described through the Level of Hydrogen (LOH), defined as the ratio between the instantaneous stored energy and the rated storage capacity:

$$LOH_k = \frac{E_{\text{tank},k}}{E_{\text{rated}}}, \tag{3.59}$$

where E_{rated} is the total rated energy capacity of the hydrogen storage system.
The storage energy is updated at each timestep according to the energy balance:

$$E_{\text{tank},k+1} = E_{\text{tank},k} + \left(P_{\text{in},k} - P_{\text{out},k}\right) \Delta t, \tag{3.60}$$

where $P_{\text{in},k}$ and $P_{\text{out},k}$ represent the LHV-based hydrogen energy flows into and out of the storage

system, respectively, while Δt is the duration of the simulation timestep expressed in hours. As specified in the main modelling assumptions, hydrogen leakage and storage losses are neglected; therefore, no additional charging or discharging efficiency terms are introduced in the storage energy balance.

The tank operating range is limited by minimum and maximum admissible storage levels. The corresponding energy limits are defined as:

$$E_{\min} = LOH_{\min} E_{\text{rated}}, \tag{3.61}$$

and

$$E_{\max} = LOH_{\max} E_{\text{rated}}. \tag{3.62}$$

Accordingly, the tank state is constrained within:

$$E_{\min} \leq E_{\text{tank},k} \leq E_{\max}. \tag{3.63}$$

The initial tank energy is determined from the given initial Level of Hydrogen:

$$E_{\text{tank},0} = LOH_{\text{init}} E_{\text{rated}}. \tag{3.64}$$

At each timestep, the available charging capacity is determined by the difference between the maximum admissible storage energy and the current tank state:

$$E_{\text{charge,avail},k} = \max\left(0, E_{\max} - E_{\text{tank},k}\right). \tag{3.65}$$

Similarly, the amount of stored hydrogen energy available for withdrawal without violating the minimum storage level is:

$$E_{\text{discharge,avail},k} = \max\left(0, E_{\text{tank},k} - E_{\min}\right). \tag{3.66}$$

These quantities define the energy margins available for charging and discharging at each timestep and are used by the energy-management logic to ensure that the storage state remains within its lower and upper operating limits.

3.4 PEM Electrolyzer Degradation Model

Electrolyzer degradation represents a relevant aspect of this modelling framework, since progressive performance deterioration can affect the relationship between electrical energy consumption and hydrogen production over the operating lifetime of the system.

The degradation model is implemented as an extension of the electrochemical PEM electrolyzer model described in the previous section. Rather than directly modifying the electrochemical

parameters governing the polarization behaviour of the cell, an empirical correction is introduced to represent the progressive degradation of the electrolyzer conversion efficiency.
For a prescribed electrical power, the adopted approach preserves the electrochemical operating point determined by the original model while introducing a degradation-dependent correction to hydrogen production and the corresponding performance indicators.

Literature-Based Degradation Curves

The degradation model adopted in this work is based on the relationship between PEM electrolyzer hydrogen production efficiency, operating time, and normalized stack power reported in the literature [35]. This formulation was selected because it provides efficiency data at different degradation states as a function of the electrolyzer load allowing the degradation behaviour to be characterized with respect to both cumulative operation and operating point. This is particularly suitable for the present analysis, in which the PEM electrolyzer operates under time-varying power conditions determined by the energy-management strategy. The stack electrical power is therefore normalized with respect to the rated stack power:

$$p_{\mathrm{pu}} = \frac{P_{\mathrm{stack}}}{P_{\mathrm{rated}}}, \tag{3.67}$$

where P_{stack} is the actual stack electrical power and P_{rated} is the rated electrical power of the electrolyzer.
Two reference efficiency curves reported in the same literature source are adopted in the present model:

$$\eta_1 = \eta_1(p_{\mathrm{pu}}) \tag{3.68}$$

and

$$\eta_{100} = \eta_{100}(p_{\mathrm{pu}}), \tag{3.69}$$

representing the reference efficiency behaviour at operating day 1 and operating day 100, respectively.
Both curves are represented through piecewise functions of the normalized stack power, allowing the degradation correction to account for the instantaneous electrolyzer operating point.
For intermediate ageing conditions, a linear interpolation between the day-1 and day-100 efficiency curves is assumed in the present model. The interpolation coefficient is defined as:

$$\alpha(d) = \frac{d-1}{100-1} = \frac{d-1}{99}, \tag{3.70}$$

where d represents the current operating day.
The interpolated reference efficiency is therefore:

$$\eta_{\mathrm{ref}}(p_{\mathrm{pu}}, d) = [1-\alpha(d)]\,\eta_1(p_{\mathrm{pu}}) + \alpha(d)\eta_{100}(p_{\mathrm{pu}}). \tag{3.71}$$

At $d = 1$, the model therefore reproduces the initial reference curve, while at $d = 100$ it reaches the degraded reference curve.

Degradation Factor and Integration into the PEM Model

The literature-based efficiency curves are not used to replace the efficiency calculated by the electrochemical PEM model. Instead, they are used to derive a relative degradation factor that quantifies the performance reduction with respect to the initial condition.
The degradation factor is defined as:

$$f_{\mathrm{deg}}\left(p_{\mathrm{pu}}, d\right) = \frac{\eta_{\mathrm{ref}}\left(p_{\mathrm{pu}}, d\right)}{\eta_1\left(p_{\mathrm{pu}}\right)}. \tag{3.72}$$

At the initial operating condition, $f_{\mathrm{deg}} = 1$, whereas progressive degradation generally results in values lower than unity.
For a given electrical power setpoint, the corresponding electrical operating point is first determined through the electrochemical PEM model according to the procedure described in the previous section.
The degradation correction is then applied to the hydrogen production calculated by the original model:

$$\dot{m}_{\mathrm{H_2,deg}} = f_{\mathrm{deg}} \dot{m}_{\mathrm{H_2,fresh}}, \tag{3.73}$$

where $\dot{m}_{\mathrm{H_2,fresh}}$ represents the hydrogen production predicted by the original electrochemical model at the same electrical operating point.
Accordingly, the LHV-based stack conversion efficiency is corrected as

$$\eta_{\mathrm{energ,deg}} = f_{\mathrm{deg}} \eta_{\mathrm{energ,fresh}}. \tag{3.74}$$

The thermoneutral ratio used as a performance indicator is also corrected using the same relative degradation factor.
This approach provides a computationally efficient method for incorporating empirical ageing behaviour while preserving the detailed nonlinear representation of the original PEM electrolyzer model.

Evolution with Operating Time

The degradation state is linked to the cumulative operating time of the electrolyzer rather than to calendar time. The operating day is defined as

$$d = 1 + \frac{t_{\mathrm{op,s}}}{86400} = 1 + \frac{t_{\mathrm{op,h}}}{24}, \tag{3.75}$$

where $t_{\mathrm{op,s}}$ and $t_{\mathrm{op,h}}$ represent the same cumulative PEM operating time expressed in seconds and hours, respectively. The operating-time counter is increased only during timesteps in which the electrolyzer is active; therefore, the degradation state evolves according to actual electrolyzer

utilization rather than elapsed calendar time.
The implementation of the operating-time counter reflects the temporal resolution of the two energy-management frameworks. In the rule-based simulation, which operates with a 15-minute timestep, each active interval contributes 900 s to the cumulative operating time. In the optimization-based framework, which operates with an hourly timestep, each implemented interval in which the electrolyzer is active contributes 1 h to the cumulative operating time. In both cases, these quantities represent the same physical variable, namely the cumulative operating time of the PEM electrolyzer. To remain within the range covered by the adopted degradation data, the operating day is limited to a maximum value of 100:

$$d_{\mathrm{deg}} = \min\left[100,\ 1 + \frac{t_{\mathrm{op,s}}}{86400}\right] = \min\left[100,\ 1 + \frac{t_{\mathrm{op,h}}}{24}\right]. \tag{3.76}$$

Once day 100 is reached, the degradation state is assumed to remain constant and the day-100 efficiency curve is used for all subsequent operation. This modelling assumption is introduced to avoid extrapolating the degradation behaviour beyond the range represented by the reference curves adopted in the present model.

Inverse Calculation under Degraded Conditions

The dependence of the degradation factor on normalized stack power also affects the inverse relationship between hydrogen output and the electrical power required by the electrolyzer. Under fresh conditions, a specified hydrogen production rate can be related to the corresponding stack current through Faraday's law, while the electrochemical model determines the associated cell voltage and stack electrical power. Under degraded conditions, however, the hydrogen output is additionally affected by the degradation factor, which itself depends on the electrical operating point. Consequently, the electrical power required to achieve a prescribed degraded hydrogen output must be determined numerically.
In general, the inverse problem can be expressed as

$$Y_{\mathrm{H_2,deg}}\left(P_{\mathrm{stack}}, d_{\mathrm{deg}}\right) = Y_{\mathrm{H_2,target}}, \tag{3.77}$$

where $Y_{\mathrm{H_2}}$ denotes the hydrogen output. Depending on the adopted formulation, this quantity may represent either the hydrogen production rate $\dot{m}_{\mathrm{H_2}}$ or the corresponding LHV-based chemical power $P_{\mathrm{H_2,LHV}}$.
The role of this inverse relationship differs between the two energy-management frameworks. In the rule-based approach, degradation is evaluated under a frozen-dispatch assumption, whereas in the optimization-based EMS the degradation-dependent PEM performance is incorporated into the energy-management decisions. The corresponding implementation is described in the following sections.

3.5 Rule-Based Energy Management

The first stage of the analysis is developed through a deterministic rule-based energy-management approach, which coordinates the operation of the integrated system according to a predefined sequence of priorities and operating conditions. This framework is used to evaluate the system response under different hydrogen-substitution targets while explicitly accounting for the detailed electrochemical behaviour of the PEM electrolyzer and the operational constraints of the hydrogen-production and storage system.

At each simulation timestep, the controller first determines the hydrogen requirement associated with the target furnace hydrogen contribution. The available energy sources and storage resources are then sequentially allocated according to photovoltaic availability, hydrogen storage state, electrolyzer and compressor operating limits of the system components.

Hydrogen Demand Determination

At the beginning of each timestep, the furnace thermal demand is evaluated and the corresponding target hydrogen contribution and required hydrogen mass flow rate are determined according to the formulation described in Section 3.3.1.

The resulting hydrogen requirement represents the target that the hydrogen production and storage system attempts to supply during the considered timestep. Since the total furnace thermal demand is assumed to be always satisfied, any portion of the target hydrogen contribution that cannot ultimately be supplied is compensated by additional natural gas.

Photovoltaic-Based Hydrogen Production

Once the furnace hydrogen requirement has been determined, the controller determines the PEM operating power according to the photovoltaic power available during the current timestep. When hydrogen storage capacity is available, the controller seeks the maximum feasible PEM operating power that can be supplied by the available photovoltaic generation while respecting the electrolyzer, compressor, storage, and electrical-balance constraints.

When no additional hydrogen can be stored, the controller instead seeks the minimum PEM operating power required to satisfy the furnace hydrogen target, subject to the available photovoltaic power and the electrolyzer operating limits.

The hydrogen produced using photovoltaic electricity is first allocated to the instantaneous furnace hydrogen demand. This establishes a direct hydrogen flow from the electrolyzer to the furnace:

$$\dot{m}_{\mathrm{H_2,direct}} = \min\left(\dot{m}_{\mathrm{H_2,PV}}, \dot{m}_{\mathrm{H_2,target}}\right). \tag{3.78}$$

If the hydrogen produced by the electrolyzer exceeds the instantaneous furnace requirement, the remaining hydrogen represents a potential surplus available for storage:

$$\dot{m}_{\mathrm{H_2,surplus}} = \max\left(0, \dot{m}_{\mathrm{H_2,PV}} - \dot{m}_{\mathrm{H_2,direct}}\right). \tag{3.79}$$

Only the hydrogen directed to storage is subjected to the compression process described in Section 3.3.3. The actual amount stored is therefore limited by the available tank capacity and by the operating capability of the compression system.

Hydrogen Storage Dispatch

When the hydrogen supplied directly from photovoltaic-based production is insufficient to satisfy the target hydrogen requirement of the furnace, the storage tank is used as the next available hydrogen source.

The residual hydrogen demand after direct photovoltaic-based production is:

$$\dot{m}_{\mathrm{H_2,res}} = \max\left(0, \dot{m}_{\mathrm{H_2,target}} - \dot{m}_{\mathrm{H_2,direct}}\right). \tag{3.80}$$

Hydrogen can then be withdrawn from the tank up to the amount required to satisfy this residual demand, while respecting the minimum admissible storage level. The storage system therefore acts as a temporal buffer: surplus hydrogen produced during previous periods can be used when instantaneous renewable-based production is insufficient.

The tank state is updated after charging or discharging according to the energy-balance formulation introduced in Section 3.3.4.

Grid-Supported Hydrogen Production

If a residual hydrogen requirement remains after the utilization of directly produced hydrogen and the available hydrogen stored in the tank, the PEM electrolyzer can be supplied with electricity imported from the grid.

The required electrolyzer operating point is determined according to the remaining hydrogen demand using the fresh electrochemical PEM model. The corresponding electrical requirement is therefore obtained through the hydrogen demand-driven calculation described previously, subject to the electrolyzer operating limits.

Grid electricity therefore provides an additional source of flexibility, allowing hydrogen production to continue during periods in which photovoltaic generation and stored hydrogen alone are insufficient to satisfy the hydrogen target, subject to the electrolyzer operating limits.

Opportunistic Grid-Based Storage Charging

In addition to supplying residual hydrogen demand, grid electricity can also be used for opportunistic hydrogen production under favourable price conditions.

When the electricity price is lower than the natural-gas price, additional grid-supported hydrogen production may be activated for storage rather than for immediate furnace consumption. The additional hydrogen is compressed and transferred to the tank, subject to the specified grid-charging limit, the available storage capacity, and the operating capabilities of the electrolyzer and compression system.

This strategy allows the storage system to accumulate hydrogen during periods identified as favourable according to the adopted price-based criterion, for possible use in subsequent timesteps.

Unlike an optimization-based strategy, however, this decision is triggered by a predefined rule and does not result from the simultaneous optimization of present and future operating decisions.

Natural Gas Fallback

After the available hydrogen supply options have been evaluated, any remaining unmet portion of the target hydrogen contribution is compensated by natural gas.
The hydrogen supplied to the furnace can be expressed as the combination of the available hydrogen supply pathways:

$$\dot{m}_{\mathrm{H_2,supplied}} = \dot{m}_{\mathrm{H_2,direct}} + \dot{m}_{\mathrm{H_2,tank}} + \dot{m}_{\mathrm{H_2,grid}}, \tag{3.81}$$

subject to the required hydrogen target and the corresponding component limitations.
Any remaining hydrogen deficit is:

$$\dot{m}_{\mathrm{H_2,unmet}} = \max\left(0, \dot{m}_{\mathrm{H_2,target}} - \dot{m}_{\mathrm{H_2,supplied}}\right). \tag{3.82}$$

The equivalent thermal contribution associated with this unmet hydrogen demand is supplied by additional natural gas. In this way, the total furnace thermal demand remains fully satisfied even when the hydrogen substitution target cannot be completely achieved.

Operating Constraints

The control actions described above are additionally subject to the physical constraints of the integrated system. While the operating limits of the electrolyzer, compressor, and hydrogen storage system are applied through the component models presented in Section 3.3, the controller must also satisfy the electrical power balance associated with photovoltaic-based hydrogen production. In particular, when photovoltaic-based hydrogen production is directed to storage, the available photovoltaic power must simultaneously supply both the electrolyzer and the compression system,

$$P_{\mathrm{stack}} + P_{\mathrm{cp}} \leq P_{\mathrm{PV}}, \tag{3.83}$$

where P_{cp} is the electrical power required for hydrogen compression. Consequently, photovoltaic-based hydrogen production for storage can only take place when sufficient photovoltaic power is available to operate both the electrolyzer stack and the compression system simultaneously.

Integration of Electrolyzer Degradation

The degradation model presented in Section 3.4 is incorporated into the rule-based simulation through a frozen-dispatch approach. The controller decisions are determined using the fresh PEM electrochemical model, while the degraded performance is subsequently evaluated at the same electrical operating point.
This formulation allows the effect of degradation on hydrogen production and electrolyzer performance to be quantified under unchanged electrical operating conditions, thereby isolating PEM performance deterioration from changes in the energy-management decisions.

Since the degraded hydrogen output is not fed back into the controller, it does not lead to a recalculation of the electrolyzer power setpoint, storage dispatch, grid electricity use, or natural-gas fallback, or the resulting furnace energy balance. The degraded case should therefore be interpreted as a performance assessment of the PEM electrolyzer under the dispatch determined using the fresh model, rather than as a separate degradation-aware system dispatch.

3.6 Optimization-Based Energy Management

The second stage of the analysis considers an optimization-based Energy Management System (EMS), in which system operation is determined by solving a mathematical optimization problem subject to the technical and operational constraints of the integrated system. The EMS determines the allocation of the available energy flows with the objective of minimizing the selected operating cost while satisfying the energy requirements of the industrial process.

The optimization framework coordinates the photovoltaic system, PEM electrolyzer, hydrogen storage system, electrical grid, natural gas supply, and glass furnace. Compared with the rule-based formulation, it also includes additional system-level energy flows and degrees of freedom, which are introduced in the following subsections.

A central methodological development of this work is the integration of the detailed PEM electrochemical and degradation models described in Sections 3.3 and 3.4 into an existing optimization-based EMS for the same industrial case study, replacing the original constant-efficiency representation of the electrolyzer. In contrast to the frozen-dispatch approach adopted in the rule-based analysis, degradation-dependent PEM performance is iteratively fed back into the EMS and can therefore influence the resulting system operation.

Since the electrochemical behaviour of the electrolyzer introduces nonlinear and operating-point-dependent relationships, the complete PEM model is not directly embedded within the optimization problem. Instead, an iterative procedure is adopted to update the electrolyzer conversion efficiency used by the EMS according to the operating points determined at each iteration.

Optimization Horizon and Sequential Operation

In contrast to the 15-minute temporal resolution adopted in the rule-based simulation, the optimization-based EMS is formulated with an hourly simulation timestep. The hourly input profiles are derived from the same original 15-minute datasets used in the rule-based framework by averaging each group of four consecutive 15-minute values, after the required unit conversions and pre-processing operations have been performed. Therefore, the two frameworks rely on the same input data, while differing in their temporal resolution. The planning horizon of the optimization-based EMS is set to 24 hours.

The energy-management problem is formulated over a finite prediction horizon. At each optimization step, the EMS considers the expected system conditions over the following 24 hours, including furnace demand, photovoltaic generation, and energy prices, while accounting for the system state resulting from the previously implemented timestep.

The optimization problem is solved over the complete planning horizon, but only the operating decisions corresponding to the current hourly timestep are implemented. The system state is subsequently updated and the optimization horizon is shifted forward by one hour before solving the problem again.
This rolling-horizon procedure allows the EMS to account for the temporal coupling introduced by hydrogen storage and for expected variations in energy availability, demand, and energy prices, while continuously updating the operating decisions as the simulation progresses.

Optimization Variables and Energy Flows

The optimization problem coordinates hydrogen production, storage, and furnace supply on the basis of predefined input profiles describing photovoltaic generation, furnace and industrial energy demands, and energy prices. Together with the technical, economic, and environmental model parameters, these inputs define the operating conditions considered by the EMS at each timestep.
The principal optimized quantities include the electrical power supplied to the PEM electrolyzer, the corresponding hydrogen energy output, hydrogen energy flows associated with storage charging and discharging, the utilized photovoltaic power, electricity imported from the grid, the electrical contribution to the furnace, and the natural-gas contribution to the furnace.
The hydrogen output of the electrolyzer is represented on an energy basis. The relationship between the electrical input of the PEM and the corresponding hydrogen energy output is expressed as

$$P_{\mathrm{ely,in},k} = \frac{P_{\mathrm{ely,out},k}}{\eta_{\mathrm{EMS},k}}, \tag{3.84}$$

where $P_{\mathrm{ely,in},k}$ is the electrical input power of the electrolyzer, $P_{\mathrm{ely,out},k}$ is the LHV-based hydrogen output power, and $\eta_{\mathrm{EMS},k}$ is the conversion efficiency adopted by the optimization model at timestep k.

System Constraints

The optimization problem is subject to a set of constraints representing the physical and operational behaviour of the integrated energy system.
At each timestep, photovoltaic generation and electricity imported from the grid supply the electrical loads of the integrated system. The electrical balance is expressed as

$$P_{\mathrm{PV},k} + P_{\mathrm{grid},k} = P_{\mathrm{load,el},k} + P_{\mathrm{ely,in},k} + P_{\mathrm{cp},k} + P_{\mathrm{ele,furnace},k}, \tag{3.85}$$

where the terms on the right-hand side represent the industrial electrical load, electrolyzer consumption, compression electricity consumption, and direct electrical contribution to the furnace, respectively. Photovoltaic utilization is constrained by the available PV generation at each timestep. The electrolyzer operation is constrained by its admissible operating range, including the rated PEM power and the ramp limits imposed on variations in hydrogen energy output between consecutive hourly intervals.
The hydrogen output of the electrolyzer is allocated either directly to the furnace or to the hydrogen

storage system. The corresponding hydrogen-energy balance is expressed as

$$P_{\text{ely,out},k} = P_{\text{ely,out,furnace},k} + P_{\text{tank,in},k}, \tag{3.86}$$

where $P_{\text{ely,out,furnace},k}$ represents the LHV-based hydrogen power supplied directly from the electrolyzer to the furnace and $P_{\text{tank,in},k}$ represents the hydrogen power directed to storage.
The total hydrogen contribution to the furnace is then obtained from the combination of directly produced and stored hydrogen:

$$P_{\text{H}_2,\text{furnace},k} = P_{\text{ely,out,furnace},k} + P_{\text{tank,out},k}. \tag{3.87}$$

Hydrogen directed to storage passes through the compression system before entering the tank, while hydrogen supplied directly to the furnace does not require the storage compression process. In the optimization framework, the corresponding compressor electricity consumption is related to the hydrogen energy flow directed to storage according to

$$P_{\text{cp},k} = P_{\text{tank,in},k} \frac{w_{\text{cp}}}{LHV_{\text{H}_2}}, \tag{3.88}$$

where w_{cp} is the specific electrical compression work obtained from the thermodynamic compressor model presented in Section 3.3.3.
The optimization framework therefore represents compressor electricity consumption through a linear relation based on the specific electrical compression work obtained from the thermodynamic compressor model. This allows consistency to be maintained in the electrical energy required to compress a given hydrogen flow, while the detailed multi-stage thermodynamic formulation is not explicitly solved within the optimization problem.
The hydrogen storage state is represented in the optimization framework through its state of charge (SOC). The storage dynamics introduce a temporal coupling between consecutive optimization intervals and are represented as

$$SOC_{k+1} = SOC_k + \frac{\eta_{\text{ch}} P_{\text{tank,in},k} \Delta t}{E_{\text{rated}}} - \frac{P_{\text{tank,out},k} \Delta t}{\eta_{\text{dis}} E_{\text{rated}}}, \tag{3.89}$$

where η_{ch} and η_{dis} are the charging and discharging efficiencies, respectively, E_{rated} is the rated energy capacity of the hydrogen storage system, and $\Delta t = 1$ h is the optimization timestep.
The storage state is constrained between the minimum and maximum admissible values:

$$SOC_{\min} \leq SOC_k \leq SOC_{\max}. \tag{3.90}$$

Although the storage state is represented through different mathematical variables in the two frameworks (LOH in the rule-based implementation and SOC in the optimization-based EMS), both formulations describe the same physical hydrogen inventory on an energy basis. The same rated storage capacity and corresponding operating limits are adopted in the comparative simulations; the difference therefore concerns the mathematical representation of the storage state rather than the

physical storage system itself.
The hydrogen contribution to the furnace is imposed as a minimum energy-share requirement:

$$P_{\mathrm{H_2,furnace},k} \geq x_{\mathrm{H_2,min}} P_{\mathrm{load,th,TOT},k}. \tag{3.91}$$

This differs from the rule-based formulation, in which an hydrogen target is sequentially pursued, while natural gas supplies the remaining furnace energy demand. In the optimization framework, the hydrogen contribution is instead imposed as a minimum constraint and may exceed this minimum.
The total fuel contribution to the furnace is obtained by combining the natural-gas and hydrogen energy flows:

$$P_{\mathrm{bur,in},k} = P_{\mathrm{NG},k} + P_{\mathrm{H_2,furnace},k}, \tag{3.92}$$

where $P_{\mathrm{bur,in},k}$ represents the total fuel-energy input to the furnace burner.
The overall furnace energy balance is then expressed as

$$P_{\mathrm{load,th,TOT},k} = \eta_{\mathrm{bur}} P_{\mathrm{bur,in},k} + P_{\mathrm{ele,furnace},k}, \tag{3.93}$$

where η_{bur} is the burner thermal efficiency and $P_{\mathrm{ele,furnace},k}$ represents the direct electrical contribution to the furnace. In the adopted optimization model, this contribution is included directly in the furnace energy balance, without introducing an additional electrical-to-thermal conversion efficiency, and is constrained within a defined range of the total furnace demand:

$$x_{\mathrm{el,min}} P_{\mathrm{load,th,TOT},k} \leq P_{\mathrm{ele,furnace},k} \leq x_{\mathrm{el,max}} P_{\mathrm{load,th,TOT},k}. \tag{3.94}$$

Objective Function

The operating schedule is determined by minimizing an objective function that accounts for both energy costs and carbon-related costs. In the implemented formulation, the active objective includes the cost of electricity imported from the grid, the cost of natural gas consumption, and the corresponding carbon-related costs associated with grid electricity and natural gas use. Component investment costs and maintenance costs are not included in the operational optimization.
The objective function can therefore be expressed in general form as:

$$\min C_{\mathrm{tot}} = C_{\mathrm{grid}} + C_{\mathrm{NG}} + C_{\mathrm{em,grid}} + C_{\mathrm{em,NG}}, \tag{3.95}$$

where C_{grid} and C_{NG} represent the energy-supply costs associated with grid electricity and natural gas, respectively, while $C_{\mathrm{em,grid}}$ and $C_{\mathrm{em,NG}}$ represent the corresponding carbon-related cost contributions.
The grid-electricity cost over the optimization horizon is evaluated as

$$C_{\mathrm{grid}} = \sum_k c_{\mathrm{el},k} P_{\mathrm{grid},k} \Delta t, \tag{3.96}$$

where $c_{\mathrm{el},k}$ is the electricity price at timestep k.
Similarly, the natural-gas cost is calculated as

$$C_{\mathrm{NG}} = \sum_k c_{\mathrm{NG},k} P_{\mathrm{NG},k} \Delta t, \tag{3.97}$$

where $c_{\mathrm{NG},k}$ is the natural-gas energy price.
The environmental cost associated with electricity imported from the grid is evaluated as

$$C_{\mathrm{em,grid}} = \sum_k c_{\mathrm{CO_2,grid}} P_{\mathrm{grid},k} \Delta t, \tag{3.98}$$

where $c_{\mathrm{CO_2,grid}}$ is the indirect carbon-cost coefficient associated with grid electricity. It is obtained by combining the grid carbon-intensity factor, $\mathrm{EF}_{\mathrm{grid}}$, with the adopted carbon price, $c_{\mathrm{CO_2}}$:

$$c_{\mathrm{CO_2,grid}} = \mathrm{EF}_{\mathrm{grid}} c_{\mathrm{CO_2}}. \tag{3.99}$$

For natural gas, the corresponding carbon dioxide emissions are first estimated from the natural-gas energy consumption as

$$m_{\mathrm{CO_2,NG},k} = \frac{P_{\mathrm{NG},k} \Delta t}{LHV_{\mathrm{NG}}} \rho_{\mathrm{NG}} r_{\mathrm{CO_2}}, \tag{3.100}$$

where LHV_{NG} is the volumetric lower heating value of natural gas, ρ_{NG} is the natural-gas density, and $r_{\mathrm{CO_2}}$ is the mass ratio between the carbon dioxide produced and the natural gas consumed.
The corresponding environmental cost is then calculated as

$$C_{\mathrm{em,NG}} = \sum_k c_{\mathrm{CO_2}} m_{\mathrm{CO_2,NG},k}, \tag{3.101}$$

where $c_{\mathrm{CO_2}}$ is the carbon-cost coefficient applied to direct natural-gas emissions.

Integration of the Detailed PEM Electrolyzer and Degradation Model

Directly embedding the detailed PEM electrolyzer model into the optimization problem would introduce nonlinear relationships between electrical power, current density, cell voltage, hydrogen production, efficiency, and degradation state, substantially increasing the complexity of the optimization problem. To preserve the tractability of the existing EMS formulation while accounting for the operating-point- and degradation-dependent PEM performance, an iterative coupling procedure is therefore adopted.
At the beginning of each rolling-horizon optimization step, the EMS assumes a constant electrolyzer efficiency over the 24-hour optimization horizon:

$$\eta^{(0)}_{\mathrm{EMS},k} = \eta_{\mathrm{init}}, \tag{3.102}$$

where η_{init} is the efficiency used to initialize the iterative procedure, k denotes the timestep within the 24-hour horizon, and the superscript (0) identifies the efficiency profile at the first iteration.

Using the assumed efficiency profile, which is treated as fixed during the optimization solve, the EMS determines the electrolyzer electrical input power $P_{\text{ely,in},k}$ and the corresponding LHV-based hydrogen output $P_{\text{ely,out},k}$ according to Equation 3.84.
The resulting hydrogen output is then used as the target for the detailed PEM model, which evaluates the electrolyzer performance at the corresponding degradation state. The latter is determined for each active timestep according to the cumulative PEM operating time.
At the beginning of each 24-hour horizon, the cumulative operating time reached up to the previously implemented hour is used as the starting value. The predicted hours are then considered sequentially. Whenever the EMS schedules the electrolyzer to operate, the cumulative operating time is increased by one hour; when the electrolyzer is inactive, it remains unchanged. The resulting cumulative operating time determines the degradation state $d_{\text{deg},k}$ associated with each active timestep.
Once the degradation state has been determined, each active timestep is therefore characterized by two quantities required for the detailed PEM evaluation: the hydrogen output $P_{\text{ely,out},k}$ determined by the EMS and the corresponding degradation state $d_{\text{deg},k}$. At this stage, the unknown quantity is the electrical stack power $P_{\text{stack},k}$ required to produce the specified hydrogen output under the corresponding degradation condition.
The detailed PEM model described in Section 3.3.2 is naturally evaluated in the opposite direction: for a given electrical stack power and degradation state, it calculates the corresponding LHV-based hydrogen output, $P_{\text{H}_2,\text{LHV,deg},k}$:

$$P_{\text{stack},k} \longrightarrow P_{\text{H}_2,\text{LHV,deg},k}. \tag{3.103}$$

By contrast, in the present coupling procedure, $P_{\text{ely,out},k}$ is already known from the EMS, while $P_{\text{stack},k}$ must be determined. The required stack power is therefore the value that satisfies

$$P_{\text{H}_2,\text{LHV,deg}}\left(P_{\text{stack},k}, d_{\text{deg},k}\right) = P_{\text{ely,out},k}. \tag{3.104}$$

The left-hand side represents the LHV-based hydrogen output calculated by the detailed PEM model for a given stack power and degradation state, whereas the right-hand side is the hydrogen output determined by the EMS and used as the target of the detailed PEM evaluation.
Since the adopted PEM formulation does not provide an explicit analytical expression for $P_{\text{stack},k}$ in terms of this hydrogen output, the required stack power is determined numerically through a bisection procedure. The search is performed within the physical operating range of the electrolyzer,

$$0 \leq P_{\text{stack},k} \leq P_{\text{rated}}. \tag{3.105}$$

Before starting the search, the maximum hydrogen output that the degraded PEM can produce at P_{rated} is evaluated. If

$$P_{\text{ely,out},k} > P_{\text{H}_2,\text{LHV,deg}}\left(P_{\text{rated}}, d_{\text{deg},k}\right), \tag{3.106}$$

the hydrogen target cannot be reproduced at the corresponding degradation state and the evaluated

stack power is limited to P_{rated}. Otherwise, the bisection search is performed.

At each bisection step, a trial value of $P_{\text{stack},k}$ is selected within the current search interval. The detailed PEM model calculates the hydrogen output associated with this trial power. The result is then compared with the EMS hydrogen output:

$$P_{\text{H}_2,\text{LHV,deg}}\left(P_{\text{stack},k}, d_{\text{deg},k}\right) \begin{cases} < P_{\text{ely,out},k}, & \text{increase } P_{\text{stack},k}, \\ > P_{\text{ely,out},k}, & \text{decrease } P_{\text{stack},k}. \end{cases} \tag{3.107}$$

The search interval is progressively reduced until the calculated hydrogen output matches the EMS target within the prescribed numerical tolerance. The resulting value of $P_{\text{stack},k}$ is therefore the electrical stack power required by the detailed degradation-dependent PEM model to produce the hydrogen output scheduled by the EMS.

For each candidate stack power tested during the bisection, the detailed PEM model must first determine the associated current density. Stack power is related to current density through

$$P_{\text{stack}} = N_{\text{cells}} V_{\text{cell}}(i)\, i\, A_{\text{cell}}. \tag{3.108}$$

Since V_{cell} itself depends on current density, the adopted PEM formulation does not provide an explicit expression for i in terms of P_{stack}. The electrochemical inversion described in Section 3.3.2 is therefore applied to each candidate stack power. The resulting current density is then used to calculate the corresponding hydrogen production, which is compared with the EMS hydrogen output $P_{\text{ely,out},k}$ within the stack-power bisection.

The determination of the required stack power therefore involves two nested numerical procedures. The stack-power bisection searches for the electrical power required to reproduce the hydrogen output determined by the EMS, while the electrochemical inversion determines the current density associated with each candidate stack power. The procedure can be represented schematically as

$$P_{\text{ely,out},k} \xrightarrow{\text{stack-power bisection}} P_{\text{stack},k} \xrightarrow{\text{electrochemical inversion}} i_k \rightarrow P_{\text{H}_2,\text{LHV,deg},k}. \tag{3.109}$$

Once the required stack power has been determined for each active timestep, the corresponding degradation-dependent PEM efficiency is calculated as

$$\eta_{\text{PEM},k} = \frac{P_{\text{ely,out},k}}{P_{\text{stack},k}}. \tag{3.110}$$

This efficiency represents the conversion efficiency predicted by the detailed electrochemical model at the corresponding degradation state. It is then fed back into the EMS, replacing the efficiency previously assumed for the corresponding timestep. Denoting the coupling iteration by r, the efficiency update can be written as

$$\eta_{\text{EMS},k}^{(r+1)} = \eta_{\text{PEM},k}^{(r)}. \tag{3.111}$$

For timesteps in which the electrolyzer is inactive, the efficiency value from the previous coupling

iteration is retained.

The EMS is then solved again using the updated efficiency profile. Since the relationship between electrical input and hydrogen output has changed, the new optimization may determine different electrolyzer operating conditions and, consequently, different system energy flows. The hydrogen output obtained from the new optimization is therefore evaluated again with the detailed degradation-dependent PEM model, and the efficiency profile is updated once more.

The coupling procedure is repeated until the efficiency used by the EMS and that returned by the detailed PEM model are sufficiently close:

$$\max_k \left| \eta^{(r)}_{\mathrm{PEM},k} - \eta^{(r)}_{\mathrm{EMS},k} \right| < \varepsilon_\eta, \tag{3.112}$$

where the maximum is evaluated over the 24-hour optimization horizon, considering only timesteps in which the electrolyzer is active.

After convergence, or after the maximum number of coupling iterations has been reached, only the decisions corresponding to the first hour of the optimized horizon are implemented. The resulting system state is carried forward to the next rolling-horizon step, while the cumulative PEM operating time is increased by one hour only if the electrolyzer operates during the implemented timestep. The operating-time increments predicted for the remaining hours are used only to evaluate degradation within the current optimization horizon and are not transferred to the following rolling-horizon step. The horizon is then shifted forward by one hour and the complete procedure is repeated.

Relationship between the Two Energy-Management Frameworks

The two energy-management approaches are applied to the same industrial case study and share the main physical component characteristics and input datasets. Where possible, consistent physical parameters are adopted for the PEM electrolyzer, hydrogen compression system, and hydrogen storage system. The same PEM degradation formulation is also applied in both frameworks, with the degradation state determined from the cumulative operating time of the electrolyzer.

However, the two approaches are developed for different analytical purposes and retain important differences associated with their respective energy-management formulations. In particular, they differ in temporal resolution, control logic, optimization horizon, representation of selected energy flows and storage operation, and strategy-specific operating constraints.

A key methodological difference concerns the interaction between PEM degradation and the energy-management strategy. In the rule-based framework, degradation is evaluated under a frozen-dispatch assumption: the degraded PEM model is evaluated at the electrical operating points determined using the fresh PEM model, without modifying the controller decisions. In the optimization-based framework, degradation-dependent PEM performance is instead iteratively fed back into the EMS, allowing changes in PEM performance to affect the electrical energy required for hydrogen production and, consequently, the optimized system dispatch.

The two frameworks should therefore be interpreted as distinct but complementary stages of the analysis rather than as alternative implementations of the same energy-management strategy. Al-

though they share the same industrial application and several common physical assumptions, each framework addresses a different aspect of the overall analysis through its specific formulation and system boundaries. These differences are therefore taken into account when interpreting the respective results.

3.7 Performance Assessment Methodology

The performance of the investigated system is assessed through a set of technical, energetic, economic, and environmental indicators. A consistent set of performance indicators is adopted where applicable, while framework-specific indicators are introduced when required by the different energy-management formulations.

Since the two numerical frameworks operate at different temporal resolutions, namely 15 min for the rule-based strategy and 1 h for the optimization-based EMS, cumulative energy quantities are evaluated over the complete simulation period according to

$$E = \sum_{k=1}^{N} P_k \Delta t, \tag{3.113}$$

where Δt is the timestep adopted by the corresponding simulation. This formulation is used to evaluate the cumulative energy flows reported in the following analyses.

Technical and Energy Performance Indicators

The utilization of the PEM electrolyzer is characterized through its cumulative operating time, considering only the intervals during which hydrogen production is active:

$$t_{\mathrm{op}} = \sum_{k=1}^{N} \delta_{\mathrm{PEM},k} \Delta t, \tag{3.114}$$

where $\delta_{\mathrm{PEM},k} = 1$ when the electrolyzer is operating and $\delta_{\mathrm{PEM},k} = 0$ otherwise.

The total electrical energy consumed by the PEM, E_{PEM}, is obtained using Equation 3.113. Electrolyzer utilization is further characterized through the capacity factor

$$CF_{\mathrm{PEM}} = \frac{E_{\mathrm{PEM}}}{P_{\mathrm{PEM,rated}} T_{\mathrm{sim}}}, \tag{3.115}$$

and the equivalent full-load hours

$$FLH_{\mathrm{PEM}} = \frac{E_{\mathrm{PEM}}}{P_{\mathrm{PEM,rated}}}. \tag{3.116}$$

The capacity factor expresses the average utilization of the installed PEM capacity over the simulation period, while the equivalent full-load hours represent the corresponding annual electrical utilization in rated-power-equivalent hours.

The hydrogen storage system is assessed through the evolution of its normalized storage state and

the energy flows exchanged with the tank. The storage state is represented by the Level of Hydrogen (LOH) in the rule-based framework and by the State of Charge (SOC) in the optimization-based EMS.

Cumulative quantities are also evaluated for storage charging and discharging, compressor electricity consumption, photovoltaic utilization, grid electricity import, and natural-gas consumption, where applicable.

The allocation of electricity sources is interpreted according to the electrical-balance formulation of each framework. In the rule-based strategy, electricity supplied specifically to the PEM can be attributed to photovoltaic generation or grid electricity, allowing the corresponding renewable and grid shares of PEM consumption to be evaluated. In the optimization-based EMS, photovoltaic generation and grid electricity instead supply a common electrical balance and are therefore assessed at system level rather than explicitly allocated to individual electrical loads.

Hydrogen Performance Indicators

The total hydrogen production over the simulation period is evaluated as

$$m_{\mathrm{H_2,prod}} = \sum_{k=1}^{N} \dot{m}_{\mathrm{H_2},k} \Delta t, \tag{3.117}$$

with the appropriate time conversion when the hydrogen mass-flow rate is expressed in $\mathrm{kg\,s^{-1}}$. The corresponding LHV-based hydrogen energy is

$$E_{\mathrm{H_2,prod}} = m_{\mathrm{H_2,prod}} LHV_{\mathrm{H_2}}. \tag{3.118}$$

The instantaneous hydrogen contribution to the furnace energy demand is defined as

$$x_{\mathrm{H_2},k} = \frac{P_{\mathrm{H_2,useful},k}}{P_{\mathrm{load,th,TOT},k}}, \tag{3.119}$$

while the overall hydrogen contribution over the complete simulation period is evaluated as

$$x_{\mathrm{H_2,overall}} = \frac{\sum_{k=1}^{N} P_{\mathrm{H_2,useful},k} \Delta t}{\sum_{k=1}^{N} P_{\mathrm{load,th,TOT},k} \Delta t}. \tag{3.120}$$

For the rule-based framework, an additional hydrogen-target coverage indicator is used:

$$C_{\mathrm{H_2}} = \frac{m_{\mathrm{H_2,supplied}}}{m_{\mathrm{H_2,target}}}. \tag{3.121}$$

This indicator quantifies the fraction of the prescribed hydrogen target that is effectively supplied. It is specific to the rule-based analysis, whereas in the optimization-based EMS the hydrogen contribution is imposed as a minimum operating constraint and may therefore be exceeded.

PEM Degradation Performance Indicators

The overall energetic performance of the PEM electrolyzer over the simulation period is characterized through its LHV-based conversion efficiency,

$$\eta_{\mathrm{PEM}} = \frac{E_{\mathrm{H_2}}}{E_{\mathrm{PEM}}}, \tag{3.122}$$

where $E_{\mathrm{H_2}}$ is the cumulative LHV-based hydrogen energy produced and E_{PEM} is the corresponding cumulative electrical energy supplied to the electrolyzer.
The specific electrical energy consumption is defined as

$$SEC_{\mathrm{PEM}} = \frac{E_{\mathrm{PEM}}}{m_{\mathrm{H_2,prod}}}, \tag{3.123}$$

and is expressed in $\mathrm{kWh\,kg^{-1}_{H_2}}$.
The degradation-related indicators are evaluated according to the different treatment of PEM ageing in the two energy-management frameworks. In the rule-based analysis, degradation is assessed under the frozen-dispatch assumption described in Section 3.5. Fresh and degraded PEM performance are therefore evaluated for the same electrical operating profile, such that

$$E_{\mathrm{PEM,fresh}} = E_{\mathrm{PEM,deg}}, \tag{3.124}$$

whereas the corresponding hydrogen production generally differs:

$$E_{\mathrm{H_2,fresh}} \neq E_{\mathrm{H_2,deg}}. \tag{3.125}$$

The relative reduction in hydrogen production due to degradation is therefore evaluated as

$$\Delta_{\mathrm{H_2,deg}} = \frac{E_{\mathrm{H_2,fresh}} - E_{\mathrm{H_2,deg}}}{E_{\mathrm{H_2,fresh}}}. \tag{3.126}$$

In the optimization-based analysis, the comparison is instead performed for the final hydrogen-output trajectory determined by the degradation-aware EMS. Fresh and degraded PEM performance are evaluated for the same hydrogen output, such that

$$E_{\mathrm{H_2,fresh}} = E_{\mathrm{H_2,deg}} = E_{\mathrm{H_2}}, \tag{3.127}$$

while the corresponding electrical energy requirements generally differ:

$$E_{\mathrm{PEM,fresh}} \neq E_{\mathrm{PEM,deg}}. \tag{3.128}$$

The corresponding fresh and degraded overall PEM efficiencies are therefore evaluated as

$$\eta_{\mathrm{fresh}} = \frac{E_{\mathrm{H_2}}}{E_{\mathrm{PEM,fresh}}}, \tag{3.129}$$

and

$$\eta_{\text{deg}} = \frac{E_{\text{H}_2}}{E_{\text{PEM,deg}}}. \tag{3.130}$$

The relative efficiency reduction due to degradation is then calculated as

$$\Delta\eta_{\text{deg}} = \frac{\eta_{\text{fresh}} - \eta_{\text{deg}}}{\eta_{\text{fresh}}}, \tag{3.131}$$

while the additional electrical energy required under degraded conditions for the same hydrogen-output trajectory is evaluated as

$$\Delta E_{\text{PEM,deg}} = E_{\text{PEM,deg}} - E_{\text{PEM,fresh}}. \tag{3.132}$$

The latter quantities represent a comparison of fresh and degraded PEM conversion performance at the operating points associated with the final degradation-aware EMS dispatch and do not correspond to two independently optimized system dispatches.

Economic and Environmental Performance Indicators

The economic assessment considers the cumulative operating costs associated with grid electricity and natural-gas consumption, together with the corresponding carbon-related cost contributions. The total energy cost is evaluated as

$$C_{\text{energy}} = C_{\text{grid}} + C_{\text{NG}}, \tag{3.133}$$

while the total carbon-related cost is given by

$$C_{\text{em}} = C_{\text{em,grid}} + C_{\text{em,NG}}. \tag{3.134}$$

The resulting total operating cost considered in the economic assessment is therefore

$$C_{\text{tot}} = C_{\text{energy}} + C_{\text{em}}. \tag{3.135}$$

Operational emissions are evaluated separately by considering direct CO_2 emissions associated with natural-gas consumption and indirect CO_2-equivalent emissions associated with electricity imported from the grid. The corresponding emission factors and carbon-cost coefficients are specified in the case-study parameters.

The same categories of energy and carbon-related contributions are considered in both energy-management frameworks, although their role differs. In the rule-based analysis, economic and environmental quantities are evaluated after the operating decisions have been determined. In the optimization-based EMS, the corresponding cost terms are included directly in the objective function and therefore influence the resulting system dispatch.

Economic and environmental performance is assessed within each framework relative to its corresponding 100% natural-gas baseline. Differences in system boundaries and electrical loads between the two formulations are taken into account when interpreting the respective results.

4. Case Study and Results

4.1 Simulation Setup

4.1.1 Simulation Parameters

The numerical simulations presented in this chapter are performed using the modelling framework described in Chapter 3. Since the mathematical formulation of the individual system components has already been presented in detail, this section focuses on the definition of the case study and the numerical parameters adopted in the simulations.
The analysis is based on an existing industrial glass manufacturing plant located in Slovenia. The annual furnace demand, photovoltaic generation, electricity-price, and natural-gas-price profiles employed in the simulations are based on data provided by the industrial company.
The following subsections first present the parameters adopted for the rule-based analysis, which is used to investigate different hydrogen-substitution scenarios. The optimization-based analysis is then defined separately in Section 4.3. The two frameworks are applied to the same industrial application and share selected input data and physical parameters where applicable, while retaining the modelling features, framework-specific parameters, and system boundaries associated with each formulation.

General Simulation and Plant Parameters

The main parameters defining the rule-based simulation are reported in Table 4.1. The simulation maintains the 15-minute temporal resolution of the original input data.

Table 4.1: General plant and simulation parameters adopted in the rule-based implementation.

Parameter	**Symbol**	**Value**
Simulation timestep	Δt	15 min
Number of simulated timesteps	N_{step}	35 136 = 1 year
Hydrogen lower heating value	LHV_{H_2}	33.33 kWh kg^{-1}
Burner thermal efficiency	η_{bur}	0.98
Maximum grid-based tank charging rate	$\dot{m}_{\text{H}_2,\text{grid,max}}$	15 kg h^{-1}
Grid carbon-intensity factor	EF_{grid}	0.173 kgCO_2eq kWh^{-1}
Carbon price	c_{CO_2}	0.07343 EUR kgCO_2^{-1}

The grid carbon-intensity factor is based on the average electricity-generation carbon intensity reported for Slovenia in 2025 [36], while the adopted carbon price corresponds to the average EU ETS auction price for 2025 reported in [37].
The maximum grid-based tank charging rate represents a control parameter of the rule-based strategy rather than a physical limitation of the storage system. A sensitivity analysis was performed by increasing this limit from 15 to 20 and 30 kg h^{-1}. Higher values mainly increased grid-based

hydrogen production and the associated electricity consumption, costs, and emissions, without improving hydrogen-target coverage or significantly affecting the main annual performance indicators. Therefore, a value of 15 $\mathrm{kg\,h^{-1}}$ was retained for the rule-based simulations.

PEM Electrolyzer Parameters

The main electrochemical, geometrical, and operating parameters adopted for the PEM electrolyzer are reported in Table 4.2.

Table 4.2: Main parameters adopted in the PEM electrochemical model.

Parameter	**Symbol**	**Value**
Number of cells	N_{cells}	670
Active cell area	A_{cell}	1000 $\mathrm{cm^2}$
Rated power	$P_{\mathrm{PEM,rated}}$	2.5 MW
Maximum current density	i_{max}	2.5 $\mathrm{A\,cm^{-2}}$
Operating temperature	T	60°C
Hydrogen pressure	$p_{\mathrm{H_2}}$	30 bar
Oxygen pressure	$p_{\mathrm{O_2}}$	30 bar
Anodic charge-transfer coefficient	α_{a}	2.0
Cathodic charge-transfer coefficient	α_{c}	0.5
Anodic exchange-current density	$i_{0,\mathrm{a}}$	2×10^{-7} $\mathrm{A\,cm^{-2}}$
Cathodic exchange-current density	$i_{0,\mathrm{c}}$	2×10^{-3} $\mathrm{A\,cm^{-2}}$
Membrane thickness	t_{mem}	0.018 cm
Membrane water content	λ_{mem}	21
Contact resistance	R_{contact}	0.02 $\Omega\,\mathrm{cm^2}$
Anodic limiting-current density	$i_{\mathrm{lim,a}}$	3 $\mathrm{A\,cm^{-2}}$
Cathodic limiting-current density	$i_{\mathrm{lim,c}}$	3 $\mathrm{A\,cm^{-2}}$

The same electrochemical model and parameterization are adopted in both energy-management frameworks. However, its integration within the control strategy differs between the rule-based and optimization-based implementations, as described in Chapter 3.

Hydrogen Compressor Unit

In the rule-based implementation, the compression process is described by the three-stage thermodynamic model introduced in Chapter 3. The main operating and design parameters adopted for the compressor are reported in Table 4.3.

Table 4.3: Main parameters adopted in the hydrogen compression model.

Parameter	Symbol	Value
Inlet pressure	p_{in}	30 bar
Outlet pressure	p_{out}	350 bar
Number of compression stages	N_{stages}	3
Intercooling temperature	T_{int}	60°C
Isentropic efficiency	η_{is}	0.75
Motor efficiency	η_{motor}	0.95
Rated compressor power	$P_{\text{comp,rated}}$	298 kW

Hydrogen Storage Unit

In Table 4.4 are reported the main parameters adopted for the hydrogen storage system.

Table 4.4: Main parameters adopted in the hydrogen storage model.

Parameter	Symbol	Value
Rated hydrogen capacity	$m_{\text{H}_2,\text{rated}}$	100 kg
Minimum storage level	LOH_{min}	0.10
Maximum storage level	LOH_{max}	0.90
Initial storage level	LOH_0	0.50
Charging efficiency	η_{ch}	1.0
Discharging efficiency	η_{dis}	1.0

The rated hydrogen storage capacity is set to 100 kg. Using the hydrogen lower heating value adopted in the model, this corresponds to an energy capacity of approximately 3333 kWh_{H_2}. The usable storage range extends from 10% to 90% of the rated capacity, while the initial hydrogen inventory is set to 50%. Charging and discharging losses are neglected in the adopted storage model.

4.1.2 Investigated Scenarios

The simulation campaign performed in this work is divided into two stages. The first stage consists of the assessment of the rule-based control strategy under different hydrogen-substitution targets, whereas the second stage focuses on the integration of the detailed PEM electrochemical and degradation models into an existing optimization-based Energy Management System (EMS) and on the evaluation of the resulting system operation.

For the rule-based analysis, five operating scenarios are investigated by progressively increasing the target hydrogen contribution to the thermal demand of the industrial furnace. The analysed hydrogen shares are equal to 5%, 10%, 15%, 20%, and 25%. This parametric analysis assesses the system's ability to accommodate increasing hydrogen penetration and its effects on the operation of the integrated PV–PEM–storage system.

The optimization-based EMS is evaluated by imposing a minimum hydrogen contribution of 5% of the furnace thermal demand. This value corresponds to the lowest hydrogen-substitution target

investigated in the rule-based analysis. However, the 5% value has a different role in the two formulations: it represents a target in the rule-based framework, whereas it is imposed as a minimum constraint in the optimization-based EMS and may therefore be exceeded.

4.2 Rule-Based Energy Management Results

The rule-based energy management framework is evaluated for the five hydrogen-share targets defined in Section 4.1, with the aim of assessing the capability of the considered system configuration to accommodate progressively increasing hydrogen substitution and identifying the resulting technical limitations of the integrated PV–PEM–storage system.

4.2.1 Scenario-Specific Operating Behaviour

5% Hydrogen-Share Scenario

The 5% hydrogen-share scenario represents the least demanding operating condition considered in the rule-based analysis and is therefore examined in greater detail to illustrate the operating behaviour of the integrated PV–PEM–compression–storage system.
Under this operating condition, the prescribed hydrogen requirement is fully satisfied over the complete simulation period. No timestep in which the target is not met is observed and the annual hydrogen-target coverage is equal to 100%.

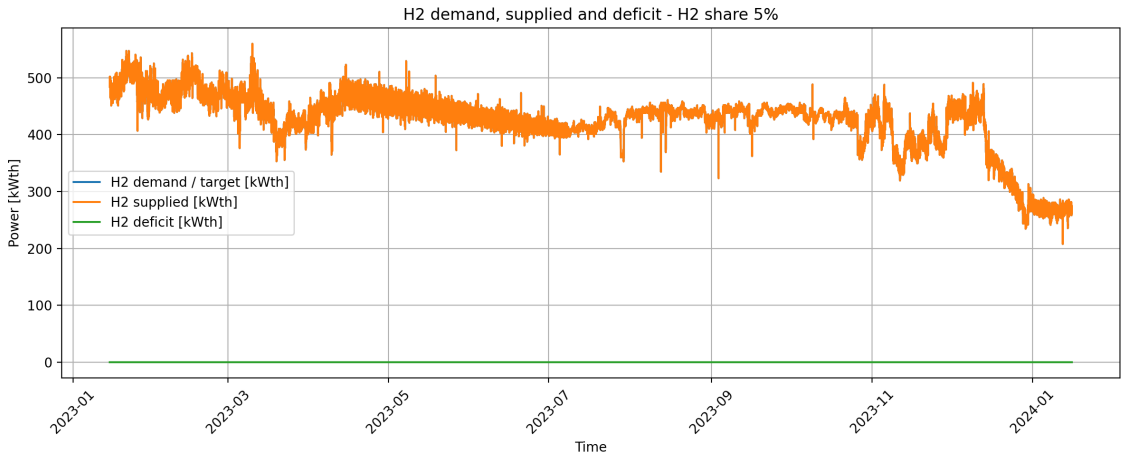


Figure 4.1: Hydrogen demand and hydrogen supplied to the furnace for the 5% hydrogen-share scenario.

As shown in Figure 4.1, the two profiles overlap throughout the complete simulated period, confirming continuous fulfilment of the prescribed 5% hydrogen contribution and resulting in an annual hydrogen supply of approximately 114.0 t, with negligible unmet demand. Consequently, no additional natural-gas fallback is required.
The complete fulfilment of the hydrogen target indicates that the installed PEM electrolyzer retains production margin under this operating condition.

The electrical operation of the hydrogen-production system during the selected period is shown in Figure 4.2.

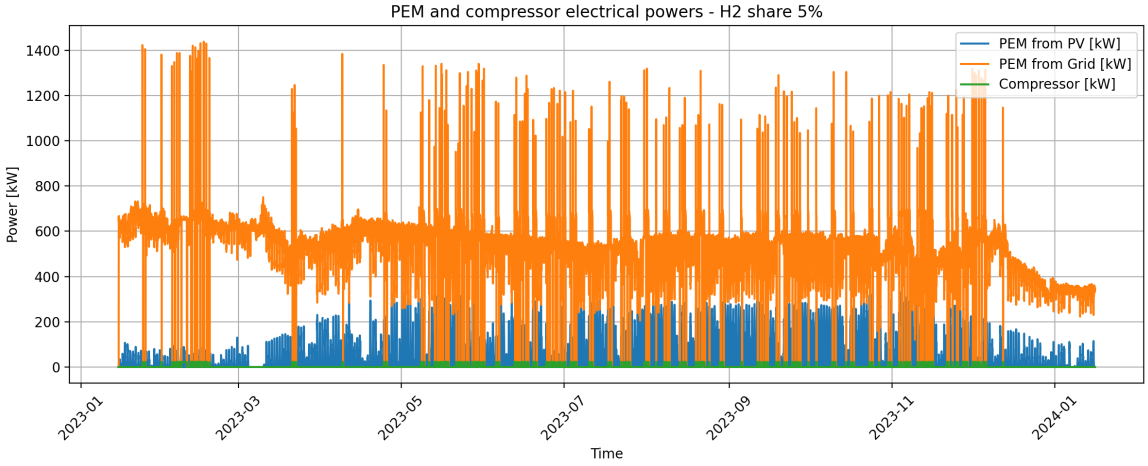


Figure 4.2: Electrical power balance during the selected operating period for the 5% hydrogen-share scenario.

The PEM operates over a broad load range and remains below its rated electrical power throughout the simulation. The maximum stack power reaches approximately 1.44 MW, corresponding to about 57.5% of the 2.5 MW rated capacity. No timestep is therefore affected by PEM power saturation. The annual electrical energy consumed by the PEM is approximately 4.91 GWh. Photovoltaic generation is prioritized by the controller whenever it is available, thereby reducing the electricity imported from the grid. Nevertheless, PV generation supplies only about 7.33% of the annual PEM electricity demand, whereas the remaining 92.67% is supplied by the grid. This low renewable fraction is not caused by significant photovoltaic curtailment, since approximately 99.95% of the available PV generation is utilized over the year. It instead reflects the relatively small annual PV energy availability compared with the electrical energy required for hydrogen production.
The available PEM production margin also allows the hydrogen storage unit to actively contribute to system operation. Its annual evolution is shown in Figure 4.3.

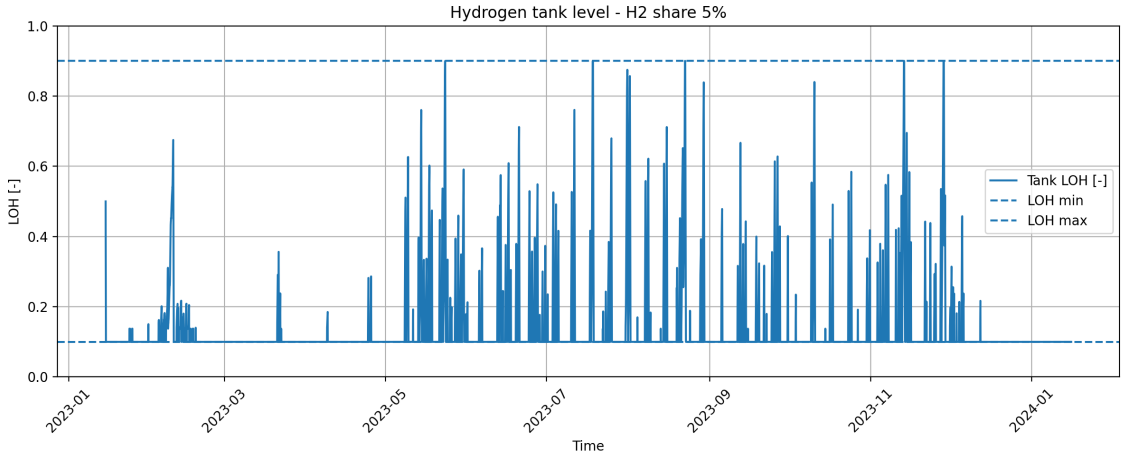


Figure 4.3: Level of Hydrogen in the storage unit for the 5% hydrogen-share scenario.

The LOH varies between 0.10 and 0.90, spanning the complete admissible operating range of the storage system. Starting from the initial LOH of 0.50, the storage level rapidly decreases towards its minimum admissible value as the hydrogen initially available in the tank is used to satisfy the furnace demand. During the subsequent operation, hydrogen produced in excess of the instantaneous furnace requirement is compressed and stored, while stored hydrogen is discharged when required by the rule-based control strategy. The repeated variation across a large fraction of the admissible storage range indicates that sufficient PEM production margin is available to periodically generate hydrogen in excess, allowing the storage system to redistribute hydrogen production over time.
Approximately 16.0 t of hydrogen are directed to storage over the year. The associated annual compressor electricity consumption is approximately 23.8 MWh and therefore remains small compared with the PEM electricity consumption.
The main electrochemical operating quantities reached by the PEM are summarized in Table 4.5.

Table 4.5: PEM operating range obtained in the 5% hydrogen-share scenario.

Operating quantity	**Observed range**
Current density	0–1.227 A cm^{-2}
Fresh PEM energy efficiency	0.717–0.959
PEM stack power	0–1437.79 kW
Fresh hydrogen production	0–30.910 kg h^{-1}
Target-not-met timesteps	0

The reported operating ranges confirm that the electrolyzer remains below both its maximum current-density and rated-power limits. The variation in fresh PEM efficiency reflects the non-linear electrochemical behaviour of the electrolyzer and its dependence on the instantaneous operating point.
The effect of PEM degradation is analysed using the frozen-dispatch approach described in Section 3.4. The electrical operating profile selected by the rule-based controller is maintained unchanged, while the same electrical operating points are evaluated using the fresh and degradation-adjusted PEM models, whose efficiency profiles are compared in Figure 4.4.

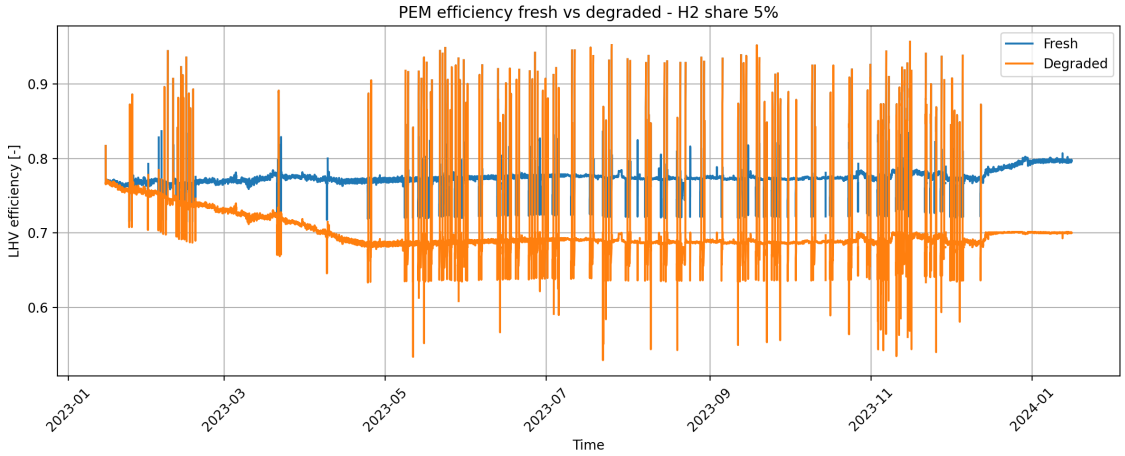


Figure 4.4: Fresh and degradation-adjusted PEM LHV efficiencies for the 5% hydrogen-share scenario.

Both efficiency profiles vary with the PEM operating point, while the degradation-adjusted efficiency is generally lower than the corresponding fresh value. Since the electrical dispatch is kept fixed in this assessment, degradation does not change the electrical power assigned to the PEM. Instead, it reduces the amount of hydrogen produced from the same electrical input.

Under the frozen-dispatch assessment, degradation reduces the annual hydrogen production from the approximately 114.0 t obtained with the fresh PEM model to approximately 103.1 t under the same electrical operating profile. This corresponds to a reduction of approximately 9.5%. The same effect is reflected in the equivalent specific electrical energy consumption.

The same effect is reflected in the equivalent specific electrical energy consumption. The fresh PEM SEC is approximately 43.1 $\mathrm{kWh\,kg_{H_2}^{-1}}$, whereas the degradation-adjusted value is approximately 47.6 $\mathrm{kWh\,kg_{H_2}^{-1}}$. The increase in SEC therefore expresses the lower hydrogen output obtained per unit of electrical energy under degraded PEM performance; it does not represent an actual increase in PEM electricity consumption in the frozen-dispatch simulation.

The annual PEM capacity factor is approximately 22.4%, corresponding to about 1964 equivalent full-load hours. These utilization indicators are consistent with the substantial unused PEM capacity observed in the instantaneous power profile.

Overall, the 5% hydrogen-share scenario represents an operating condition in which system capacity does not limit the required hydrogen contribution. The prescribed hydrogen contribution is continuously satisfied, the PEM retains substantial unused production capacity, and the storage system can exploit its complete admissible operating range. At the same time, hydrogen production remains strongly dependent on grid electricity because the available photovoltaic generation is small relative to the PEM electrical demand.

10% Hydrogen-Share Scenario

The 10% hydrogen-share scenario doubles the target hydrogen contribution compared with the 5% case. Despite the increased hydrogen demand, the installed PEM electrolyzer retains sufficient production capability to satisfy the target throughout the complete simulation period. The resulting hydrogen demand and supply profiles are shown in Figure 4.5.

As in the 5% scenario, the demand and supply profiles overlap throughout the simulation. No target-not-met timestep is observed and the annual hydrogen-target coverage remains equal to 100%. The complete fulfilment of the hydrogen target therefore eliminates the need for additional natural-gas fallback. The total hydrogen supplied to the furnace increases to approximately 228.0 t over the simulated year.

The higher hydrogen demand substantially increases PEM utilization. The maximum stack power reaches approximately 2.32 MW, corresponding to about 92.7% of the 2.5 MW rated capacity. Although the electrolyzer therefore operates considerably closer to its capacity limit than in the 5% case, the rated-power constraint is never reached.

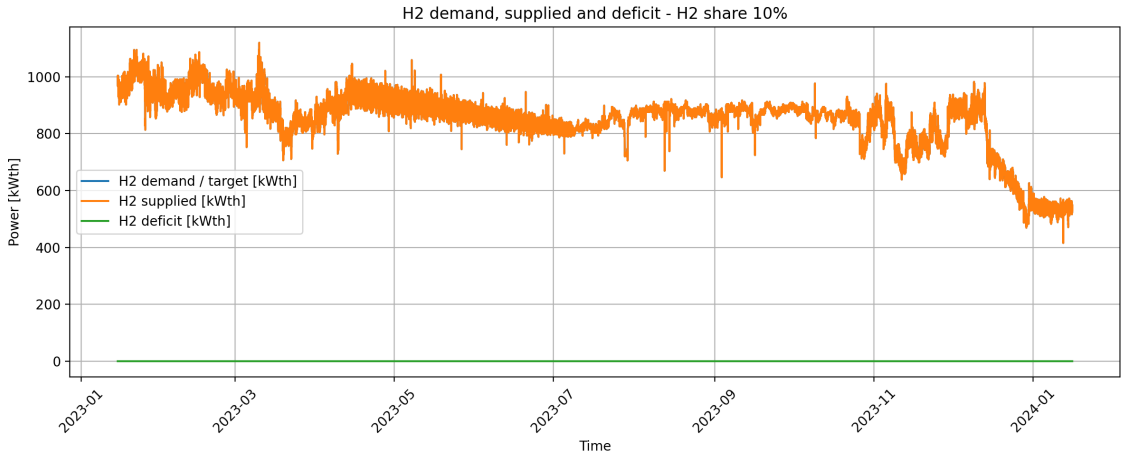


Figure 4.5: Hydrogen demand and hydrogen supplied to the furnace for the 10% hydrogen-share scenario.

Annual PEM electricity consumption increases to approximately 10.41 GWh. Since almost all the available photovoltaic generation is already utilized, the additional PEM electricity demand is supplied predominantly by the grid. The renewable share of PEM electricity consequently decreases from 7.33% in the 5% scenario to approximately 3.46%, while grid electricity accounts for the remaining 96.54%.

The increased hydrogen requirement also modifies storage operation. Figure 4.6 shows the corresponding evolution of the Level of Hydrogen.

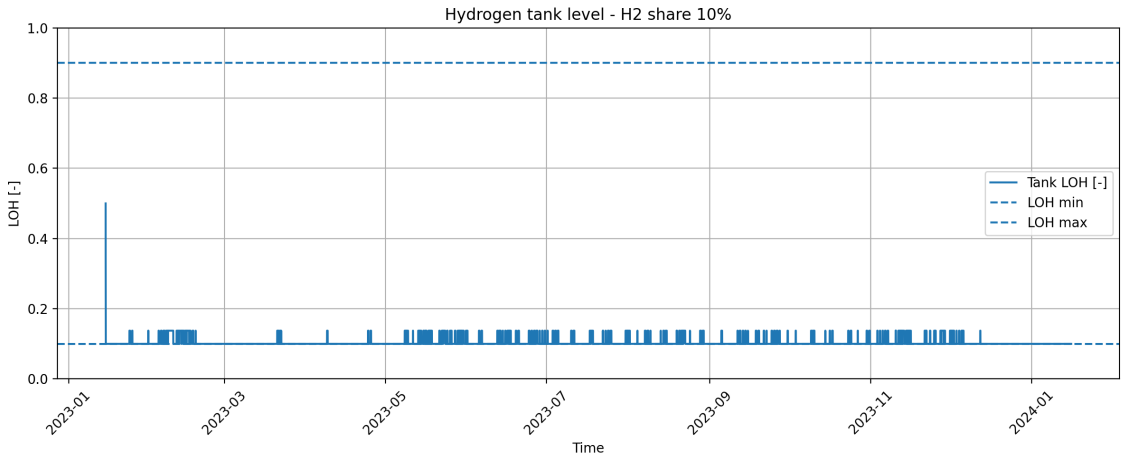


Figure 4.6: Level of Hydrogen in the storage unit for the 10% hydrogen-share scenario.

The storage starts from the initial LOH of 0.50 and rapidly decreases to the lower operating region during the initial simulation steps. After this initial transient, the LOH remains between 0.10 and approximately 0.138 throughout the remainder of the simulation. Compared with the 5% scenario, in which the storage reaches the upper operating limit of 0.90, the 10% case therefore exhibits a substantially narrower storage operating range. This indicates that a larger fraction of the hydrogen produced by the PEM is required directly by the furnace, reducing the production margin available for storage charging. Nevertheless, approximately 16.1 t of hydrogen are directed to storage over

the year. The associated annual compressor electricity consumption is approximately 23.8 MWh. The higher PEM utilization compared with the 5% scenario is also reflected in the electrochemical operating range reported in Table 4.6. Reported values are rounded to the displayed precision.

Table 4.6: PEM operating range obtained in the 10% hydrogen-share scenario.

Operating quantity	**Observed range**
Current density	0.192–1.858 A cm^{-2}
Fresh PEM energy efficiency	0.674–0.819
PEM stack power	196.4–2316.5 kW
Fresh hydrogen production	4.83–46.82 kg h^{-1}
Target-not-met timesteps	0

Compared with the 5% scenario, the PEM operates at substantially higher loads and approaches its rated electrical power. The corresponding LHV efficiency range is shifted towards lower values, consistently with the higher current densities reached by the electrolyzer and the resulting increase in electrochemical losses.

The effect of degradation is again evaluated under the frozen-dispatch assumption. For the same electrical operating profile, annual hydrogen production decreases from approximately 228.0 t under fresh conditions to 205.2 t with degradation-adjusted PEM performance, corresponding to a reduction of approximately 10.0%.

The equivalent specific electrical energy consumption thus increases from approximately 45.7 kWh $kg_{H_2}^{-1}$ under fresh conditions to 50.7 kWh $kg_{H_2}^{-1}$ under degraded conditions. As in the 5% scenario, this increase results from the lower hydrogen production obtained for the same electrical dispatch and does not represent an increase in the electricity actually assigned to the PEM.

The annual PEM capacity factor increases from approximately 22.4% in the 5% scenario to about 47.4%, corresponding to approximately 4163 equivalent full-load hours. The 10% scenario therefore still represents a capacity-unconstrained operating condition, achieving complete hydrogen-target coverage without reaching the PEM rated-power constraint, although the electrolyzer operates substantially closer to its capacity limit than in the 5% case.

15% Hydrogen-Share Scenario

The 15% hydrogen-share scenario represents the transition towards capacity-limited operation. Compared with the 10% case, the higher hydrogen requirement substantially increases PEM utilization and, for the first time, causes the electrolyzer to reach its imposed rated-power limit of 2.5 MW.

Despite the occurrence of capacity-limited operation, the prescribed hydrogen contribution remains essentially fully satisfied. Only four 15-minute timesteps are characterized by a residual hydrogen deficit, corresponding to 0.011% of the simulated timesteps. The resulting annual hydrogen-target coverage is approximately 99.9998%. The hydrogen demand, supply, and residual deficit profiles are shown in Figure 4.7.

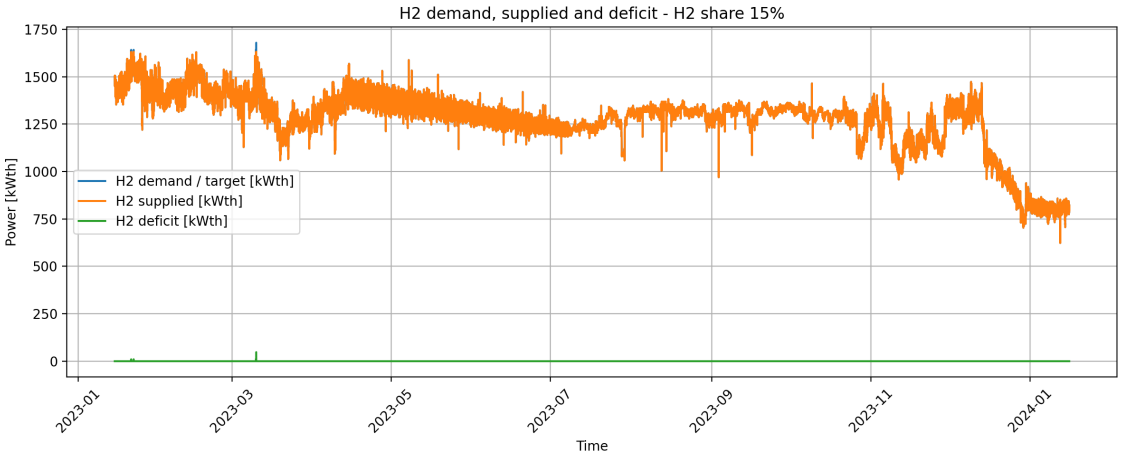


Figure 4.7: Hydrogen demand, supplied hydrogen, and residual deficit for the 15% hydrogen-share scenario.

The supplied hydrogen follows the prescribed demand throughout almost the complete simulation period. The total hydrogen supplied to the furnace is approximately 342.0 t, while the annual unmet hydrogen demand amounts to only about 0.62 kg. The additional natural-gas fallback required to compensate for this deficit is therefore negligible at the annual scale. Nevertheless, the appearance of the first target-not-met timesteps indicates that the available PEM and storage flexibility is no longer sufficient under every instantaneous operating condition.

The PEM operates considerably closer to its rated capacity than in the lower-share scenarios. Annual PEM electricity consumption increases to approximately 16.96 GWh and the rated power of 2.5 MW is reached during approximately 10.83% of the simulated timesteps. Once this limit is reached, the controller cannot further increase PEM production in response to an increase in the instantaneous hydrogen requirement.

The increasing electrical demand also further reduces the relative contribution of photovoltaic generation. The renewable share of PEM electricity decreases to approximately 2.12%, while grid electricity provides the remaining 97.88%. As in the previous scenarios, approximately 99.95% of the available photovoltaic generation is utilized.

The transition towards capacity-limited operation also substantially changes the role of the hydrogen storage system, whose LOH evolution is shown in Figure 4.8.

Starting from an initial LOH of 0.50, the storage level decreases rapidly and subsequently remains between 0.10 and approximately 0.138. Only approximately 1.81 t of hydrogen are directed to storage over the year, compared with approximately 16.1 t in the 10% scenario. The associated compressor electricity consumption consequently decreases to approximately 2.69 MWh.

This sharp reduction in storage charging indicates that most of the hydrogen produced by the PEM is now required directly by the furnace, leaving little production surplus available for storage. The tank can still provide short-term buffering using the available hydrogen inventory, but its ability to compensate for persistent production shortages is limited by the reduced opportunity for subsequent recharging.

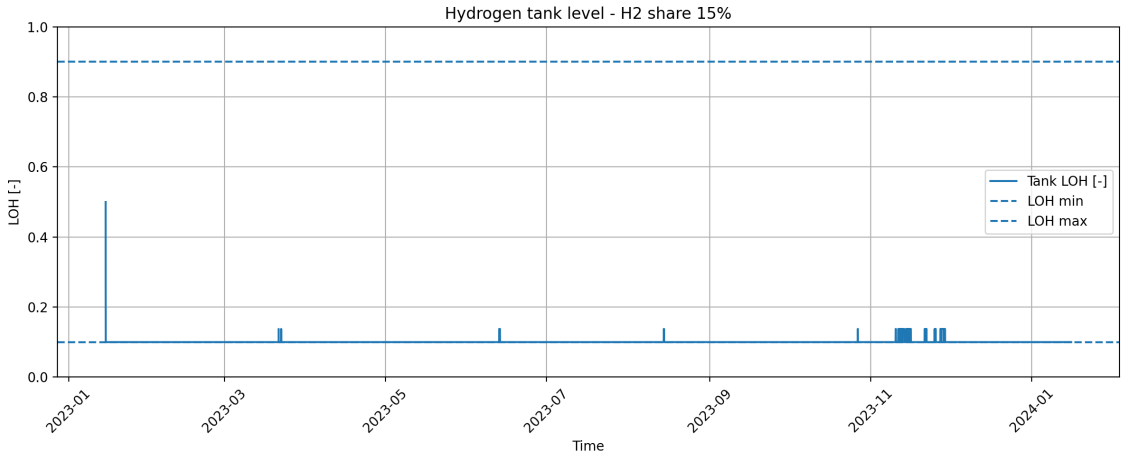


Figure 4.8: Level of Hydrogen in the storage unit for the 15% hydrogen-share scenario.

The electrochemical operating range reached by the PEM is summarized in Table 4.7.

Table 4.7: PEM operating range obtained in the 15% hydrogen-share scenario.

Operating quantity	**Observed range**
Current density	0.585–1.982 A cm^{-2}
Fresh PEM energy efficiency	0.666–0.770
PEM stack power	638.0–2500 kW
Fresh hydrogen production	14.74–49.94 kg h^{-1}
PEM saturation	10.83% of simulated timesteps
Target-not-met timesteps	4

The operating range confirms the substantial increase in PEM utilization. In contrast with the 5% and 10% scenarios, the electrolyzer now reaches its rated electrical power and its maximum current density approaches 2 A cm^{-2}. The fresh LHV efficiency range also shifts towards lower values as PEM operation becomes increasingly concentrated at higher electrical loads.

The effect of PEM degradation remains significant under the same frozen-dispatch assessment adopted in the previous scenarios. Annual hydrogen production decreases from approximately 350.7 t under fresh conditions to 315.6 t with degradation-adjusted PEM performance, corresponding to a reduction of approximately 10.0%.

The equivalent specific electrical energy consumption thus increases from approximately 48.35 kWh $\mathrm{kg}_{\mathrm{H_2}}^{-1}$ under fresh conditions to 53.73 kWh $\mathrm{kg}_{\mathrm{H_2}}^{-1}$ under degraded conditions.

The annual PEM capacity factor increases to approximately 77.2%, corresponding to about 6784 equivalent full-load hours. The electrolyzer is therefore utilized much more intensively than in the 5% and 10% scenarios.

Overall, the 15% hydrogen-share scenario marks the transition to capacity-limited operation. The PEM reaches its rated power, storage charging decreases sharply, and the first hydrogen deficits appear. However, their magnitude remains negligible at the annual scale, with a hydrogen-target coverage of approximately 99.9998%. The 15% case can therefore be regarded as the highest investigated hydrogen-share target that is achieved with nearly complete annual demand coverage

under the adopted system configuration.

20% Hydrogen-Share Scenario

Increasing the target hydrogen contribution to 20% produces a clear change in the operating behaviour of the rule-based system. While the 15% scenario marks the onset of capacity-limited operation, at 20% the PEM rated-power constraint becomes a dominant operating condition and the prescribed hydrogen requirement can no longer be continuously satisfied.
Figure 4.9 compares the hydrogen demand with the hydrogen effectively supplied to the furnace and the corresponding residual deficit.

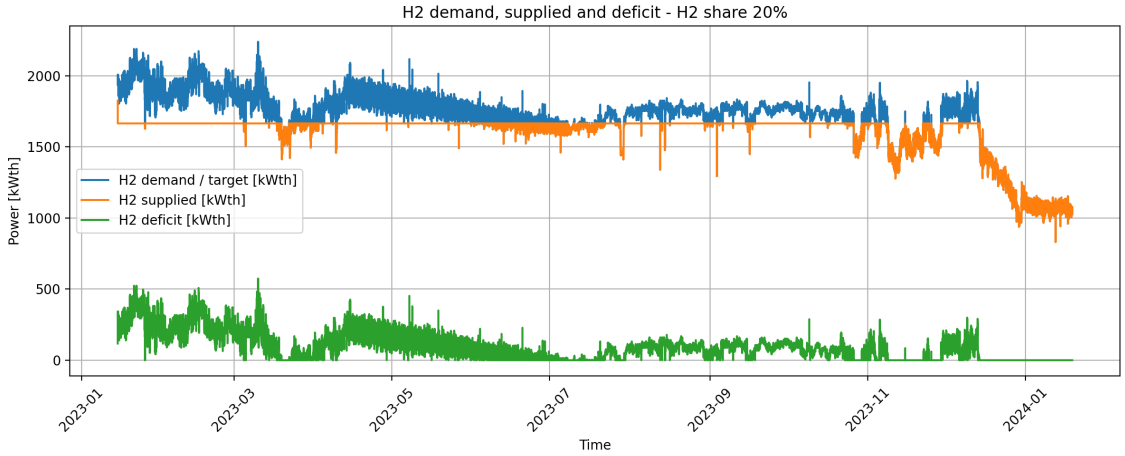


Figure 4.9: Hydrogen demand, supplied hydrogen, and residual deficit for the 20% hydrogen-share scenario.

Unlike the lower-share scenarios, the hydrogen supplied to the furnace no longer continuously follows the prescribed demand. A hydrogen deficit is observed during 28 028 timesteps, corresponding to approximately 79.77% of the simulated timesteps. The annual hydrogen-target coverage consequently decreases to approximately 93.12%, with a total unmet hydrogen demand of approximately 31.4 t.
The total hydrogen supplied to the furnace is approximately 424.7 t over the year. During the deficit periods, the missing thermal contribution is provided by natural gas in order to preserve the required furnace thermal balance. As a result, the effective annual hydrogen contribution is approximately 18.62% of the furnace useful thermal demand, below the 20% target.
The inability to continuously satisfy the hydrogen requirement is primarily associated with the installed PEM capacity. The electrolyzer reaches its rated electrical power of 2.5 MW during approximately 81.63% of the simulated timesteps, compared with 10.83% in the 15% scenario. Once this limit is reached, hydrogen production cannot be further increased even when additional grid electricity is available.
Annual PEM electricity consumption increases to approximately 21.20 GWh. The renewable contribution represents only approximately 1.70% of the PEM electricity supply, while grid electricity

accounts for approximately 98.30%. Photovoltaic curtailment remains negligible, with approximately 99.95% of the available PV generation utilized over the simulated year.
The persistent operation close to the PEM rated capacity also changes the role of hydrogen storage. Figure 4.10 shows the corresponding evolution of the Level of Hydrogen.

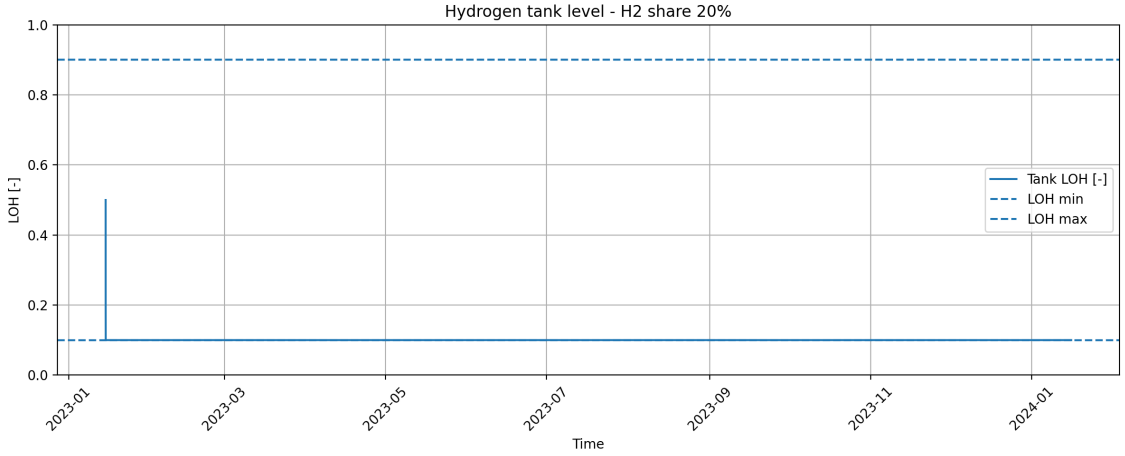


Figure 4.10: Level of Hydrogen in the storage unit for the 20% hydrogen-share scenario.

Starting from the initial LOH of 0.50, the storage level rapidly decreases to its minimum admissible value of 0.10 and remains close to this limit for almost the entire simulation period. In contrast with the lower-share scenarios, no significant hydrogen production surplus is available for storage charging, and the amount of hydrogen transferred to storage over the year is consequently negligible. Compressor electricity consumption also becomes negligible. The storage system therefore loses most of the buffering function observed at lower hydrogen shares, since persistent PEM saturation prevents the generation of the surplus hydrogen required for tank recharging.
The high utilization of the PEM also produces a markedly different electrochemical operating profile. Figure 4.11 compares the fresh and degradation-adjusted LHV efficiencies evaluated under the frozen-dispatch assumption.

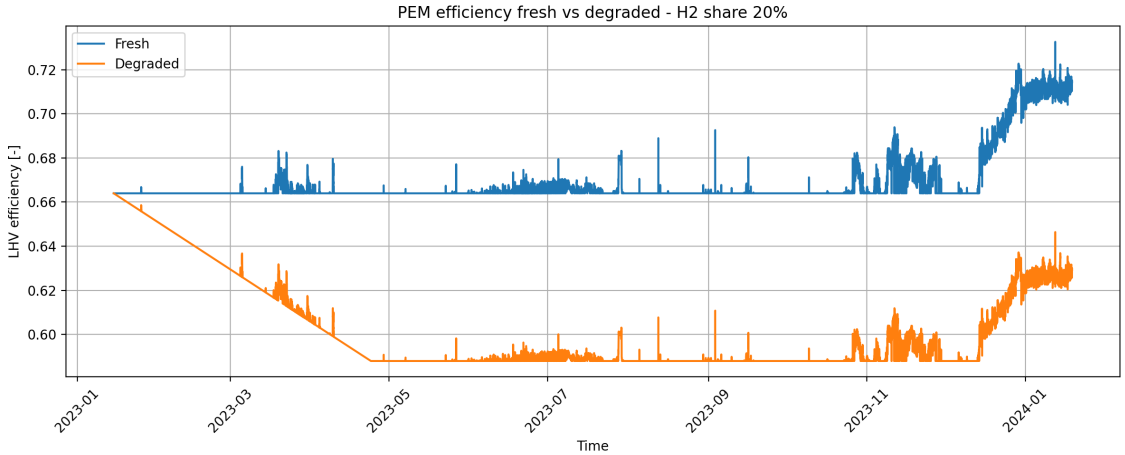


Figure 4.11: Fresh and degradation-adjusted PEM LHV efficiencies for the 20% hydrogen-share scenario.

Compared with the lower hydrogen-share scenarios, the efficiency profiles show considerably less variation over most of the simulation period. This behaviour results from the prolonged operation of the PEM at its rated power, which concentrates the electrolyzer operation around a much narrower range of high-load operating points. The fresh LHV efficiency ranges from approximately 0.664 to 0.748, with an annual average of approximately 0.668.

At identical electrical operating points, the degradation-adjusted efficiency remains below the corresponding fresh value. Under the frozen-dispatch assessment, annual PEM hydrogen production decreases from approximately 425.2 t under fresh conditions to approximately 383.2 t with degradation-adjusted performance, corresponding to a reduction of approximately 9.88%.

The equivalent specific electrical energy consumption consequently increases from approximately 49.85 $\mathrm{kWh\,kg_{H_2}^{-1}}$ under fresh conditions to 55.31 $\mathrm{kWh\,kg_{H_2}^{-1}}$ under degraded conditions. Again, this increase reflects the lower hydrogen production obtained from the same electrical input rather than an increase in the electricity assigned to the PEM.

The annual PEM capacity factor reaches approximately 96.5%, corresponding to about 8479 equivalent full-load hours. The electrolyzer is therefore operated close to its maximum annual electrical utilization, leaving very limited scope for further hydrogen production with the installed capacity.

Overall, the 20% scenario represents a clearly established capacity-limited operating regime. Persistent PEM saturation prevents the target hydrogen contribution from being continuously achieved and simultaneously eliminates most of the production surplus required for storage charging. The annual hydrogen-target coverage decreases to approximately 93.12%, resulting in an effective hydrogen contribution of approximately 18.62%.

25% Hydrogen-Share Scenario

The 25% hydrogen-share scenario represents the most demanding operating condition investigated in the rule-based analysis. Compared with the 20% case, the hydrogen requirement increases further while the installed PEM electrolyzer and the remaining system capacities remain unchanged. The capacity limitations identified in the previous scenario therefore here become even more pronounced. Figure 4.12 compares the target hydrogen demand with the hydrogen effectively supplied to the furnace and the corresponding residual deficit. The supplied-hydrogen profile deviates substantially from the target demand over most of the simulation period, with the hydrogen target not being met during approximately 92.99% of the simulated timesteps. Consequently, the annual hydrogen-target coverage decreases to approximately 76.14%, while the total unmet hydrogen demand reaches approximately 136.0 t. The corresponding missing thermal contribution is supplied by natural gas. This behaviour is primarily associated with the almost continuous saturation of the PEM. The electrolyzer operates at its rated electrical power of 2.5 MW during approximately 92.99% of the simulated timesteps, compared with 81.63% in the 20% scenario. Additional grid-electricity availability therefore cannot produce a corresponding increase in hydrogen output, since the installed electrolyzer capacity is already fully exploited.

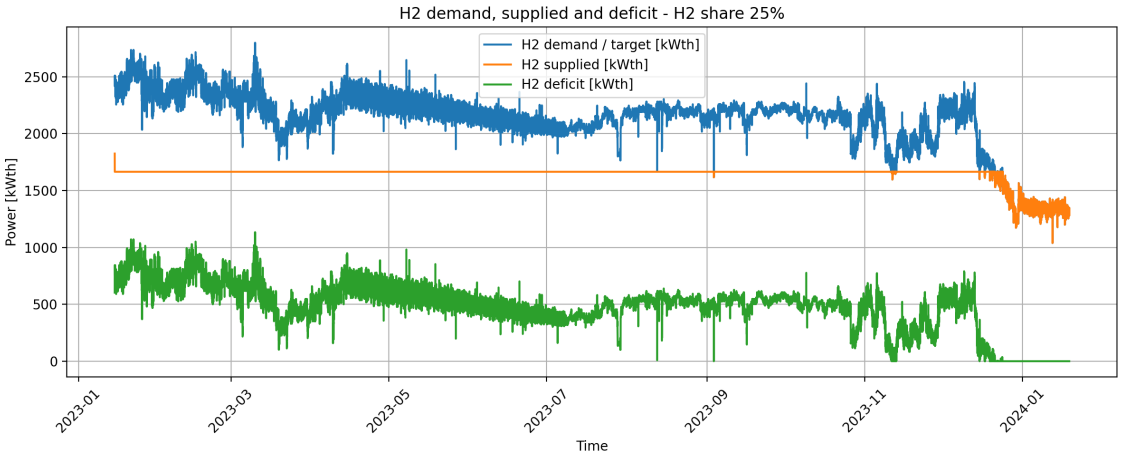


Figure 4.12: Hydrogen demand, supplied hydrogen, and residual deficit for the 25% hydrogen-share scenario.

Annual PEM electricity consumption thus increases only from approximately 21.20 GWh in the 20% scenario to 21.69 GWh at 25%, despite the five-percentage-point increase in the target hydrogen share. Grid electricity provides approximately 98.34% of the PEM electricity supply, while the renewable contribution decreases slightly to approximately 1.66%.

The annual PEM capacity factor reaches approximately 98.8%, corresponding to about 8676 equivalent full-load hours. The limited increase compared with the 20% scenario confirms that almost the entire annual production capability of the installed electrolyzer is already being exploited. Consistently, increasing the target hydrogen contribution from 20% to 25% raises the annual hydrogen supplied to the furnace only from approximately 424.7 t to 434.1 t, corresponding to an increase of about 9.4 t. The effective annual hydrogen contribution therefore increases only from approximately 18.62% to 19.04%, further indicating that the 2.5 MW PEM electrolyzer is operating close to its practical production ceiling under the adopted system configuration.

Storage operation is similarly constrained. No meaningful hydrogen surplus is available for tank charging and the associated compressor electricity consumption is therefore essentially zero. Once the initial inventory is depleted, persistent PEM saturation prevents effective replenishment of the tank.

The degradation results are consistent with the high-load operating regime already observed in the 20% scenario. Under the frozen-dispatch assessment, annual PEM hydrogen production decreases from approximately 434.0 t under fresh conditions to 391.1 t with degradation-adjusted performance, corresponding to a reduction of approximately 9.9%.

The equivalent specific electrical energy consumption increases from approximately 49.98 kWh $kg_{H_2}^{-1}$ under fresh conditions to 55.46 kWh $kg_{H_2}^{-1}$ under degraded conditions. These values are only slightly higher than those obtained in the 20% scenario, consistently with the PEM operating regime being already concentrated close to its rated-power condition.

Overall, the 25% scenario confirms the production limitation of the adopted system configuration. Increasing the target hydrogen share beyond 20% produces only a marginal increase in the hydrogen effectively supplied to the furnace, while the electrolyzer operates at rated power for almost the entire

simulation period. A substantial further increase in hydrogen substitution would therefore primarily require additional hydrogen-production capacity, since increasing storage capacity alone would provide limited benefit when practically no surplus hydrogen is available for tank replenishment.

4.2.2 Comparative Assessment of the Rule-Based Scenarios

The scenario-specific results presented in the previous sections reveal substantial changes in system operation as the target hydrogen share is progressively increased. A comparative assessment is therefore performed to identify the transition from unconstrained to capacity-limited operation and to evaluate how the main system indicators evolve as the hydrogen target increases, including hydrogen supply, PEM utilization and degradation, electrical energy requirements, storage operation, and economic and environmental performance.
The main indicators obtained for the five investigated scenarios are summarized in Table 4.8.

Table 4.8: Main indicators of the investigated rule-based scenarios.

Indicator	**5%**	**10%**	**15%**	**20%**	**25%**
H_2 target coverage [%]	100.00	100.00	99.9998	93.12	76.14
Effective annual H_2 share [%]	5.00	10.00	15.00	18.62	19.04
PEM saturation [% simulation time]	0.00	0.00	10.83	81.63	92.99
PEM capacity factor [%]	22.4	47.4	77.2	96.5	98.8
PEM electricity [GWh]	4.91	10.41	16.96	21.20	21.69
Renewable share of PEM supply [%]	7.33	3.46	2.12	1.70	1.66
Annual PEM energy efficiency, fresh [%]	77.4	73.0	68.9	66.9	66.7
Annual PEM energy efficiency, degraded [%]	70.0	65.7	62.0	60.3	60.1
Fresh SEC [kWh $kg_{H_2}^{-1}$]	43.08	45.65	48.35	49.85	49.98
Degraded SEC [kWh $kg_{H_2}^{-1}$]	47.60	50.73	53.73	55.31	55.46
Degradation-related H_2 loss [%]	9.5	10.0	10.0	9.9	9.9

The indicators identify three characteristic operating regimes. At hydrogen targets of 5% and 10%, the PEM operates below its rated capacity and the hydrogen target is fully achieved. The 15% scenario represents a transition condition: the electrolyzer reaches its rated power during part of the simulation, although hydrogen-target coverage remains essentially complete. At 20% and 25%, PEM saturation becomes a dominant operating condition and hydrogen production can no longer increase proportionally to the hydrogen target.

Hydrogen-Target Fulfilment and PEM Utilization

The first comparison concerns the capability of the rule-based strategy to provide the prescribed hydrogen contribution as the hydrogen target is progressively increased.
Complete target coverage is obtained for the 5% and 10% scenarios. The 15% scenario also maintains essentially complete coverage, equal to approximately 99.9998%, despite the first occurrence of PEM saturation. Only four simulation timesteps do not fully meet the hydrogen target, cor-

responding to an annual hydrogen deficit of approximately 0.62 kg. The initial activation of the rated-power constraint therefore has a negligible effect on annual hydrogen delivery.

A markedly different behaviour appears at higher hydrogen targets. Coverage decreases to approximately 93.12% in the 20% scenario and 76.14% in the 25% scenario. This reduction coincides with a rapid increase in PEM saturation, from 10.83% of the simulated timesteps at 15% hydrogen share to 81.63% at 20% and 92.99% at 25%. At these higher targets, the electrolyzer therefore operates at its rated power for most of the simulation, while its maximum hydrogen-production capacity is no longer sufficient to fully meet the required hydrogen demand.

The same transition is reflected in the PEM capacity factor, which increases from 22.4% at 5% hydrogen share to 47.4% at 10% and 77.2% at 15%, before reaching 96.5% and 98.8% in the 20% and 25% scenarios, respectively. The increasing capacity factor therefore confirms the progressively higher utilization of the electrolyzer as the hydrogen target increases.

The effect of the PEM rated-power limit on the achievable hydrogen contribution becomes particularly clear when the target hydrogen share is compared with the effective annual hydrogen share, as shown in Figure 4.13.

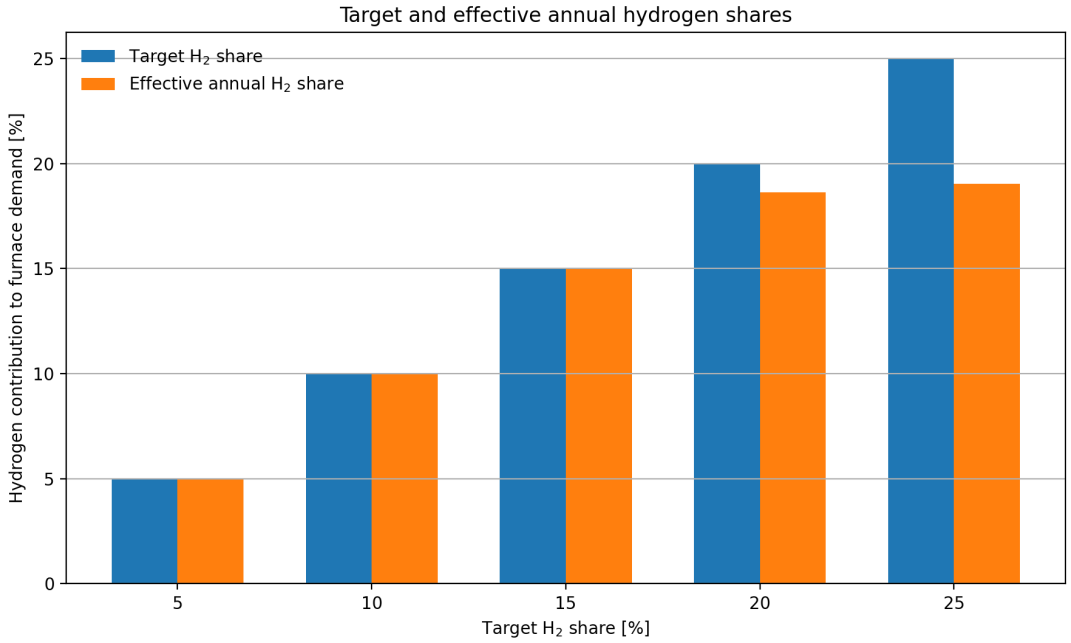


Figure 4.13: Comparison between the target hydrogen share and the effective annual hydrogen contribution achieved for the investigated rule-based scenarios.

The effective annual hydrogen contribution coincides with the target up to 15%. Above this level, however, the increase becomes strongly sub-linear. A prescribed target of 20% results in an effective annual hydrogen share of approximately 18.62%, while increasing the target to 25% raises the effective contribution to only 19.04%.

Consequently, a five-percentage-point increase in the target hydrogen share between the two highest-share scenarios produces an increase of only approximately 0.42 percentage points in the effective annual hydrogen contribution. The corresponding hydrogen supplied to the furnace increases by

only about 9.4 t over the year. These results identify a practical production plateau associated with the installed 2.5 MW PEM capacity.

PEM Degradation and Energy Efficiency

PEM degradation represents an additional aspect of system performance that evolves with the cumulative operating time of the electrolyzer and depends on its electrical operating point. The frozen-dispatch assessment adopted in the rule-based framework allows the electrochemical effect of degradation to be separated from changes in controller decisions. For each scenario, the same PEM electrical operating profile is therefore evaluated using both the fresh and degradation-adjusted PEM models.
Figure 4.14 compares the corresponding annual hydrogen production.

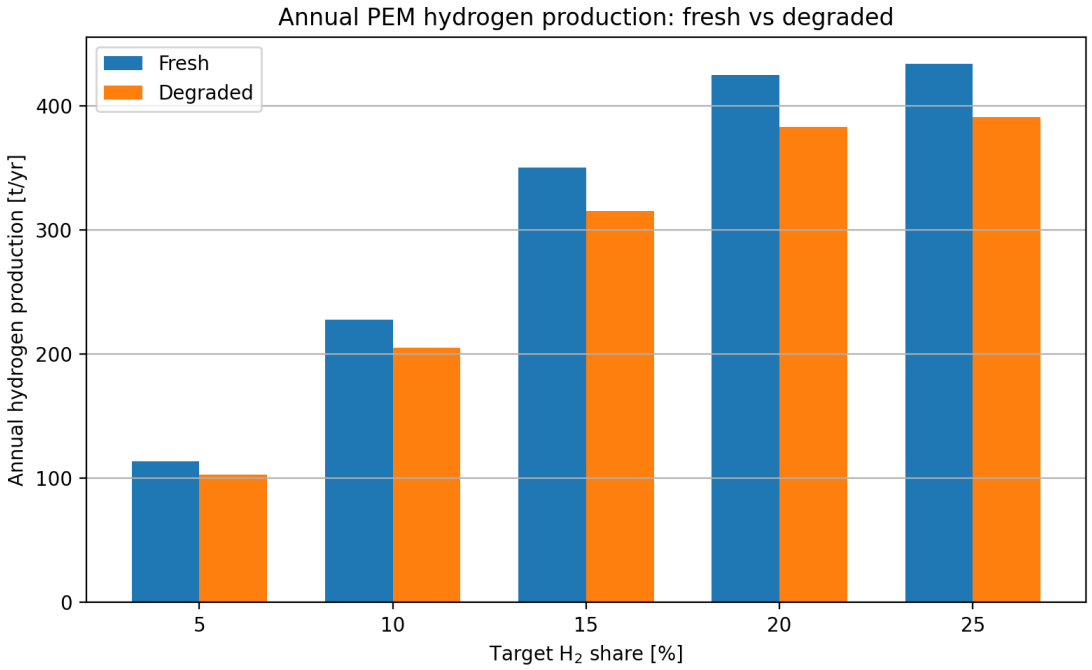


Figure 4.14: Annual hydrogen production obtained with the fresh and degradation-adjusted PEM models for the investigated rule-based scenarios.

Under fresh PEM conditions, annual hydrogen production increases from approximately 114.0 t in the 5% scenario to 228.0 t at 10%, 350.7 t at 15%, 425.2 t at 20%, and 434.0 t at 25%. When degradation-adjusted performance is evaluated at the same electrical operating points, the corresponding values decrease to approximately 103.1, 205.2, 315.6, 383.2, and 391.1 t, respectively. As the amount of hydrogen produced increases across the investigated scenarios, the absolute difference between the fresh and degraded PEM models also increases, from approximately 10.9 t in the 5% scenario to 42.9 t in the 25% scenario. In relative terms, however, the degradation-related hydrogen-production loss remains nearly constant across the investigated scenarios.
Figure 4.15 compares the corresponding relative degradation-related hydrogen-production loss with the hydrogen-target coverage across the investigated scenarios.

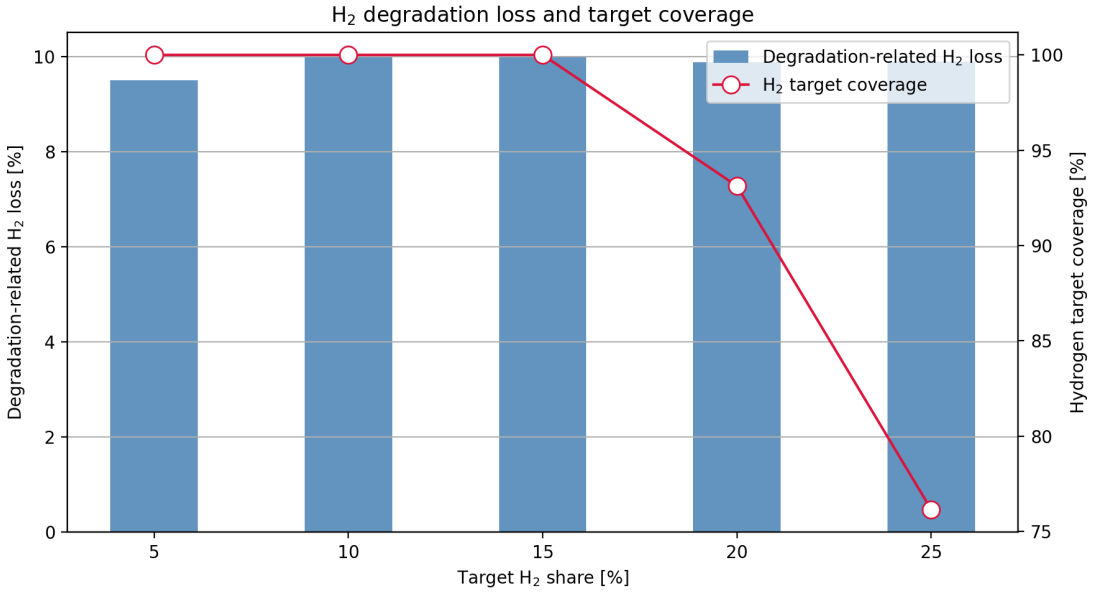


Figure 4.15: Degradation-related hydrogen-production loss and hydrogen-target coverage for the investigated rule-based scenarios.

The relative degradation-related hydrogen-production loss varies only slightly, between approximately 9.5% and 10.0%, despite the substantial change in hydrogen-target fulfilment as the target share increases. Coverage remains essentially complete up to the 15% scenario, before decreasing to 93.12% and 76.14% at hydrogen targets of 20% and 25%, respectively. This different evolution reflects distinct underlying mechanisms: the degradation penalty remains similar across the investigated PEM operating regimes, whereas the reduction in hydrogen-target coverage at higher hydrogen shares is primarily associated with the installed PEM capacity and the increasing occurrence of rated-power operation.

Since degradation is evaluated under the frozen-dispatch assumption, the two indicators shown in Figure 4.15 should not be interpreted as having a direct causal relationship. Hydrogen-target coverage is determined by the rule-based control strategy using the fresh PEM model, whereas the degradation-related hydrogen-production loss is evaluated afterwards at the same electrical operating points, without modifying the controller decisions.

The effect of the operating regime and degradation can also be quantified in terms of annual PEM energy efficiency. This indicator is defined as the ratio between the LHV-based hydrogen energy produced and the electrical energy supplied to the electrolyzer. As reported in Table 4.8, under fresh conditions, the annual efficiency decreases from approximately 77.4% at a 5% hydrogen target to 73.0% at 10%, 68.9% at 15%, and approximately 66.9% and 66.7% at 20% and 25%, respectively. When degradation-adjusted hydrogen production is evaluated at the same electrical dispatch, the corresponding annual efficiencies decrease to approximately 70.0%, 65.7%, 62.0%, 60.3%, and 60.1%. The progressive reduction in fresh efficiency reflects the increasing concentration of PEM operation at high electrical loads, while the difference between fresh and degraded conditions quantifies the electrochemical performance penalty associated with the adopted degradation model. The reduction in PEM energy efficiency is reflected in the corresponding increase in specific

electrical energy consumption (SEC), as shown in Figure 4.16.

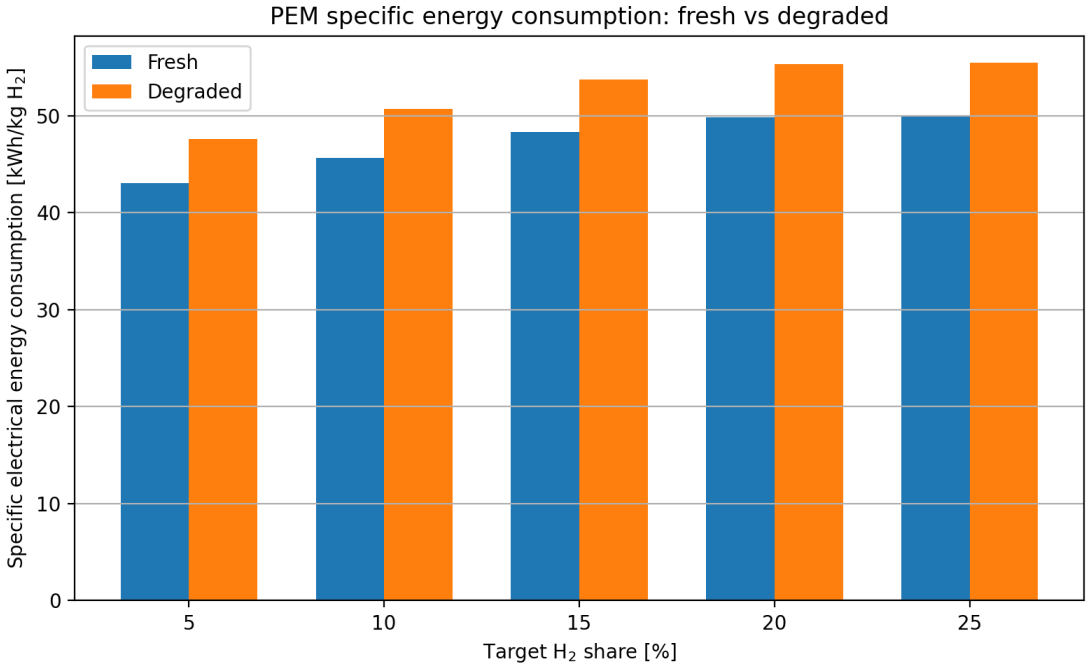


Figure 4.16: Specific electrical energy consumption obtained with the fresh and degradation-adjusted PEM models for the investigated rule-based scenarios.

Even under fresh PEM conditions, the SEC progressively increases with the hydrogen target, from approximately 43.08 kWh $kg_{H_2}^{-1}$ at 5% to 49.98 kWh $kg_{H_2}^{-1}$ at 25%. This evolution is associated with the progressive shift towards higher-load operating conditions and reflects the load-dependent electrochemical efficiency of the PEM. Degradation introduces an additional increase in the equivalent SEC, which rises from approximately 47.60 kWh $kg_{H_2}^{-1}$ at 5% to 55.46 kWh $kg_{H_2}^{-1}$ at 25%.
Under the frozen-dispatch formulation, the degradation-adjusted SEC should be interpreted as an equivalent specific electrical energy requirement. The electrical energy assigned to the PEM remains identical to the fresh case, while degradation reduces the hydrogen produced from that same electrical input. The ratio between PEM electricity and hydrogen production then increases even though the electrical dispatch itself is unchanged.
Overall, the results show that PEM energetic performance is strongly dependent on the operating regime and is further affected by electrochemical degradation. Accounting for both effects is therefore important when evaluating the hydrogen-production capability and electrical energy requirements of the electrolyzer.

Electrical Supply and Storage Utilization

The progressive increase in PEM utilization is directly reflected in the annual electrical energy requirement. Figure 4.17 compares the annual electricity supplied to the PEM from photovoltaic generation and from the electrical grid across the investigated scenarios.

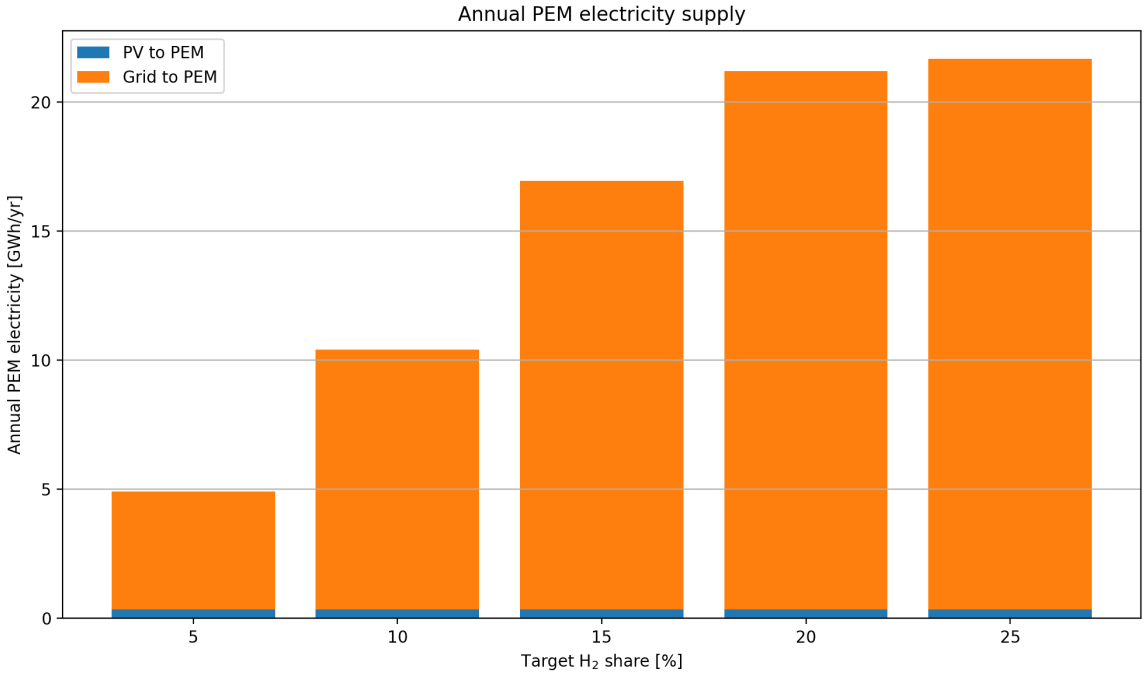


Figure 4.17: Annual PEM electricity supply from photovoltaic generation and from the electrical grid for the investigated rule-based scenarios.

Annual PEM electricity consumption increases from approximately 4.91 GWh at a 5% hydrogen share to 10.41 GWh at 10% and 16.96 GWh at 15%. The increase becomes considerably smaller at the highest targets, reaching approximately 21.20 GWh at 20% and 21.69 GWh at 25%. This plateau reflects the progressive saturation of the installed PEM capacity, which limits any further increase in electrical consumption and hydrogen production.

The annual photovoltaic contribution to the PEM remains close to 0.36 GWh across all investigated scenarios. However, its relative contribution decreases rapidly as PEM electricity consumption increases, with the renewable share falling from 7.33% at a 5% hydrogen share to 1.66% at 25%. Conversely, the grid contribution increases from 92.67% to more than 98% over the same range. The decreasing renewable fraction therefore does not result from increasing photovoltaic curtailment. Instead, since the installed PV capacity remains unchanged across the investigated scenarios, the almost fully utilized PV generation represents a progressively smaller fraction of the increasing electricity demand for hydrogen production.

The changing PEM operating regime also strongly affects hydrogen storage utilization. Approximately 16.0 t of hydrogen are directed to storage in both the 5% and 10% scenarios. This quantity decreases sharply to approximately 1.81 t at 15% and becomes essentially zero at 20% and 25%. The associated compressor electricity consumption follows the same trend, decreasing from approximately 23.8 MWh in the 5% and 10% scenarios to only about 2.7 MWh at 15%, before becoming negligible in the two highest-share cases.

This behaviour highlights the close relationship between PEM production flexibility and storage utilization. At low hydrogen targets, unused PEM capacity allows surplus hydrogen to be transferred to storage. As PEM utilization increases, this production margin progressively decreases, until tank

charging becomes negligible in the 20% and 25% scenarios. Once the initial hydrogen inventory is depleted, the storage level therefore remains close to its minimum operating limit. Increasing storage capacity alone would consequently provide limited benefit under these conditions, since the main limitation is the lack of surplus hydrogen available for tank replenishment.

Economic and Environmental Performance

The increasing dependence on grid-supported hydrogen production has important economic and environmental consequences. The main trade-off is between the reduction in natural-gas consumption achieved through hydrogen substitution and the additional grid electricity required for PEM operation.

To assess the environmental benefit of hydrogen integration, the investigated scenarios are compared with a 100% natural-gas baseline, in which the complete furnace thermal demand is supplied by natural gas. This configuration results in annual direct CO_2 emissions of approximately 14.308 $ktCO_2/yr$.

Figure 4.18 shows the direct emissions from natural-gas combustion and the indirect emissions associated with grid electricity for the baseline and the five hydrogen-share scenarios.

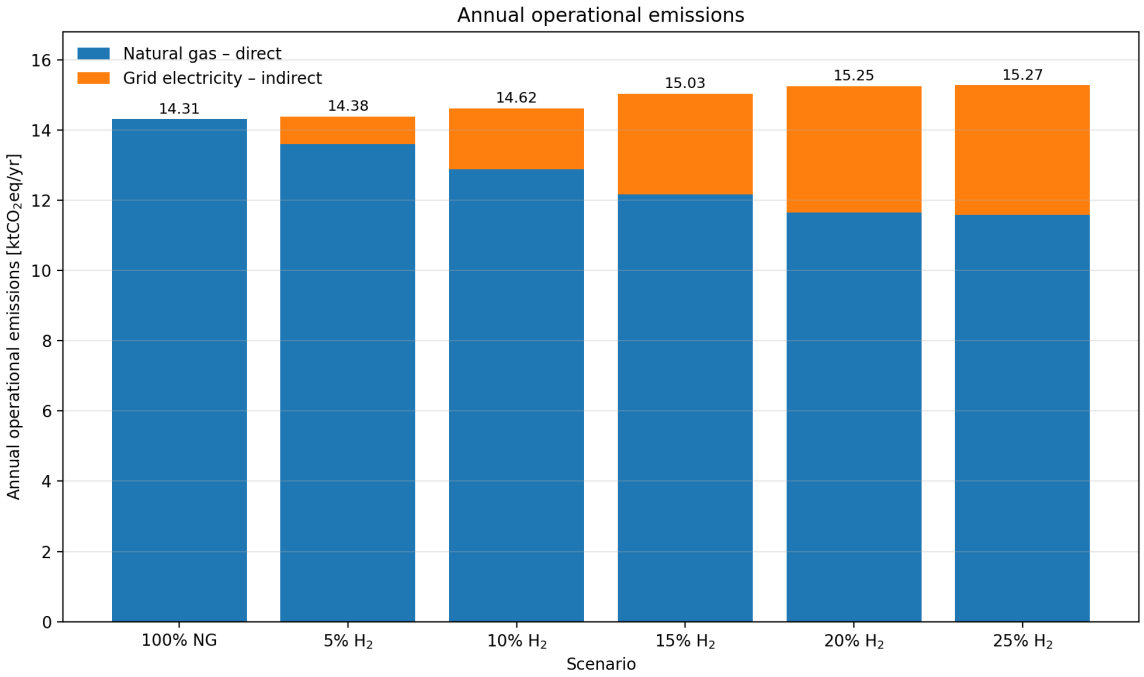


Figure 4.18: Annual operational emissions for the 100% natural-gas baseline and the investigated rule-based hydrogen-share scenarios, including direct natural-gas and indirect grid-electricity contributions.

Hydrogen substitution progressively reduces direct emissions from natural-gas combustion, from 14.308 $ktCO_2/yr$ in the baseline to 11.584 $ktCO_2/yr$ at the 25% hydrogen target. However, the electricity required for hydrogen production is supplied predominantly by the grid. With the adopted grid carbon intensity of 0.173 $kg_{CO_2eq}\,kWh^{-1}$, the associated indirect emissions increase from 0.791 $ktCO_2eq/yr$ at 5% H_2 to 3.690 $ktCO_2eq/yr$ at 25% H_2.

Consequently, the reduction in direct emissions is more than offset by the additional grid-related contribution. Total operational emissions range from 14.384 $ktCO_2eq/yr$ in the 5% scenario to 15.275 $ktCO_2eq/yr$ at 25%, compared with 14.308 $ktCO_2eq/yr$ for the baseline. This corresponds to an increase of approximately 0.53% at 5% H_2, rising to 6.76% at 25% H_2.

The investigated configuration therefore achieves a reduction in direct on-site emissions, but not in total operational emissions. Under the considered electricity-supply conditions, the limited availability of local photovoltaic generation leads to substantial grid dependence, preventing hydrogen substitution from delivering an overall decarbonization benefit. A larger contribution from low-carbon electricity would therefore be required to reverse this result.

In practical terms, this condition could be approached either by increasing on-site renewable generation or by reducing the carbon intensity of the electricity supplied to the electrolyzer or by combining both strategies. The present results therefore do not indicate an intrinsic environmental disadvantage of hydrogen substitution, but rather highlight the importance of the electricity-supply pathway in determining its actual decarbonization potential.

The flattening of the emission trend at the highest hydrogen targets is mainly associated with PEM saturation. Once the electrolyzer reaches its rated power, further increases in the prescribed hydrogen share cannot be fully translated into additional hydrogen production and grid-electricity consumption.

A similar trade-off is observed from an economic perspective. Figure 4.19 compares the annual energy and carbon-related operating costs with the 100% natural-gas baseline.

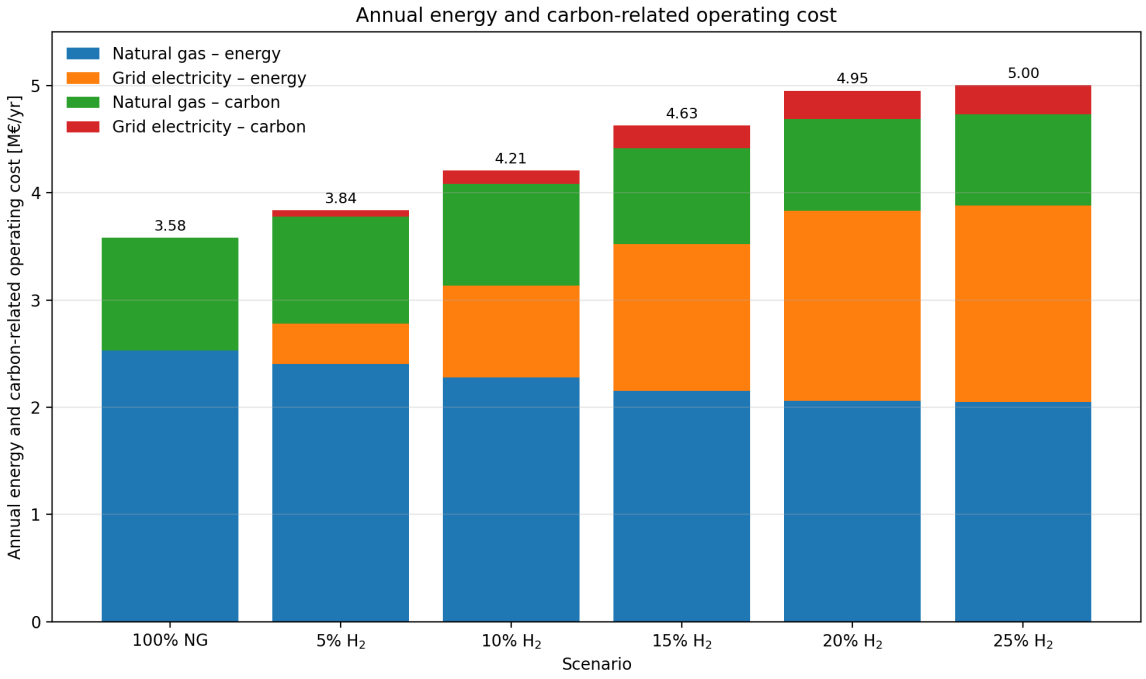


Figure 4.19: Annual energy and carbon-related operating costs for the 100% natural-gas baseline and the investigated rule-based hydrogen-share scenarios.

The baseline results in an annual natural-gas expenditure of approximately 2.532 M€ and a carbon cost of 1.051 M€, corresponding to a combined annual energy and carbon-related operating cost of

3.583 M€. Although hydrogen substitution reduces both natural-gas expenditure and the associated carbon cost, these savings are outweighed by the increasing cost of grid electricity and its related emissions.

The resulting annual energy and carbon-related operating cost increases from 3.839 M€ at 5% H_2 to 5.004 M€ at 25% H_2. Relative to the baseline, this represents an additional annual expenditure ranging from approximately 256,000€ to 1.421 M€. Therefore, under the adopted energy-price and carbon-price assumptions, none of the investigated hydrogen-share scenarios provides an economic advantage over the natural-gas baseline within the operating-cost boundaries considered in the analysis.

To further quantify the economic effect of hydrogen substitution, the net incremental energy and carbon-related cost per kilogram of hydrogen supplied is evaluated. This indicator represents the increase in annual energy and carbon-related operating costs relative to the 100% natural-gas baseline, normalized by the mass of hydrogen effectively supplied to the furnace. It therefore accounts for the additional grid-electricity and indirect carbon costs, while subtracting the avoided natural-gas and associated direct carbon costs. Natural-gas fallback is included whenever the target hydrogen contribution cannot be fully achieved.

Figure 4.20 shows the resulting net incremental cost per unit of hydrogen supplied to the furnace.

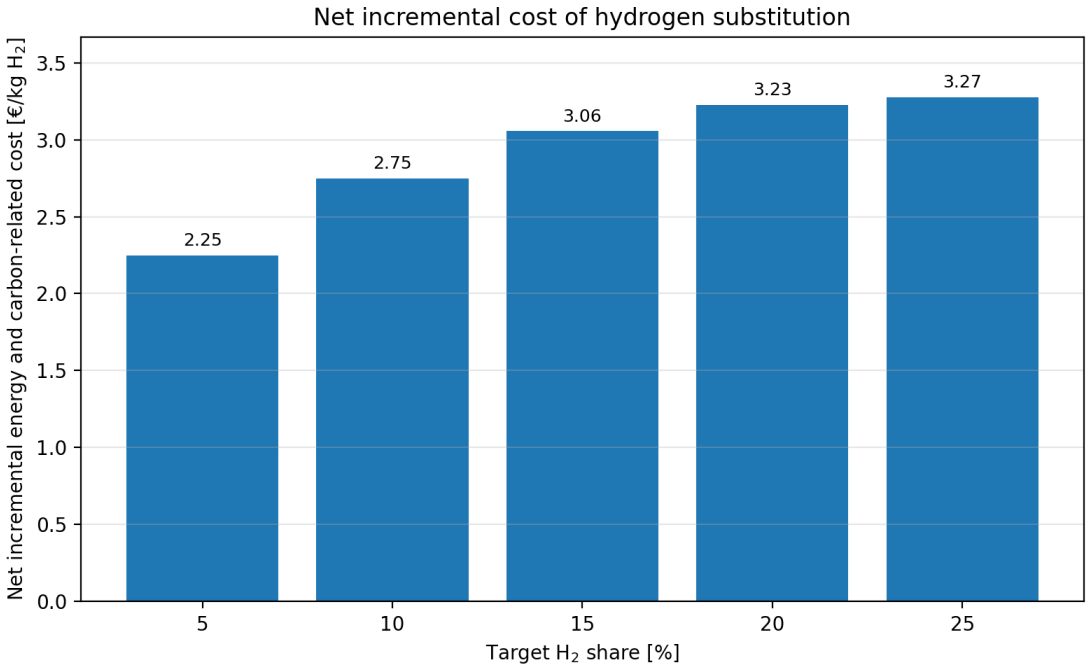


Figure 4.20: Net incremental energy and carbon-related operating cost per unit of hydrogen effectively supplied to the furnace for the investigated rule-based scenarios.

The net incremental cost increases from approximately 2.25 € $kg_{H_2}^{-1}$ at a 5% hydrogen target to 3.27 € $kg_{H_2}^{-1}$ at 25%. The increase reflects the progressively less favourable balance between avoided natural-gas expenditure and the additional electricity required for hydrogen production. Its tendency to stabilize at the highest hydrogen targets is again consistent with PEM saturation, which limits further increases in hydrogen production and associated operating costs.

Overall Assessment

The comparative analysis identifies a clear transition in the operation of the integrated hydrogen-production system. The 5% and 10% scenarios remain capacity-unconstrained, while the 15% scenario marks the transition towards capacity-limited operation. At 20% and 25%, PEM saturation becomes dominant and prevents the hydrogen target from being fully achieved.

The installed 2.5 MW PEM electrolyzer therefore represents the principal technical limitation at high hydrogen shares. Increasing the target hydrogen contribution from 20% to 25% raises the effective annual share only from approximately 18.62% to 19.04%, indicating that the installed hydrogen-production capacity has approached a practical production ceiling.

A second limitation concerns the electricity source used for hydrogen production. Although almost all available photovoltaic generation is utilized, the installed PV generation remains small compared with the increasing PEM electricity requirement. Higher hydrogen production is therefore achieved primarily through greater grid-electricity consumption, while the renewable contribution to PEM supply progressively decreases.

The storage results further demonstrate that storage capacity cannot be considered independently from hydrogen-production flexibility. At low hydrogen targets, available PEM capacity allows surplus hydrogen to be produced and transferred to storage. As PEM utilization increases, this production margin progressively disappears, and tank replenishment becomes negligible in the highest-share scenarios. Increasing storage capacity alone would therefore not resolve the hydrogen deficit without additional hydrogen-production capability.

PEM degradation introduces an additional long-term performance penalty. Under the frozen-dispatch assessment, degradation reduces the hydrogen production obtained from the same electrical dispatch by approximately 9.5–10.0% across the investigated scenarios. In parallel, increasing the hydrogen target shifts PEM operation towards higher-load conditions, reducing fresh annual energy efficiency and increasing specific electrical energy consumption even before degradation is considered. The results therefore highlight the combined influence of load-dependent electrochemical performance and PEM degradation on the long-term energetic performance of the electrolyzer.

These technical characteristics directly affect the economic and environmental performance of the system. Increasing hydrogen substitution reduces natural-gas consumption, direct furnace CO_2 emissions, and natural-gas expenditure. However, under the adopted electricity mix and energy-price assumptions, the corresponding increase in grid-electricity demand more than offsets these benefits, resulting in higher total operational CO_2eq emissions and higher annual energy and carbon-related operating costs than in the 100% natural-gas baseline.

Overall, the rule-based assessment indicates that increasing hydrogen substitution beyond the level achievable with the current 2.5 MW PEM electrolyzer would require additional hydrogen-production capacity. However, the environmental benefit of higher hydrogen substitution also depends on the electricity used for hydrogen production. Under the investigated electricity-supply conditions, the strong dependence on grid electricity offsets the reduction in direct emissions achieved through natural-gas substitution. A greater contribution from on-site renewable generation and/or lower-

carbon electricity could therefore improve the overall decarbonization performance of the system.

4.3 Optimization-Based Energy Management System

The second part of the analysis investigates the operation of the industrial microgrid under the optimization-based Energy Management System (EMS) described in Chapter 3. In this framework, the operating schedule is determined through the simultaneous coordination of hydrogen production, storage operation, grid electricity imports, natural-gas consumption, and direct furnace electrification.

A central objective of this second stage is to evaluate the integration of the detailed PEM electrochemical and degradation models developed in this work within an existing optimization-based EMS, replacing its original constant-efficiency representation. The analysis is developed for the same industrial application and retains the main component characteristics, annual input data, and PEM electrochemical parameterization introduced in the previous sections. However, the formulation includes additional optimization-specific operating assumptions and degrees of freedom, which are summarized below.

4.3.1 Optimization-Specific Simulation Parameters

Table 4.9 summarizes the main parameters and operating constraints specific to this EMS formulation.

Table 4.9: Main simulation parameters specific to the optimization-based EMS.

Parameter	**Symbol**	**Value**
Simulation timestep	Δt	1 h
Planning horizon	N_{hor}	24 h
Minimum hydrogen contribution	$x_{\text{H}_2,\text{min}}$	5%
Minimum direct electrical contribution	$x_{\text{el,min}}$	8%
Maximum direct electrical contribution	$x_{\text{el,max}}$	12%
Hydrogen-output ramp limit	$\Delta P_{\text{ely,out,max}}$	1000 kW_{H_2} h^{-1}
Initial efficiency estimate	η_{init}	0.65
Maximum coupling iterations	$N_{\text{iter,max}}$	20
Efficiency convergence tolerance	ε_η	10^{-3}
Specific electrical compression work	w_{comp}	1.484 $\text{kWh}\,\text{kg}_{\text{H}_2}^{-1}$

The economic and environmental parameters adopted in the rule-based analysis are retained unchanged in the optimization-based framework, including the grid carbon intensity and the carbon price. In the optimization-based EMS, however, the corresponding carbon-emission costs are included directly in the objective function and therefore contribute to the determination of the optimal dispatch.

4.3.2 Selected-Day Operating Behaviour

One day of the annual simulation is analysed in detail to better illustrate the operating behaviour resulting from the optimization-based EMS. Day 180 is selected because it represents a high photovoltaic- generation day, thus providing a particularly useful operating condition for observing how the EMS coordinates the available renewable electricity with PEM operation, hydrogen storage, electricity prices and furnace energy supply. The selected day is not intended to represent average annual operating conditions, which are assessed separately through the annual performance indicators presented in the following sections.

PEM and Hydrogen-Storage Operation

Figure 4.21 compares the electrical input power of the PEM electrolyzer with the electricity-price profile during the selected day.

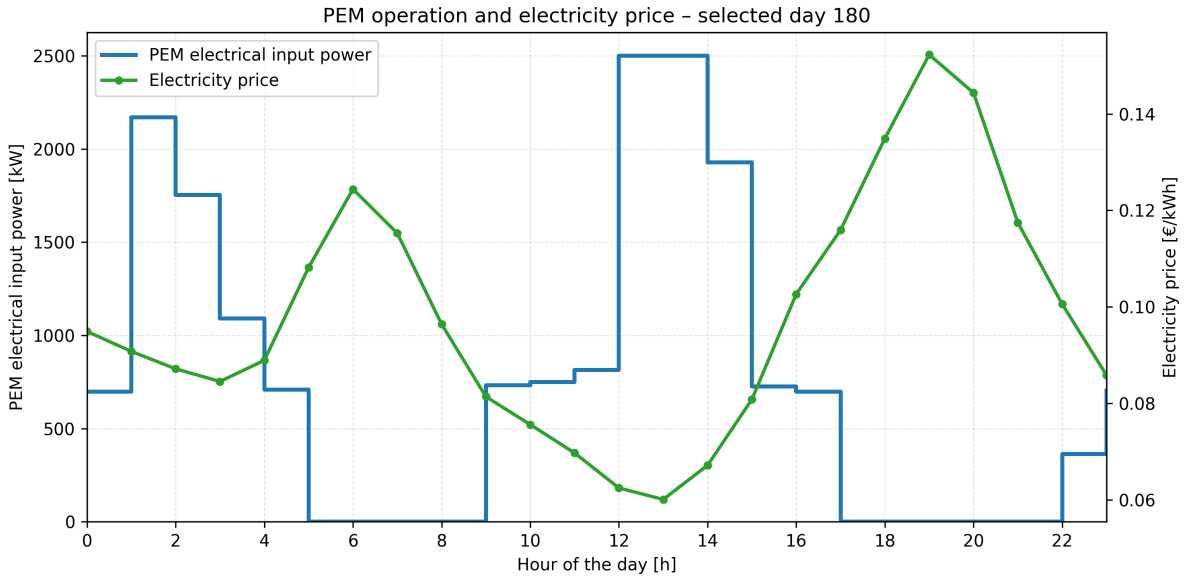


Figure 4.21: PEM electrical input power and electricity-price profile during selected day 180.

The optimized PEM dispatch shows a clear response to the variation in electricity price over the selected day. During the first hours, the electrolyzer operates at moderate-to-high power, reaching approximately 2.2 MW around hours 1–2, when electricity prices are relatively low. PEM operation is subsequently reduced and is interrupted between approximately hours 5 and 9, before resuming as electricity prices decrease.

The most pronounced operating period occurs between hours 12 and 14. During these hours, which coincide with the lowest electricity prices of the day and with daytime photovoltaic availability, the PEM reaches its rated electrical power of 2.5 MW. After hour 14, PEM power is progressively reduced. From approximately hour 17 until hour 22, when electricity prices are comparatively high, the electrolyzer remains switched off. Operation resumes towards the end of the day as the electricity price decreases again.

The correspondence between several of these variations indicates that electricity price plays an important role in determining the economically optimized PEM schedule. However, the dispatch does not simply follow the instantaneous electricity price, since PEM operation is determined jointly with hydrogen-storage operation and the other system constraints over the 24-hour planning horizon. The resulting hydrogen-storage operation is shown in Figure 4.22.

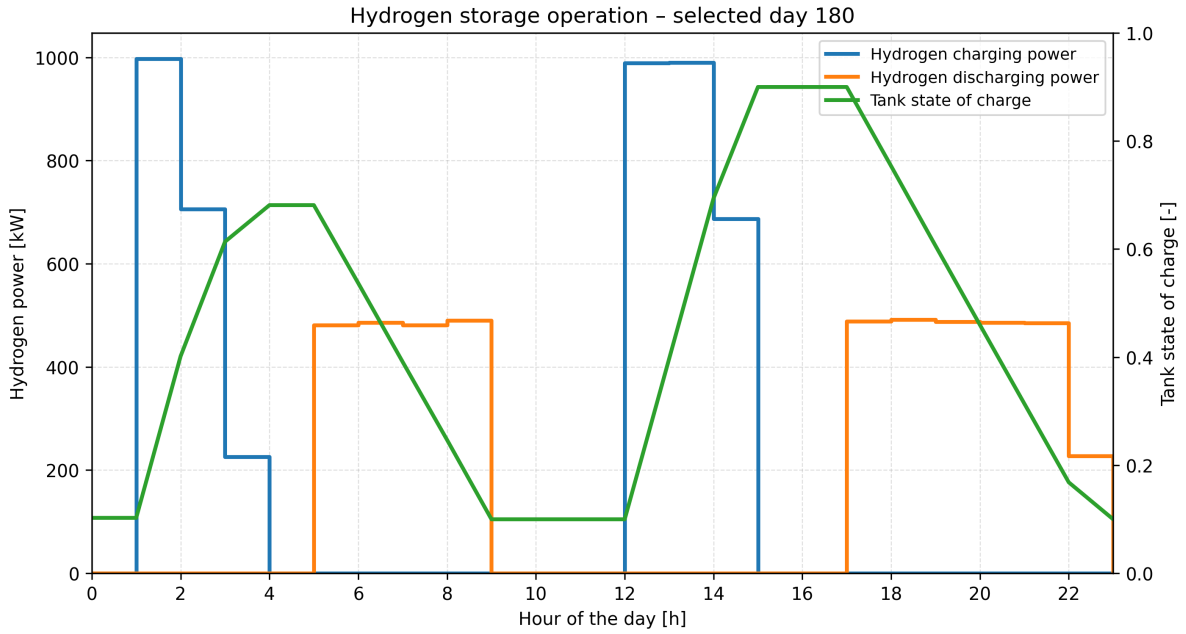


Figure 4.22: Hydrogen charging and discharging power and tank state of charge during selected day 180.

The hydrogen-storage operation is characterized by a clear sequence of charging and discharging periods throughout the selected day. During approximately the first hour, the storage remains close to its minimum state of charge. Between hours 1 and 4, the tank is charged, with the charging power progressively decreasing as the state of charge increases from approximately 0.1 to about 0.7. This is followed by a sustained discharge between approximately hours 4 and 9, which progressively returns the tank to its minimum state of charge. The storage then remains nearly inactive until around hour 12.

A second, more pronounced charging phase occurs between approximately hours 12 and 15. During this period, the tank state of charge rapidly increases and reaches its upper operating limit of approximately 0.9. This charging phase coincides with the period identified in Figure 4.21 in which the PEM operates at high power, reaching its rated value while electricity prices are at their lowest levels of the day. After remaining close to its maximum state of charge for approximately two hours, the tank begins to discharge from around hour 17 and continues supplying hydrogen during most of the evening. This corresponds to the period in which electricity prices increase significantly and PEM operation is progressively reduced and eventually interrupted.

The combined PEM and storage profiles therefore illustrate how system operation evolves under the 24-hour rolling-horizon EMS. At each simulation hour, the optimization considers the electricity-price and photovoltaic-generation profiles over the following planning horizon, together with the

hydrogen requirement, storage state and system constraints. This allows hydrogen production to be shifted towards favourable operating periods and stored for later use. The storage system therefore decouples hydrogen production from its instantaneous use at the furnace, avoiding the need for the PEM to directly follow the hourly hydrogen demand.

Furnace Energy Supply

The composition of the furnace energy supply during the same selected day is shown in Figure 4.23.

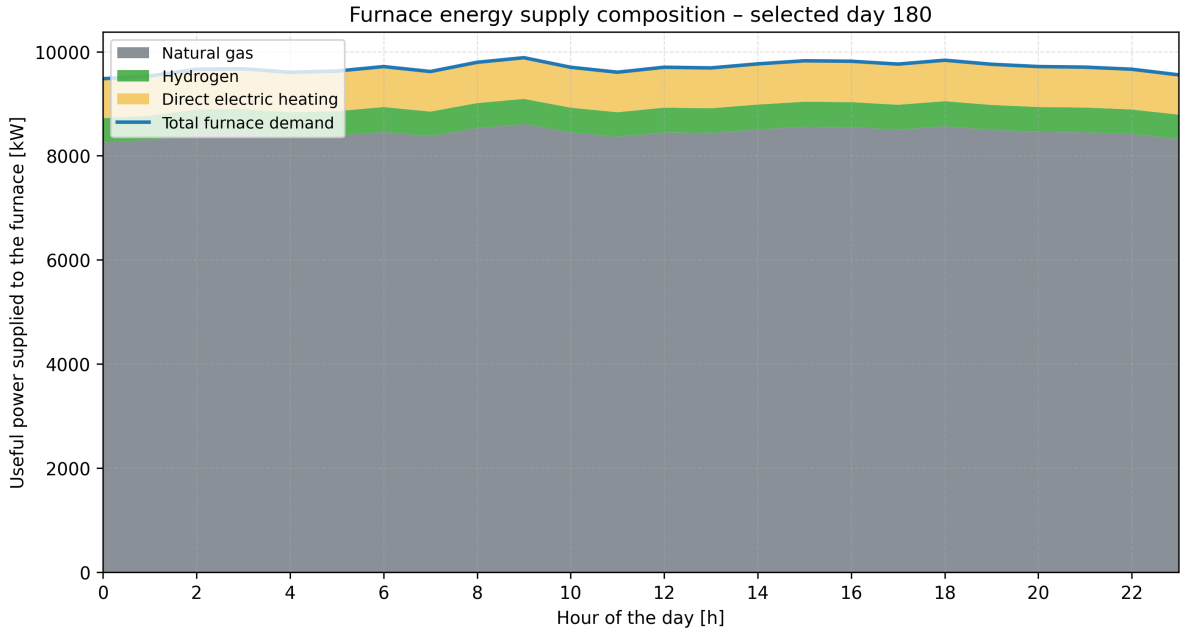


Figure 4.23: Composition of the useful energy supplied to the furnace during selected day 180.

Throughout the day, natural gas remains the dominant energy source, while hydrogen and direct electrical heating provide additional contributions to the furnace energy supply. The three energy carriers are jointly coordinated by the EMS to continuously satisfy the furnace demand.
The hydrogen contribution remains close to the imposed minimum level over the entire day. Since the hydrogen constraint is formulated as a lower bound rather than a fixed setpoint, the EMS can exceed this minimum when this is consistent with the optimized system operation. Hydrogen continues to be supplied to the furnace also during periods in which PEM operation is reduced or interrupted. Together with the storage behaviour shown in Figure 4.22, this illustrates how stored hydrogen allows the furnace supply to be maintained independently of the instantaneous PEM production profile.
Direct electrical heating also contributes continuously within the operating range imposed in the optimization problem. During day 180, its maximum useful thermal contribution reaches approximately 790.75 kW, while the total useful energy supplied through direct electrical heating amounts to approximately 18.61 MWh.

4.3.3 Annual Technical and Energy Performance

The selected-day analysis illustrates the operating behaviour of the optimization-based EMS, whereas its overall technical performance is assessed over the complete annual simulation. The main annual indicators related to hydrogen supply, PEM utilization and storage operation are summarized in Table 4.10.

Table 4.10: Main annual technical performance indicators of the optimization-based EMS.

Indicator	Symbol	Value
Minimum hourly hydrogen contribution	$x_{H_2,min}$	5.000%
Average hourly hydrogen contribution	$\overline{x}_{H_2}$	5.527%
Effective annual hydrogen contribution	$x_{H_2,annual}$	5.536%
PEM electricity consumption	E_{PEM}	7.247 GWh
PEM operating hours	$t_{PEM,op}$	5779 h
PEM equivalent full-load hours	t_{EFLH}	2899 h
PEM capacity factor	CF_{PEM}	33.09%
Hydrogen energy charged into storage	$E_{H_2,tank,in}$	1.627 GWh_{H_2}

Hydrogen-Share Compliance and PEM Utilization

The annual results confirm that the hydrogen requirement imposed in the optimization formulation is satisfied over the complete simulated period. The minimum hourly hydrogen contribution is equal to 5.000%, within numerical tolerance, while the average hourly contribution reaches 5.527%. On an annual energy basis, the effective hydrogen contribution is slightly higher, at 5.536%.

The difference between the imposed minimum and the resulting hydrogen contribution reflects the formulation of the hydrogen constraint as a lower bound rather than an exact operating setpoint. The EMS can therefore exceed the minimum contribution when this is consistent with the overall optimized dispatch. The slight difference between the average hourly and effective annual values results from their different aggregation: the former is calculated as the arithmetic mean of the hourly hydrogen shares, whereas the latter is obtained as the ratio between the cumulative annual hydrogen contribution and the cumulative annual furnace energy demand.

The PEM electrolyzer consumes approximately 7.247 GWh of electricity over the annual simulation and operates for 5779 h. Its equivalent full-load operating time is approximately 2899 h, corresponding to a capacity factor of 33.09%. The difference between physical operating hours and equivalent full-load hours confirms that the electrolyzer operates predominantly under part-load conditions. Considering only the hours in which the PEM is active, its average equivalent load remains close to 50% of the rated power.

Annual Hydrogen Production and Storage Operation

Figure 4.24 presents the daily hydrogen production together with the average daily state of charge of the hydrogen-storage system over the annual simulation.

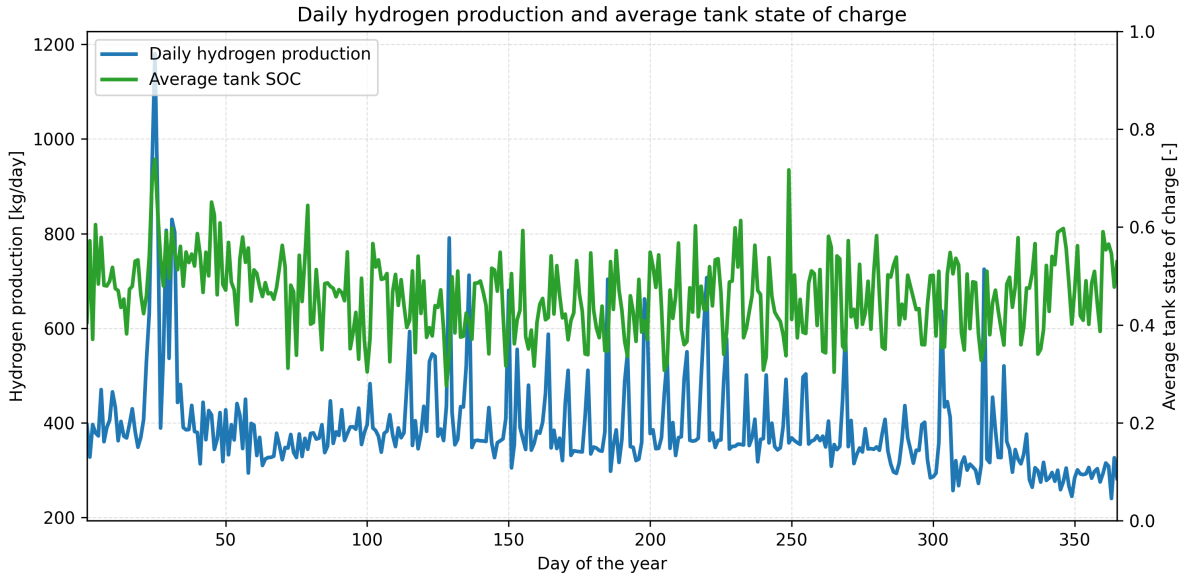


Figure 4.24: Daily hydrogen production and average hydrogen-tank state of charge over the annual simulation.

Daily hydrogen production varies considerably over the annual simulation, with most days characterized by moderate production levels and a limited number of pronounced peaks. These variations reflect the flexibility of the optimization-based EMS, which can modify PEM operation according to the economic and operating conditions of the system rather than maintaining a constant hydrogen-production rate.

The most pronounced peak occurs around day 25, when hydrogen production reaches approximately 1.19 t/day. During this day, particularly low electricity prices make electrolyzer operation economically favourable, and the PEM operates at its rated electrical power of 2.5 MW for the entire 24-hour period. As the hydrogen requirement is imposed as a lower bound rather than an exact setpoint, the EMS can increase hydrogen production beyond the minimum required level and substitute a larger fraction of natural gas when this is economically advantageous.

The average daily tank state of charge also exhibits repeated variations over the year, indicating that storage is regularly involved in the operation of the hydrogen subsystem. In total, approximately 1.627 GWh_{H_2} is charged into the tank during the annual simulation. This recurring storage utilization extends the behaviour observed for the selected day to the annual scale, confirming that the tank repeatedly decouples hydrogen production from furnace consumption.

Annual Energy Balance

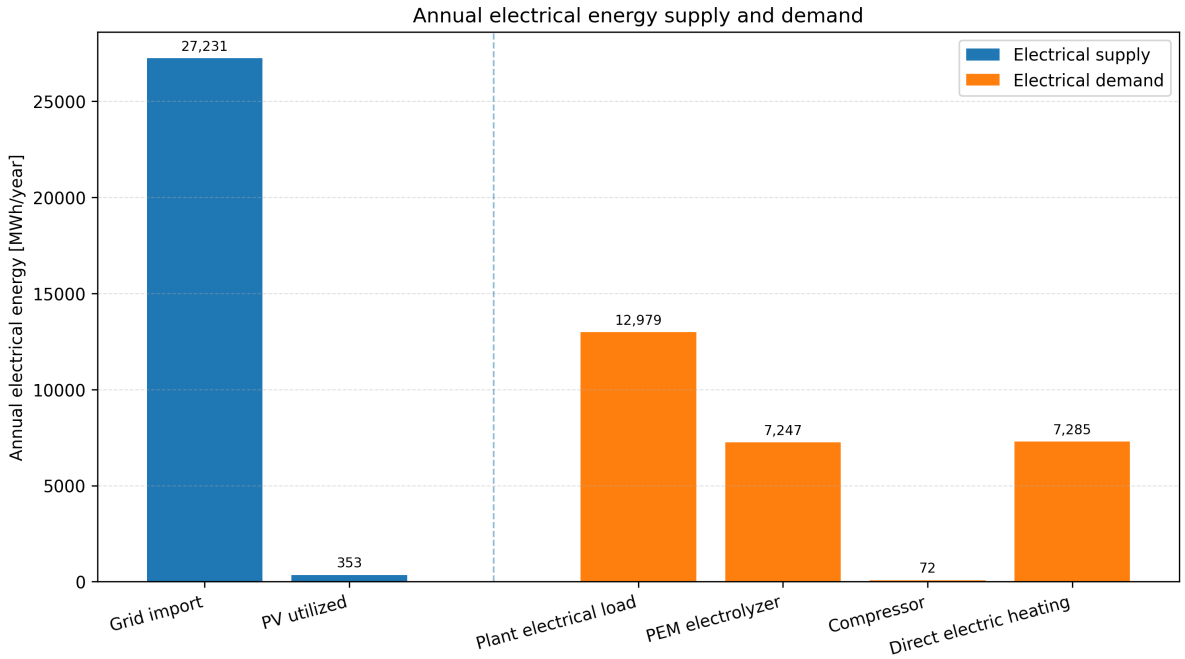


Figure 4.25: Annual electrical-energy supply and demand of the optimization-based system.

The annual electrical-energy balance presented in Figure 4.25 highlights the strong dependence of the investigated configuration on grid electricity. Of the total 27.584 GWh electrical demand, approximately 27.231 GWh, corresponding to 98.72%, is supplied by the grid, while photovoltaic generation contributes approximately 0.353 GWh, or 1.28%.

On the demand side, the original plant electrical load accounts for approximately 12.979 GWh, while direct furnace electrification and PEM operation require approximately 7.285 GWh and 7.247 GWh, respectively. Hydrogen compression represents only a minor contribution, with an annual electricity consumption of approximately 72.45 MWh. Overall, PEM operation and direct furnace electrification account for approximately 52.7% of the total electrical demand.

The limited contribution of local photovoltaic generation means that most of the electricity required for hydrogen production and direct furnace electrification must be supplied by the grid. This result is particularly relevant when assessing the economic and environmental performance of the system in the following sections.

Considering the combustible energy supplied to the furnace burner, approximately 4.739 GWh_{H_2} of hydrogen and 75.179 GWh of natural gas are supplied over the annual simulation. Natural gas therefore remains the dominant combustible energy carrier, while hydrogen provides a smaller contribution according to the optimized dispatch.

4.3.4 Effect of the Detailed PEM Representation and Degradation

An important aspect of the optimization-based analysis is the representation of PEM conversion efficiency. Rather than retaining a single constant efficiency throughout the simulation, the EMS is

coupled with the electrochemical model described in Chapter 3, allowing the conversion efficiency to depend on the PEM operating point and to evolve with degradation.
The impact of this modelling approach is assessed in two steps. First, the fresh electrochemical efficiency is compared with the constant efficiency assumption used to initialize the iterative coupling. Second, the additional effect of PEM degradation is evaluated by comparing fresh and degradation-adjusted performance.

Effect of the Electrochemical Efficiency Model

Figure 4.26 quantifies the difference between the PEM efficiency predicted by the fresh electrochemical model and the constant value of 65% used as the initial efficiency estimate in the EMS. The relative efficiency difference is evaluated at the operating points associated with the final degradation-aware EMS dispatch and subsequently averaged on a daily basis. This comparison is intended to quantify the discrepancy between the two efficiency representations at the same operating conditions, rather than to compare two independently optimized annual dispatches.

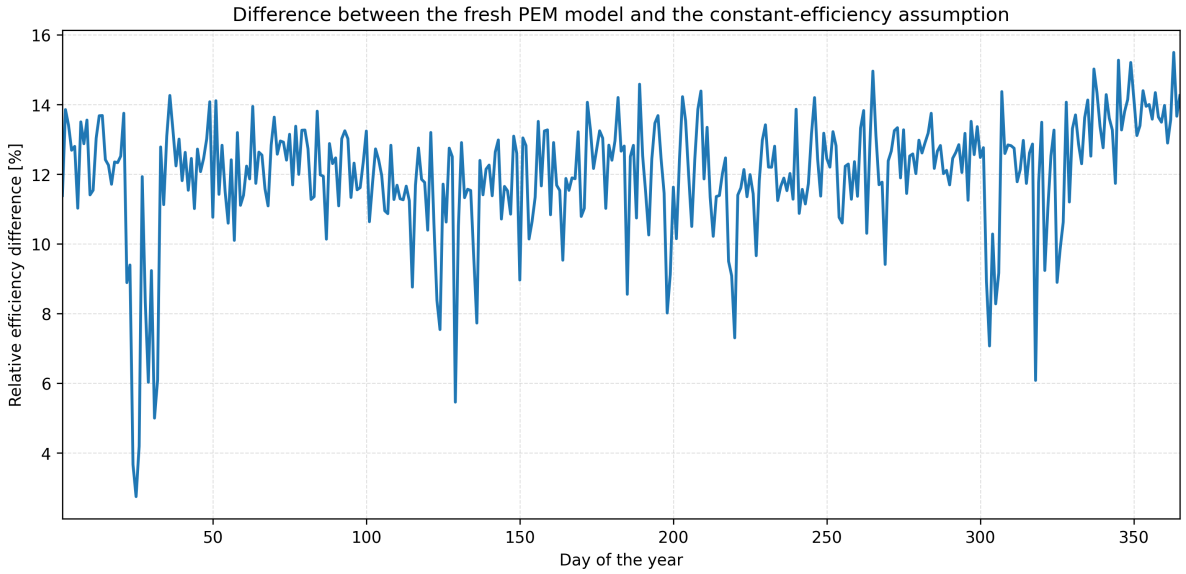


Figure 4.26: Daily average relative difference between the fresh electrochemical PEM efficiency and the constant 65% efficiency assumption at the operating points associated with the final degradation-aware EMS dispatch.

As shown in Figure 4.26, the discrepancy between the two efficiency representations varies over the annual simulation. This variation results from the dependence of the electrochemical efficiency on PEM operating conditions, which cannot be captured by the constant-efficiency representation.
The relative difference is calculated with respect to the fresh electrochemical efficiency. When evaluated over the individual PEM operating hours, its annual average is approximately 11.96%. When the hourly relative differences are first averaged for each day, the corresponding annual average of the daily values is approximately 12.00%.
These results demonstrate that the constant 65% efficiency provides a simplified representation of PEM conversion performance. The electrochemical model instead captures the dependence of

conversion performance on electrolyzer operating conditions, providing a more physically representative description of PEM behaviour.

Effect of PEM Degradation

The additional impact of PEM degradation is evaluated by comparing the fresh electrochemical performance with the degradation-adjusted performance at the operating points associated with the final degradation-aware EMS dispatch. This comparison isolates the effect of ageing on PEM conversion performance under the same operating conditions.

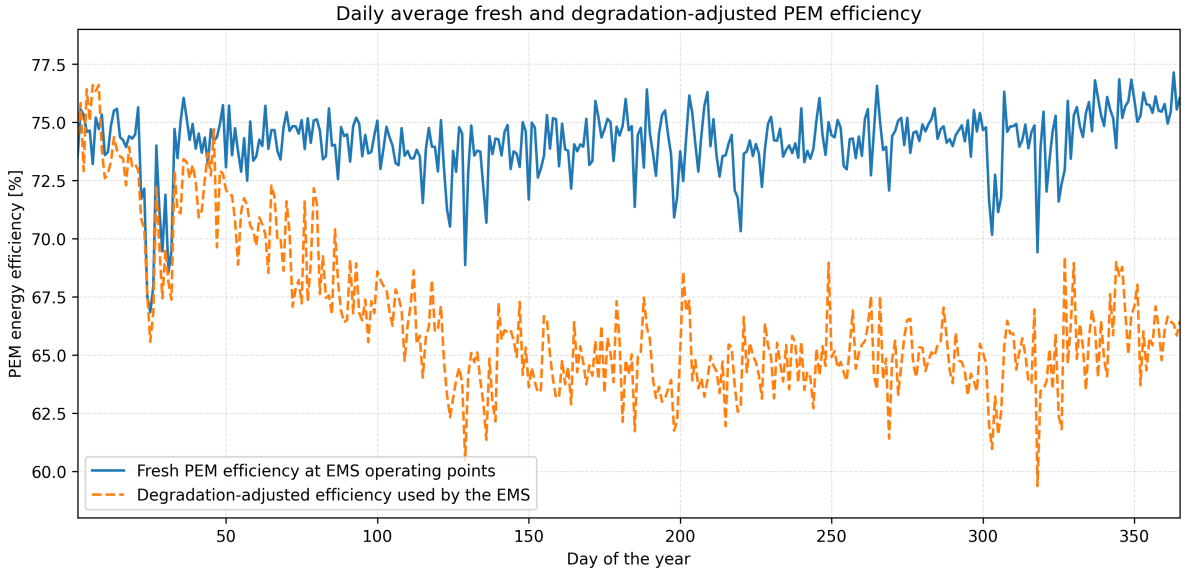


Figure 4.27: Daily fresh and degradation-adjusted PEM efficiency over the annual simulation.

As shown in Figure 4.27, the fresh efficiency varies over the year according to the PEM operating point, while the degradation-adjusted profile additionally reflects the evolution of PEM performance with ageing. During the initial part of the simulation, the two profiles remain relatively close. As cumulative PEM operation increases, a progressively larger separation develops, after which the degradation-adjusted efficiency remains generally below the corresponding fresh value.

The magnitude of the difference continues to vary according to the operating point selected by the EMS. Towards the end of the simulation, a partial reduction in the separation between the two profiles can be observed. This behaviour does not indicate a recovery of PEM performance, but results from the combined influence of degradation and the changing electrolyzer operating conditions on conversion efficiency.

When weighted according to the hydrogen production associated with the final degradation-aware EMS dispatch, the fresh PEM efficiency is approximately 71.72%, whereas the corresponding degradation-adjusted efficiency decreases to approximately 64.60%. The relative reduction between the two weighted values is therefore approximately 9.93%.

The energetic consequence of this performance deterioration can be quantified by evaluating the same hydrogen-output profile with the fresh and degradation-adjusted PEM representations. The

degraded representation requires approximately 728.5 MWh of additional electrical energy to provide the same hydrogen output.

It should be recalled that, unlike the performance comparison above, degradation is not treated exclusively as a post-processing correction in the optimization framework, since the degradation-adjusted efficiency is iteratively fed back into the EMS and can therefore influence the final optimized dispatch.

4.3.5 Economic and Environmental Performance

The optimized energy dispatch determines both the annual operating expenditure and the associated operational carbon emissions. Since the objective function includes energy-purchasing costs together with the monetized cost of carbon emissions, the different contributions are reported separately.

For the economic and environmental assessment, the optimization-based configuration is also compared with a same-boundary reconstructed 100% natural-gas baseline. The total furnace energy demand is kept unchanged, while hydrogen supply and direct furnace electrification are removed and their contributions are entirely replaced by natural gas. The furnace is therefore supplied exclusively by natural gas in the baseline.

The original plant electrical load is retained, since it represents a pre-existing electricity demand independent of the furnace energy-supply configuration. With PEM electrolysis, hydrogen compression, and direct electric heating absent, this plant load represents the only electrical demand in the baseline and is supplied by the available photovoltaic generation and grid imports. This definition preserves a consistent system boundary for comparing the integrated configuration with a conventional 100% natural-gas furnace configuration.

The main annual economic and environmental indicators of the optimization-based configuration and the reconstructed 100% natural-gas baseline are summarized in Table 4.11.

Table 4.11: Annual economic and environmental performance of the reconstructed 100% natural-gas baseline and the optimization-based configuration.

Indicator	**100% NG baseline**	**Optimization**
Grid-electricity cost [M€/yr]	1.089	2.086
Natural-gas cost [M€/yr]	2.904	2.499
Total energy cost [M€/yr]	3.993	4.585
Grid carbon cost [M€/yr]	0.160	0.346
Natural-gas carbon cost [M€/yr]	1.208	1.039
Total carbon cost [M€/yr]	1.368	1.385
Total energy and carbon-related cost [M€/yr]	5.361	5.970
Grid-related emissions [ktCO_2eq/yr]	2.183	4.711
Natural-gas emissions [ktCO_2/yr]	16.446	14.154
Total operational emissions [ktCO_2eq/yr]	18.629	18.865

Economic Performance

The reported costs should be interpreted according to the economic boundaries of the optimization model. They include grid-electricity and natural-gas expenditure together with their associated carbon costs, but do not represent a complete levelized system cost including investment, replacement, maintenance, and other cost components outside the adopted objective function.
The economic effect of the integrated configuration is further illustrated in Figure 4.28, which shows how the individual energy and carbon-related cost contributions change relative to the reconstructed 100% natural-gas baseline.

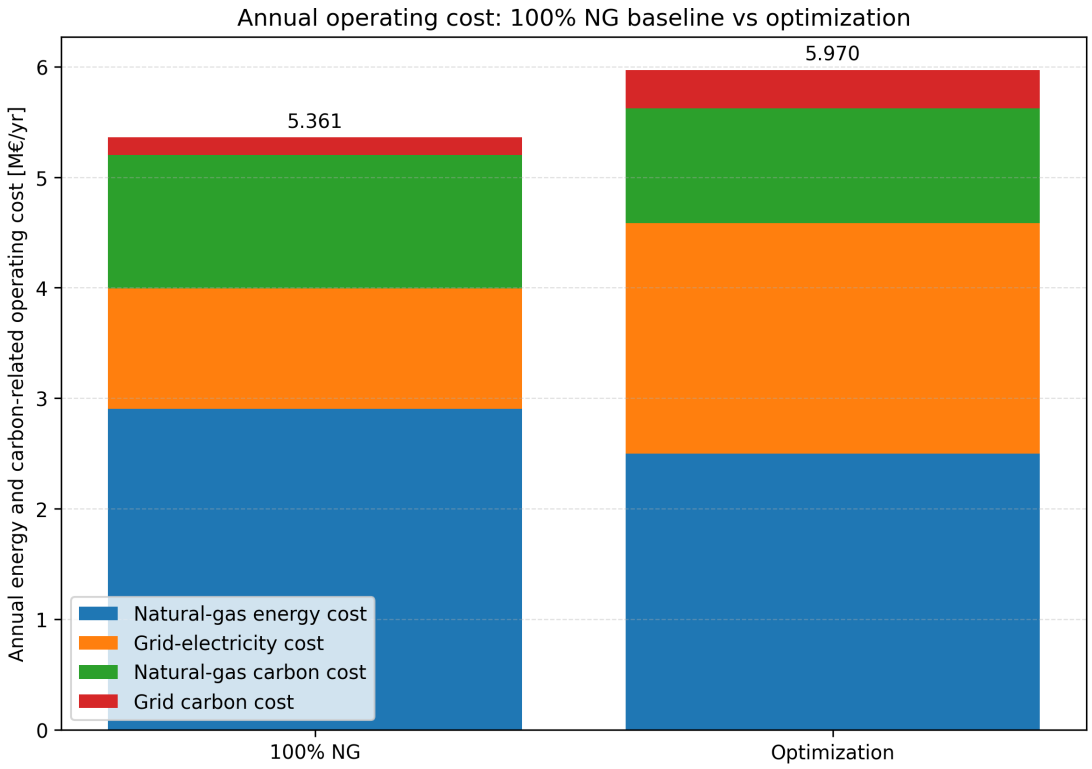


Figure 4.28: Annual energy and carbon-related operating costs for the reconstructed 100% natural-gas baseline and the optimization-based configuration.

Although the integrated configuration reduces natural-gas expenditure, this saving is outweighed by the increase in grid-electricity cost. Consequently, the total annual energy and carbon-related operating cost increases from 5.361 M€ in the baseline to 5.970 M€ in the optimization-based configuration, corresponding to an increase of approximately 0.609 M€/yr, or 11.4%.
This increase is primarily associated with energy expenditure, which rises by approximately 0.592 M€/yr, whereas the carbon-cost contribution increases by only about 0.017 M€/yr. Under the adopted energy-price and carbon-price assumptions, the reduction in natural-gas consumption is therefore insufficient to compensate for the additional electricity expenditure associated with PEM electrolysis and direct furnace electrification. The optimization-based configuration therefore does not provide an operating-cost advantage over the reconstructed 100% natural-gas baseline under the investigated conditions.

Operational Carbon Emissions

Hydrogen integration and direct furnace electrification reduce natural-gas-related emissions from 16.446 $ktCO_2/yr$ in the reconstructed 100% natural-gas baseline to 14.154 $ktCO_2/yr$ in the optimization-based configuration, corresponding to a reduction of approximately 2.292 $ktCO_2/yr$. However, the higher electricity demand increases grid-related emissions from 2.183 $ktCO_2eq/yr$ to 4.711 $ktCO_2eq/yr$, corresponding to an increase of approximately 2.528 $ktCO_2eq/yr$.
The resulting change in the composition of operational emissions is shown in Figure 4.29.

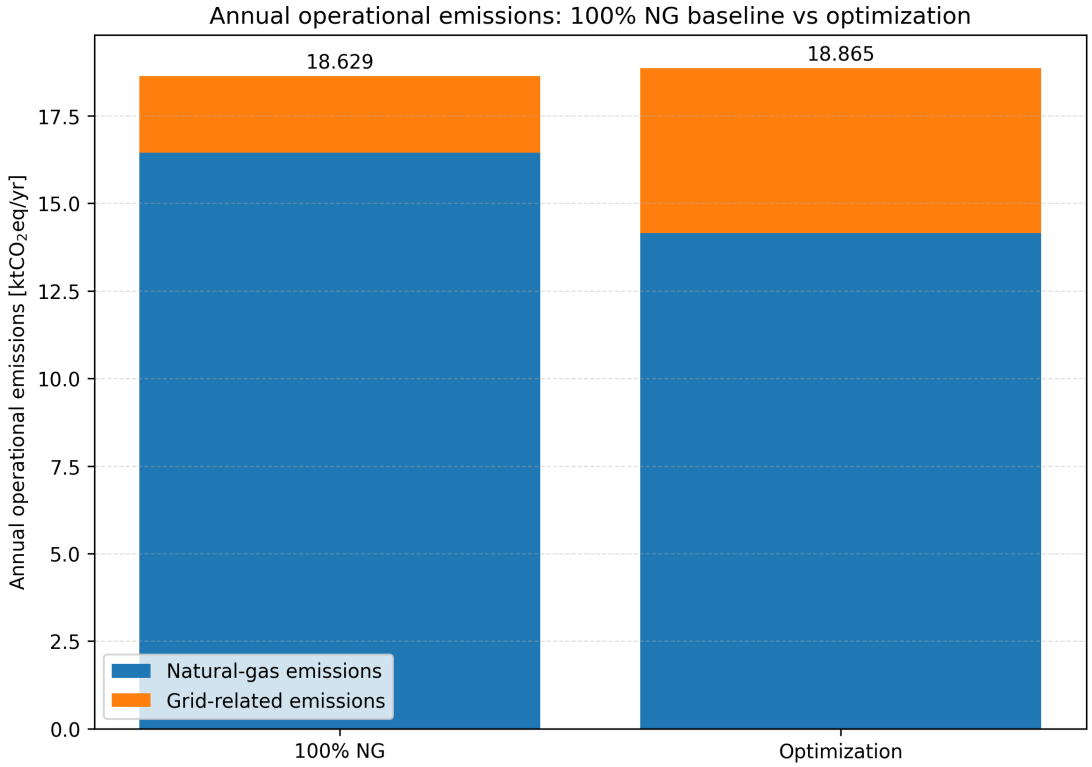


Figure 4.29: Annual operational emissions for the reconstructed 100% natural-gas baseline and the optimization-based configuration, including direct natural-gas and indirect grid-electricity contributions.

The additional grid-related emissions slightly exceed the direct emission savings obtained through natural-gas substitution. Consequently, total operational emissions increase from 18.629 $ktCO_2eq/yr$ in the baseline to 18.865 $ktCO_2eq/yr$ in the optimization-based configuration. The resulting increase is approximately 0.236 $ktCO_2eq/yr$, corresponding to 1.27% relative to the baseline.
The optimization-based configuration therefore achieves a reduction in direct natural-gas-related emissions, but not in total operational emissions. Under the investigated electricity-supply conditions, the additional indirect emissions associated with grid electricity offset the direct emission savings obtained through natural-gas substitution.
As in the rule-based analysis, this result does not indicate an intrinsic environmental disadvantage of hydrogen integration or direct electrification. Rather, it highlights the strong dependence of their decarbonization potential on the electricity-supply pathway. A greater contribution from on-site renewable generation and/or lower-carbon electricity would reduce grid dependence and the

associated indirect emission burden, potentially allowing the integrated configuration to achieve an overall operational decarbonization benefit.

4.4 Cross-Framework Discussion

4.4.1 Interpretation of the Two Analyses

The rule-based and optimization-based analyses represent two distinct stages of the present work and address complementary aspects of hydrogen integration in the considered glass-industry application. They originate from the same case-study basis and adopt a consistent electrochemical representation of the PEM electrolyzer. However, their energy-management formulations, system boundaries, and analytical purposes are not fully equivalent.

The rule-based analysis is primarily used to investigate the capability of the considered system configuration to accommodate progressively increasing hydrogen substitution. By evaluating hydrogen-share targets from 5% to 25%, it identifies how PEM operation, hydrogen storage, grid-supported hydrogen production, and natural-gas fallback evolve as the hydrogen requirement increases. The results show that the lower hydrogen targets can be fully accommodated, while increasing PEM utilization progressively leads to capacity-limited operation at higher substitution levels.

The optimization-based analysis addresses a different objective. In this second stage, the detailed PEM electrochemical and degradation models adopted in this work are integrated into an existing optimization-based EMS, replacing the original constant-efficiency representation of the electrolyzer. The resulting formulation coordinates hydrogen production and storage together with grid electricity, natural-gas consumption, and direct furnace electrification within a cost-minimizing dispatch problem. This second stage therefore extends the role of the PEM model from component-level performance assessment to an active representation within the system-level optimization.

Although both analyses include a 5% hydrogen case, the role of this hydrogen share differs between the two formulations. In the rule-based analysis, 5% represents the target hydrogen contribution, whereas in the optimization-based EMS it defines the minimum hourly contribution and can therefore be exceeded. The optimization-based formulation also represents a broader system boundary, including the original plant electrical load and direct electrical heating of the furnace. These differences are taken into account when interpreting the results across the two frameworks.

Economic and environmental performance is consequently assessed within each framework relative to its corresponding 100% natural-gas baseline. This provides a consistent basis for evaluating the effect of hydrogen integration within each system configuration, rather than directly comparing absolute annual costs and emissions obtained from different system boundaries.

4.4.2 PEM Operation and Degradation

The detailed PEM model provides the main methodological link between the two stages of the analysis. Although a consistent electrochemical representation and physical parameterization are

adopted, the operating conditions imposed on the electrolyzer differ according to the corresponding energy-management formulation. As a result, the PEM experiences different annual load distributions, which in turn affect its conversion efficiency.

For example, considering the 5% rule-based case and the optimization-based analysis, the annual fresh PEM energy efficiency is approximately 77.36% and 71.72%, respectively. This difference does not indicate a change in the intrinsic characteristics of the electrolyzer, but reflects the different operating points resulting from the two system-level formulations. Since PEM electrochemical efficiency is load dependent, energy-management decisions therefore indirectly influence its annual conversion performance.

The treatment of degradation further distinguishes the two stages. In the rule-based analysis, degradation is evaluated under a frozen-dispatch assumption. The fresh and degraded PEM models are therefore evaluated at the same electrical operating points, allowing the effect of ageing on hydrogen production and conversion performance to be isolated from changes in the controller decisions. Under this assumption, degradation reduces annual hydrogen production by approximately 10% for the same electrical dispatch, demonstrating a significant performance penalty even when the energy-management decisions remain unchanged.

In the optimization-based analysis, the interaction between PEM degradation and system operation is extended further. The degradation-dependent efficiency is iteratively fed back into the EMS, allowing the modified relationship between electrical input and hydrogen production to influence the optimized dispatch. The PEM model therefore no longer acts only as a post-processing representation of electrolyzer performance, but becomes coupled with the system-level energy-management problem. Under the resulting operating conditions, the hydrogen-production-weighted efficiency decreases from approximately 71.72% under fresh conditions to 64.60% when degradation is included. When the same hydrogen-output profile is evaluated with the fresh and degradation-adjusted PEM representations, this performance penalty corresponds to approximately 728.5 MWh of additional annual PEM electricity requirement.

Taken together, the two stages illustrate two complementary roles of detailed PEM modelling. The frozen-dispatch rule-based analysis isolates the performance penalty associated with degradation, whereas the optimization-based analysis allows degradation-dependent performance to interact with system-level dispatch. Overall, the results show that both the load dependence of PEM efficiency and its evolution with ageing are relevant when assessing electrolyzer performance at system level.

4.4.3 System-Level Implications

Despite their different formulations, the two analyses identify several common factors governing the performance of hydrogen integration. In particular, electrolyzer capacity, electricity-supply conditions, hydrogen-storage flexibility, and PEM performance determine how effectively hydrogen can contribute to the furnace energy demand.

The rule-based analysis highlights the physical limitation imposed by the installed 2.5 MW PEM electrolyzer as the target hydrogen share is increased. The 5% and 10% targets can be fully

accommodated, while the 15% case marks the onset of capacity-limited operation. At 20% and 25%, PEM saturation prevents continuous achievement of the prescribed hydrogen contribution and progressively reduces the production margin available for storage replenishment.

The optimization-based analysis complements this capacity-oriented assessment by considering a broader set of interacting energy flows and economic signals. PEM production and hydrogen storage are coordinated with grid imports, natural-gas consumption, and direct furnace electrification, while the degradation-dependent PEM representation allows electrolyzer performance to interact with the resulting dispatch.

A particularly important outcome common to both analyses is the influence of the electricity-supply pathway. The available photovoltaic generation is limited relative to the electrical demand associated with the integrated system, resulting in substantial dependence on grid electricity. Consequently, reducing direct natural-gas consumption does not automatically translate into lower total operational emissions or operating costs. The environmental and economic effectiveness of hydrogen integration depends not only on the amount of natural gas displaced, but also on the carbon intensity and cost of the electricity required to produce hydrogen and, in the optimization-based configuration, to support direct furnace electrification.

The two stages therefore provide complementary rather than competing perspectives on the investigated system. The rule-based analysis identifies the technical response and capacity limitations associated with progressively increasing hydrogen substitution, while the optimization-based analysis investigates the integration of detailed, degradation-dependent PEM behaviour within a broader cost-minimizing energy-management framework. Together, they show that the performance of hydrogen integration cannot be attributed to a single factor, but emerges from the interaction among component sizing, PEM electrochemical performance and degradation, energy-management formulation, and electricity-supply conditions

5. Conclusion

The objective of this thesis was to investigate the integration of on-site electrolytic hydrogen as a partial substitute for natural gas in a continuous glass-melting furnace, with particular attention to the influence of PEM electrolyzer performance and degradation on the overall energy-management problem. The results show that hydrogen can technically contribute to reducing natural-gas consumption in the investigated industrial process, but the achievable substitution level is strongly linked to the sizing and operation of the hydrogen-production system. Increasing the hydrogen requirement progressively increases PEM utilization until the installed electrolyzer capacity becomes the dominant constraint. Hydrogen integration should therefore not be assessed independently of component sizing, storage flexibility, and the operating strategy adopted at system level.

A second main conclusion concerns the representation of the PEM electrolyzer itself. Its conversion efficiency varies with the operating point and, according to the adopted degradation representation, progressively decreases with cumulative operation, meaning that a constant efficiency or fresh-only representation cannot fully describe its long-term behaviour. The rule-based analysis demonstrated the direct performance penalty associated with degradation under unchanged operating conditions, while the optimization-based analysis showed that degradation-dependent PEM performance can be coupled directly with the EMS and can consequently influence the optimized system operation. Accounting for degradation is therefore relevant not only for estimating electrolyzer performance, but also for obtaining a more representative description of the interaction between the PEM and the surrounding energy system.

Finally, the study shows that replacing natural gas with electrolytic hydrogen does not automatically result in lower overall operational emissions or costs. Although hydrogen substitution reduces direct furnace-related emissions, its actual decarbonization potential depends strongly on the electricity used for hydrogen production. Under the specific conditions of the investigated case study, the amount of electricity available from on-site photovoltaic generation is insufficient to cover a substantial fraction of the electricity required for hydrogen production, resulting in substantial dependence on the grid. The associated indirect emissions therefore offset the direct benefits of natural-gas substitution. This outcome is consequently linked to the considered system configuration and electricity-supply conditions and should not be interpreted as a general limitation of electrolytic hydrogen. Rather, it shows that its effectiveness as a decarbonization pathway for continuous glass production depends on the availability of sufficiently low-carbon electricity and on an appropriately sized and managed hydrogen-production system.

Overall, this work highlights the importance of evaluating hydrogen integration through an integrated system perspective. Detailed PEM electrochemical behaviour, degradation, component sizing, energy-management decisions, and electricity-supply conditions are strongly interconnected. The technical, economic, and environmental performance of hydrogen integration therefore depends from their combined effect and from the specific characteristics of the considered industrial case

study, rather than from the hydrogen-substitution level alone.

5.1 Limitations and Future Developments

The results of this work should be interpreted within the assumptions and boundaries of the adopted models. First, PEM degradation is represented through an efficiency evolution derived from the available electrochemical degradation data and extrapolated over the simulated operating period. Although this approach captures the influence of ageing on conversion performance, it does not represent all degradation mechanisms that may occur during the complete lifetime of an industrial PEM stack. Future work could therefore extend the degradation model to the full expected stack lifetime and include additional dependencies on operating history, start–stop events, load cycling, temperature, and other ageing mechanisms.

Second, the installed capacities of the photovoltaic system, PEM electrolyzer, and hydrogen storage were prescribed rather than jointly optimized. The rule-based results in particular showed that the 2.5 MW PEM rating becomes a limiting factor as the hydrogen target increases. A natural extension of the present work would therefore combine operational optimization with component sizing in order to determine economically and environmentally preferable combinations of PV capacity, electrolyzer rating, and hydrogen-storage capacity for different hydrogen-substitution objectives.

The electricity supply represents another important aspect for further investigation. Given the strong role of grid electricity in the investigated system, future work could explore alternative electricity-supply scenarios, including larger on-site renewable generation and lower-carbon grid electricity. Moreover, the use of time-dependent grid-emission factors instead of the constant value adopted in the present analysis could provide a more detailed representation of the environmental impact of electricity imports and, within the optimization framework, allow the EMS to account for temporal variations in grid carbon intensity when determining system operation.

Further developments could extend the economic assessment beyond the operating costs considered in the present analysis. The current evaluation includes energy-purchasing and carbon-related costs but does not constitute a complete techno-economic assessment of the system. Investment costs, maintenance, component replacement, electrolyzer-stack lifetime, and storage costs could therefore be included to assess the overall economic feasibility of hydrogen integration over the system lifetime.

Finally, the optimization framework could be further extended by considering uncertainty in electricity prices and renewable generation, as well as a more complete representation of PEM degradation over the electrolyzer lifetime. This would make it possible to investigate how energy-management decisions are affected by uncertain operating conditions and by the progressive evolution of electrolyzer performance. In a longer-term perspective, degradation-related effects on stack lifetime and replacement requirements could also be incorporated into the optimization framework.

These developments would provide a more complete basis for determining under which technical, economic, and electricity-supply conditions on-site electrolytic hydrogen can contribute effectively to the decarbonization of continuous glass production.

Bibliography

[1] European Commission. A hydrogen strategy for a climate-neutral europe. COM(2020) 301 final, 2020.

[2] European Commission. Repowereu plan. COM(2022) 230 final, 2022.

[3] International Energy Agency. Global hydrogen review 2024. Technical report, IEA, 2024.

[4] Michael Zier, Peter Stenzel, Leander Kotzur, and Detlef Stolten. A review of decarbonization options for the glass industry. *Energy Conversion and Management: X*, 10:100083, 2021.

[5] H2GLASS Consortium. H2glass: Introducing hydrogen fuel technologies and smart energy management systems in glass manufacturing. European Union Horizon Europe Project, 2023.

[6] Yousef S. H. Najjar. Hydrogen safety: The road toward green technology. *International Journal of Hydrogen Energy*, 38(25):10716–10728, 2013.

[7] Nikolas Schöne and Boris Heinz. Semi-systematic literature review on the contribution of hydrogen to universal access to energy in the rationale of sustainable development goal target 7.1. *Energies*, 16(4):1658, 2023.

[8] Zine Labidine Messaoudani, Fotis Rigas, Mahar Diana Binti Hamid, and Che Rosmani Che Hassan. Hazards, safety and knowledge gaps on hydrogen transmission via natural gas grid: A critical review. *International Journal of Hydrogen Energy*, 41(39):17511–17525, 2016.

[9] Sanjay Kumar Dwivedi and Manish Vishwakarma. Hydrogen embrittlement in different materials: A review. *International Journal of Hydrogen Energy*, 43(46):21603–21616, 2018.

[10] J. Incer-Valverde, C. Bauer, and M. Mazzotti. "colors" of hydrogen: Definitions and carbon intensity. *Energy*, 282:128697, 2023.

[11] M. Hermesmann and T. E. Müller. Green, turquoise, blue, or grey? environmentally friendly hydrogen production in transforming energy systems. *Progress in Energy and Combustion Science*, 90:100996, 2022.

[12] Mustafa Ergin Şahin. An overview of different water electrolyzer types for hydrogen production. *Energies*, 17(19):4944, 2024.

[13] Ahmed Rufai Dahiru, Ari Vuokila, and Mika Huuhtanen. Recent development in power-to-x: Part i – a review on techno-economic analysis. *Journal of Energy Storage*, 56:105861, 2022.

[14] Paula Muñoz-Peña, Lorenzo Bruno, Aleix Señís, Marina Fajardo, Marc Cheah-Mane, Oriol Gomis-Bellmunt, and Eduardo Prieto-Araujo. Optimal design of a hydrogen system of grid-connected flexible industrial microgrids. In *23rd Wind and Solar Integration Workshop*, Helsinki, Finland, 2024.

[15] Lorenzo Bruno, Esteban D. Gonzalez-Iakl, and Eduardo Prieto-Araujo. Optimisation-based energy management system for hydrogen integration in a grid-connected microgrid: A case study in the glass industry. In *24th Wind and Solar Integration Workshop*, Berlin, Germany, 2025.

[16] Paolo Marocco, Marta Gandiglio, Davide Audisio, and Massimo Santarelli. Assessment of the role of hydrogen to produce high-temperature heat in the steel industry. *Journal of Cleaner Production*, 388:135969, 2023.

[17] Georg Daurer, Stefan Schwarz, Martin Demuth, Christian Gaber, and Christoph Hochenauer. On the use of hydrogen in oxy-fuel glass melting furnaces: An extensive numerical study of the fuel switching effects based on coupled cfd simulations. *Fuel*, 380:133576, 2025.

[18] European Commission. H2glass: Advancing hydrogen technologies and smart production systems to decarbonise the glass and aluminium sectors. CORDIS – EU Research Results, 2023. Grant Agreement No. 101092153.

[19] A. Mohammadi and M. Mehrpooya. A comprehensive review on coupling different types of electrolyzer to renewable energy sources. *Energy*, 158:632–655, 2018.

[20] E. et al. Norman. Steam electrolysis for green hydrogen generation: State of the art and research perspective. *Renewable and Sustainable Energy Reviews*, 202:114725, 2024.

[21] E. S. et al. Akyüz. Hydrogen generation electrolyzers: Paving the way for sustainable energy. *International Journal of Hydrogen Energy*, 81:1338–1362, 2024.

[22] Q. et al. Feng. A review of proton exchange membrane water electrolysis on degradation mechanisms and mitigation strategies. *Journal of Power Sources*, 366:33–55, 2017.

[23] D. S. Falcão and A. M. F. R. Pinto. A review on pem electrolyzer modelling: Guidelines for beginners. *Journal of Cleaner Production*, 261:121184, 2020.

[24] Joakim Andersson and Stefan Grönkvist. Large-scale storage of hydrogen. *International Journal of Hydrogen Energy*, 44(23):11901–11919, 2019.

[25] G. AlZohbi et al. An overview on the technologies used to store hydrogen. *Energy Reports*, 2023.

[26] Nejc Klopčič et al. A review on metal hydride materials for hydrogen storage. *Journal of Energy Storage*, 2023.

[27] Gaël Sdanghi, Gaël Maranzana, Alain Celzard, and Vanessa Fierro. Review of the current technologies and performances of hydrogen compression for stationary and automotive applications. *Renewable and Sustainable Energy Reviews*, 102:150–170, 2019.

[28] Alessandro Franco and Caterina Giovannini. Hydrogen gas compression for efficient storage: Balancing energy and increasing density. *Hydrogen*, 5(2):293–311, 2024.

[29] Edwin K. P. Chong and Stanislaw H. Zak. *An Introduction to Optimization*. Wiley, 2013.

[30] Daniel E. Olivares, Amir H. Mehrizi-Sani, Amin H. Etemadi, Claudio A. Cañizares, Reza Iravani, Mehrdad Kazerani, Amir H. Hajimiragha, Oriol Gomis-Bellmunt, Mehrdad Saeedifard, Rodrigo Palma-Behnke, et al. Trends in microgrid control. *IEEE Transactions on Smart Grid*, 5(4):1905–1919, 2014.

[31] Stephen Boyd and Lieven Vandenberghe. *Convex Optimization*. Cambridge University Press, 2004.

[32] Jorge Nocedal and Stephen J. Wright. *Numerical Optimization*. Springer, 2006.

[33] Dimitris Bertsimas and John N. Tsitsiklis. *Introduction to Linear Optimization*. Athena Scientific, 1997.

[34] Alessandra Parisio, Evangelos Rikos, and Luigi Glielmo. A model predictive control approach to microgrid operation optimization. *IEEE Transactions on Control Systems Technology*, 22(5):1813–1827, 2014.

[35] Tingfeng Kuang, Jie Chen, Jun Liu, Yuchao Zhang, and Hongyin Bao. Optimization of user-side electrolytic hydrogen production system considering electrolyzer efficiency degradation. *International Journal of Hydrogen Energy*, 88:545–556, 2024.

[36] Nowtricity. Co2 emissions per kwh in slovenia. https://www.nowtricity.com/country/slovenia/, 2026. Historical electricity-generation data for 2025. Accessed: September 2026.

[37] International Carbon Action Partnership. Emissions trading worldwide: Icap status report 2026, 2026.